

## Stellingen

behorende bij het proefschrift  
Technology and applications of single-electron tunneling devices  
van Erik Visscher

1.

Het feit dat het NOC zich verzekert tegen teveel gouden medailles geeft aan dat de Olympische spelen moreel failliet zijn.

2.

Het beoordelen van patenten in de biochemie op inventiviteit stuit op problemen omdat in veel gevallen de natuur zelf de uitvinder is.

3.

De geschiedenis van de ontwikkeling van de Nucleaire Magnetische Resonantie leert ons dat uitspraken over de toekomst van de mesoscopische fysica niet zinvol zijn.

4.

Wetenschappelijk gezien is het interessant om de uitstoot van kooldioxide te vergroten. (W. Kurschner, F. Wagner, E. H. Visscher and H. Visscher, *Predicting the response of leave stomata to future enriched CO<sub>2</sub> atmosphere; constraints for paleobotanical and experimental observations* in Predictions in Geology, Vrije Universiteit Amsterdam, 1996)

5.

Ondanks het feit dat een plant fysiologisch zeer gevoelig reageert op een kleine gemiddelde verandering van de CO<sub>2</sub> concentratie in de atmosfeer, kan dit niet worden gebruikt als een absolute meting van de CO<sub>2</sub> concentratie in vroegere tijden.  
(<http://mloserv.mlo.hawaii.gov/mloco2.html>)

6.

De experimentele waarneming van odd-even effecten in een supergeleidend SET circuit is sterk gerelateerd aan de koppeling naar zijn electromagnetische omgeving.  
(Hoofdstuk 5 van dit proefschrift)

7.

Het door de regering voorgestelde fiscale stelsel voor de 21-ste eeuw, waar commercie in plaats van arbeid wordt belast, zal het Calvinisme in Nederland in ere herstellen.

8.

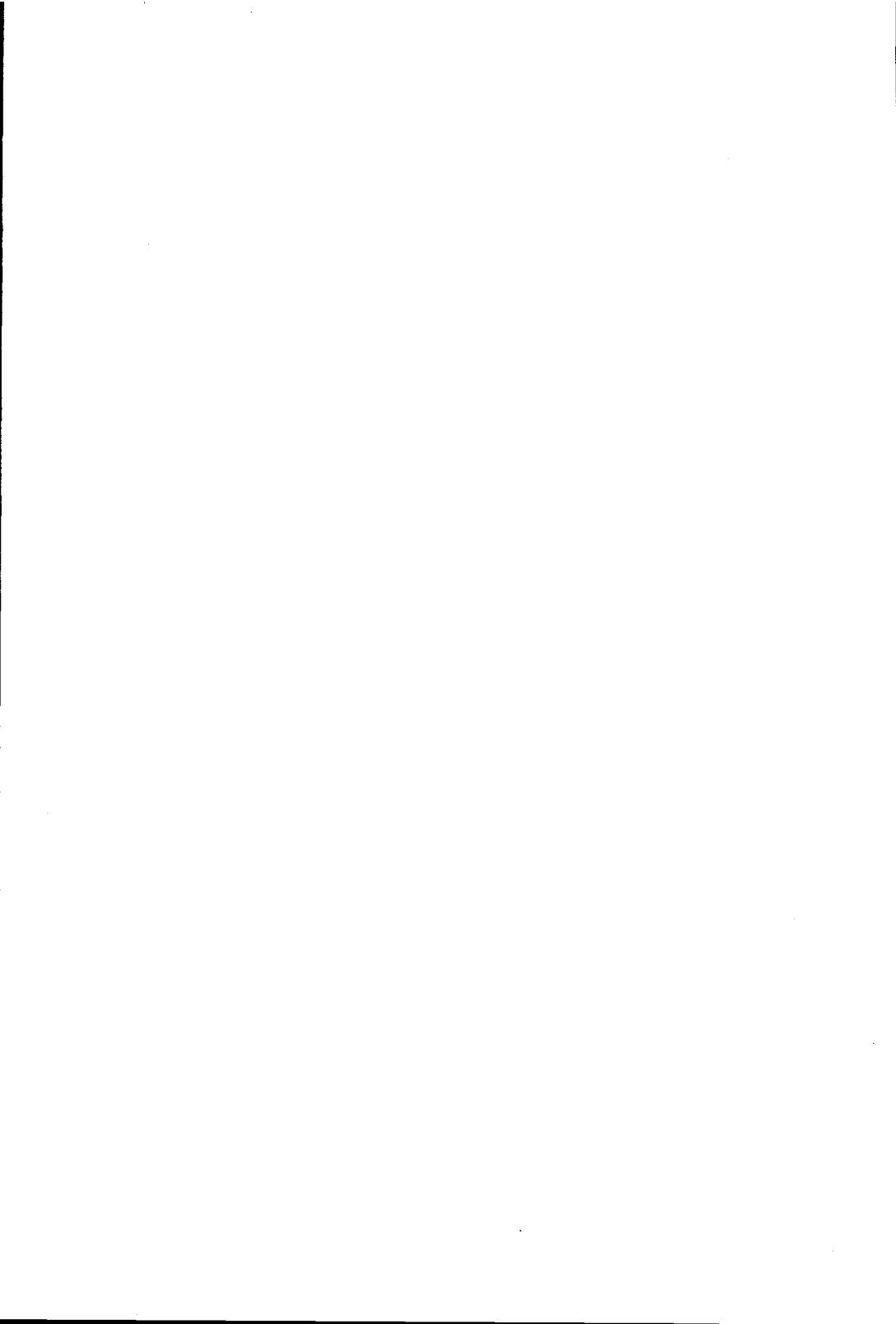
De overeenkomst tussen het paarse kabinet en de regering Clinton is dat beide hun succes te danken hebben aan een sterk aantrekkende economie.

9.

Het verschil tussen de SET-multilaags fabrikagetechniek beschreven door Visscher *et al.* (Appl. Phys. Lett. 66, 305 (1995)) en het NEC patent (JP5145062) is laatst genoemde alleen op papier werkt.

10.

De uitvinding van het wiel laat zien dat technologische doorbraken triviaal lijken.



**Technology and applications of  
single-electron tunneling devices**

714075

3191000-

TR diss 2820



# Technology and applications of single-electron tunneling devices

## Proefschrift

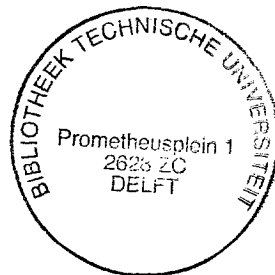
ter verkrijging van de graad van doctor  
aan de Technische Universiteit Delft,  
op gezag van de Rector Magnificus Prof. ir. K. F. Wakker,  
in het openbaar te verdedigen ten overstaan van een commissie  
door het College van Dekanen aangewezen,

op vrijdag 18 oktober 1996 te 10.30 uur

door

**Erik Henk VISSCHER**

natuurkundig ingenieur  
geboren te Utrecht.



Dit proefschrift is goedgekeurd door de promotor:

Prof. dr. J. E. Mooij

Samenstelling van de promotiecommissie:

Rector Magnificus, voorzitter

Prof. dr. J. E. Mooij, promotor

Dr. P. Hadley, toegevoegd promotor

Prof. dr. S. Radelaar (T. U. Delft)

Prof. dr. A. H. M. van Roermund (T. U. Delft)

Prof. dr. H. Visscher (U. Utrecht)

Dr. M. H. Devoret (C. E. A. Sarclay, Paris, France)

Prof. dr. T. Claeson (T.U. Chalmers, Göteborg, Sweden)

Published and distributed by:

Delft University Press

Stevingweg 1

2618 CN Delft

The Netherlands

telephone: +31-15-2783254

fax: +31-15-2781661

CIP-GEGEVENS KONINKLIJKE BIBLIOTHEEK, DEN HAAG

Visscher, Erik Henk

Technology and applications of single-electron tunneling devices.

Erik Visscher. - Delft:

Delft University Press. -Ill.

Thesis Delft University of Technology. -

With ref. - With summary in Dutch.

ISBN 90-407-1381-2

NUGI 812

Subject headings: single-electron tunneling devices, Josephson junctions, tunneling spectroscopy, mesoscopic physics.

Copyright © 1996 by E. H. Visscher

All rights reserved.

*No part of this book may be reproduced in any form by print, photoprint, microfilm or any other means without written permission from the publisher or the author.*

Printed in the Netherlands

---

## Preface

This thesis describes experimental work on ultra-small metallic tunnel junction systems. Due to the small dimensions of these systems, the electron transport through such systems can be controlled on the scale of one electron and therefore one usually refers to these devices as single-electron tunneling (SET) devices. When I started my Ph.D. in 1992 in the quantum transport group of professor Mooij such devices could already be made routinely, using what one would call now standard submicron technology. Although these devices have generated a wealth of new physics, at that time it already became apparent that in order to realize the numerous proposed experiments and applications a more mature technology was needed. At that time the European EC ESPRIT project SETTRON was initiated, which was focussed on technological issues of SET devices. Our participation in this project was the development of a multilayer process for SET devices, for which we used the excellent lithography facilities at DIMES to our advantage. Later, using the experience of the multilayer technology we also focussed on the integration of SET devices with semiconductor devices. The SETTRON project was an interesting experience, introducing me already very early to the European "single-electron tunneling community". Parallel to the development of the SET technology, we also tried to develop shunted aluminium Josephson junctions. Shunted junctions form the key to the Josephson junction technology and was already a desired technology for a long time in our group. Initially this project had a slow start, however in the summer of 1994 it made a big step forward when we choose platinum as the shunting element. At this point I left for the US to stay for three month period in professor Tinkham's group at Harvard. Working in a different environment was a welcome change. Although three months is a very short period, the work on cold amplifiers together with Jack Hergenrother was an interesting side step. Returning to Delft, in January 1996 I started the last part of my Ph.D. work, which was the combination of the multilayer SET fabrication and the shunted Josephson junctions. Personally for me this work formed the most rewarding part of the work I did. In a sense this project is a perfect example of the new approach of many research labs have adapted now, in which the development of new technologies, with a focus on applications, generates new interesting physics.

The work presented in this thesis is a result of collaboration with many people. First of all I would like to thank Peter Hadley, my tutor who thought me to develop the American approach to physics and always had time to discuss the always present physics problems. Furthermore, I would like to thank Hans Mooij, for his stimulating and enthusiastic way to manage the group. During my first two years of my Ph.D. we worked closely with a number of people, generating a very stimulating working environment. Therefore I first would like to mention the "old bunch" Huub Appelboom, Bart Geerligs, Stefan Verbrugh, Wiveka Elion,

---

Marco Matters, Nijs van der Vaart, Luuk Mur and professor Lydia Sohn. These first two years were very intensive both in terms of physics and (unforgettable) social events. The last two years of my Ph.D. many new people joined the group. I would like to thank Sander (polymer) Tans and Tjerk (quench) Oosterkamp being my roommates in the last year, sharing both the frustrations and joys of doing experimental physics. I would like to thank my students Jan Lindeman for his work on the integration of the SET - HEMT system, Walter Hoogeveen for the work on the shunted junctions and Dirk Schraven for his work on the Josephson junction generator - SET system. Not only the work, but also the numerous beers at the TPKV and the meetings at the squash court were intensive. Furthermore, I would like mention all the other people who make the group what it is, in particular Herre van der Zant, Cees Dekker, Leo Kouwenhoven and Kees Harmans. Last but not least I would like to thank Bram van der Enden for his interesting coffee table conversations and his good humor. Leo Lander, Chris Gorter, Wim Schot and Willem den Braver for their valuable technical help. In particular I would like to mention Raymond Schouten who taught me "the art of electronics". I would like to thank my brother Mark, the theorist from upstairs and my parents for their support. Finally, I would like to thank Cindy, who shared with me both the difficult and the exciting moments of my Ph.D. and who at the end knew more people in the physics community than I did.

Erik Visscher  
September 2, 1996.



# Contents

<b>1</b>	<b>Introduction</b>	<b>3</b>
1.1	Single-electron tunneling effects . . . . .	3
1.2	Single-electron tunneling technology . . . . .	6
1.3	The normal SET transistor . . . . .	7
1.4	The superconducting SET transistor . . . . .	10
1.5	The electromagnetic environment . . . . .	12
1.6	A Josephson junction microwave generator . . . . .	13
1.7	Microwave spectroscopy on Josephson junction systems . . . . .	14
1.8	General framework and scope of this thesis . . . . .	16
	References . . . . .	18
<b>2</b>	<b>Multilayer single-electron tunneling devices</b>	<b>23</b>
2.1	Introduction . . . . .	23
2.2	Multilayer fabrication . . . . .	23
2.3	Applications of multilayer SET devices . . . . .	27
2.4	Noise and offset charges in a SET transistor . . . . .	31
2.5	Filtering and shielding . . . . .	34
2.6	Operation temperature . . . . .	35
2.7	Conclusions and future prospects . . . . .	37
	References . . . . .	38
<b>3</b>	<b>High frequency operation of SET devices</b>	<b>41</b>
3.1	Introduction . . . . .	41
3.2	Experimental considerations . . . . .	42
3.3	On-chip HEMT impedance matching . . . . .	42
3.4	The electron counter . . . . .	48
3.5	Further developments . . . . .	50
	References . . . . .	51
<b>4</b>	<b>Josephson junction microwave generators</b>	<b>53</b>
4.1	Introduction . . . . .	53
4.2	A tunable SQUID microwave source . . . . .	54

---

4.3	Microwave interaction between a JJ generator and a single Josephson junction . . . . .	57
	References . . . . .	65
<b>5</b>	<b>Microwave spectroscopy on a superconducting SET transistor</b>	<b>67</b>
5.1	Introduction . . . . .	67
5.2	Quasiparticle tunneling and parity effects in a superconducting SET transistor . . . . .	68
5.3	Photon-assisted tunneling in a superconducting SET transistor . .	72
	References . . . . .	77
	<b>Summary</b>	<b>79</b>
	<b>Samenvatting</b>	<b>81</b>
	<b>Curriculum Vitae</b>	<b>83</b>

# Chapter 1

## Introduction

### 1.1 Single-electron tunneling effects

In 1911 Millikan[1] observed that the charge on small drops of oil only appeared in multiples of the electron charge,  $e = 1.6 \times 10^{-19}$  C. This was the first observation of the discreteness of charge and the first determination of the charge of an electron. An important aspect of Millikan's experiment was that the capacitance of the oil drops was small, which means that the energy to add an electron to the drop  $E_C = e^2/2C$ , was larger than the thermal energy of the drop. For the same reason, the charging of a small metallic grain can only appear in multiples of the electron charge. Reducing the capacitance will increase the charging energy, which can exceed the thermal energy at low enough temperatures and therefore becomes a observable quantity. Therefore, charge quantization can be observed in a metallic grain, if its capacitance is small enough and can be sufficiently decoupled from its environment. Furthermore, the charging energy can block the entrance of an additional electron to the grain, which is know as the Coulomb blockade.[2]

The Coulomb blockade in the small metallic grain, usually referred to as an island, can only be observed in a transport measurement. Therefore the island has to be connected to the macroscopic outside world, without increasing the capacitance and thereby destroying the charging energy. Using ultra-small tunnel junctions, electrons can be added to or removed from the island. A tunnel junction is realized if two metallic electrodes are separated only by a very thin insulating layer. The wave functions of the electrons on both side of the barrier can overlap and the probability that electrons can tunnel through this barrier quantum mechanically becomes non negligible. The tunnel junction behaves as an ultra small capacitor  $C$  with capacitances between  $10^{-15}$  to  $10^{-16}$  F, and corresponding Coulomb energies of 1 to 10 K. For bias voltages  $V$  larger than a certain threshold voltage, electrons start to tunnel through the junction with a rate of  $V/eR_T$ , where  $R_T$  is the tunnel resistance. Therefore connecting submicron tunnel junctions to the metal island provides a way to add or remove electrons form

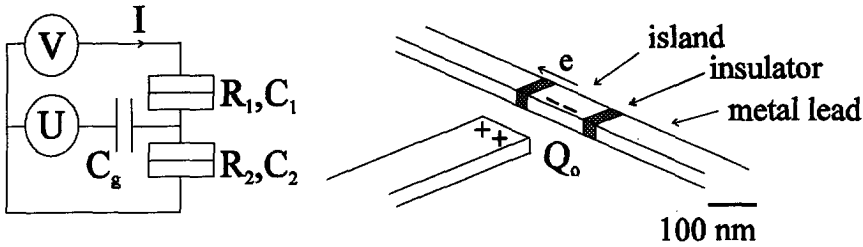


Figure 1.1: (a) Schematic of a voltage biased SET transistor. The boxes indicate the tunnel junctions. (b) Schematic of the physical layout of the SET transistor. The tunnel current through the junctions is determined by de gate charge  $Q_0$ .

the island in a *discrete* way. An extra capacitor coupled to the metallic island, usually referred to as the gate, can induce a *continuous* polarization charge. The gate provides a way to tune the potential of the island, thereby controlling the electron transport through the circuit. Building circuits out of these tunnel junctions and metallic islands, one can control the electron transport on the scale of one electron. Therefore these devices are usually referred to as single-electron tunneling (SET) devices. The most simple SET devices is called a SET transistor, which is schematically shown in Fig.1.1. Beside the charge quantization, in these tunnel devices the discreteness of the electron charge is also reflected in the shot noise, which is experimentally hard to observe. Only recently the shot noise in a SET transistor was measured.[3]

In order to have charge quantization the electron should be well localized on either side of the tunnel barrier. Therefore thermal and quantum fluctuations of the charge[20] on the island should be small. Thermal fluctuations are small if the charging energy is large compared to the thermal energy,  $E_C \gg k_B T$ . Furthermore, perturbative calculations show that quantum fluctuations are negligible in the limit where the tunnel resistance is much larger than the resistance quantum,  $R_K = h/e^2 \approx 25.8 \text{ k}\Omega$ , where  $h$  is Planck's constant. In the 1960s, the influence of charge quantization was studied in small metal grains coupled via tunnel barriers, which are formed naturally in ultra-thin metallic films.[4, 5, 6] In the late 1980s, due to the advances in micro fabrication, controlled three terminal Coulomb blockade devices were realized experimentally.[7] Using these devices a solid state analog of Millikan's famous experiment has been demonstrated, monitoring single electrons entering a small piece of metal.[8, 9]

There are a number of experimental systems in which charging effects can be studied. A widely used experimental system in the study of single-electron tunneling is a two-dimensional electron gas (2DEG), which can be obtained in semiconductor heterostructures.[10] Heterostructures are fabricated using molec-

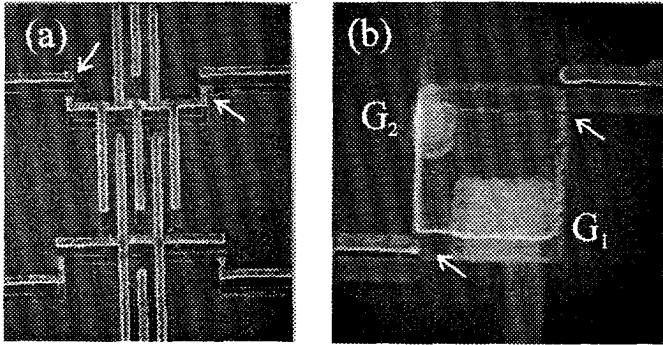


Figure 1.2: (a) SET circuit made by conventional shadow evaporation and (b) SET transistor made by a multilayer fabrication technique. The arrows indicate the overlap junctions.  $G_1$  and  $G_2$  are two gates which are situated under the island.

ular beam epitaxy (MBE) growth techniques. Using either a split gate geometry or etching techniques the electrons can be confined laterally forming a small dot of electrons. One advantage of this system is that the low electron density of the 2DEG provides large Fermi wave lengths. Therefore small dots of a few hundred nanometers contain only a few hundred electrons and not only show Coulomb blockade but also exhibit quantum confinement effects. Such devices are known as quantum dots[11] and can be considered as artificial atoms.[12]

An other popular system for studying charging effects are metal circuits, usually fabricated using a double-angle shadow evaporation technique.[13] Fig.1.2 (a) shows a typical aluminum SET circuit with interdigitated coupling capacitors. In Fig.1.2 (b) an example is shown of a SET circuit fabricated using an improved multilayer fabrication technique, presented in chapter 2. Contrary to the 2DEG systems, the Fermi wave length of conduction electrons in metals is in the order of 0.1 nm and thus much smaller than the dimensions of most metallic devices. Although recently quantum confinement in a metallic grain has been observed[14], in general it is not of importance in metallic devices. Contrary to 2DEG systems, at low temperatures, certain metals exhibit superconductivity below a certain critical temperature. Using aluminium charging devices, which are superconducting below 1.2 K, the interplay between superconductivity and charging effects can be studied.[15] Therefore in terms of physics these devices form a complementary family of charging devices in the study of quantum mechanical transport properties in submicron circuits. Apart from the fact that the electron transport in metallic devices can be governed by different type of physics, metallic devices are relatively simple to realize and robust in use com-

pared to 2DEG systems. In this thesis this technological advantage is maximally exploited, yielding hybrid metal charging devices. The integration of a SET transistor with a 2DEG high-electron mobility transistor (chapter 3) and a Josephson junction generator (chapter 5) [16, 17] will be demonstrated.

Beside the metal and 2DEG systems, the Coulomb blockade has been observed with a scanning tunneling microscope (STM) placed over a tiny metallic droplet.[18] The role of the island is played by the droplet. Due to the small dimensions (few nm) a Coulomb blockade at room temperature has been reported. Furthermore, silicon SET transistors have been fabricated, using the controlled oxidation of small silicon nanowires.[19]

## 1.2 Single-electron tunneling technology

In the last decade, SET devices have generated a wealth of new physics in quantum electron transport from the physics of artificial atoms[21, 22] to the demonstration of Heisenberg's uncertainty principle in a solid state device.[23] In a practical sense they have been proven to be very versatile electrometers with sub-electron sensitivity and have been recognized theoretically to be suitable for current standards, and even memory and logic circuits in which one single electron or a few electrons carry the information. For a good review of these subjects, see ref.[2] While in theory the performance of these devices is promising, for instance the simplest SET logic circuit, an inverter, has not been demonstrated experimentally. A number of different technological issues first have to be solved in order to focus on these more complex circuits. Therefore, in the beginning of the 1990's the relevance of a more systematic research on the technology of SET devices became apparent. The slow technological progress thus far can be illustrated for instance by noticing that since the development of the celebrated shadow-evaporation technique[7] in the late 1980's, there has been no single alternative for fabricating metal controlled multi-junction SET devices. Numerous projects partially pushed by industry have been initiated in the US, Europe and Japan. This work formed part of the ESPRIT SETTRON project that was started in 1993, with its main goal to focus on the technological issues invoked by the development of practical SET devices which can be used in precision measurements and metrology: *to identify the limitations of the present day devices and to define the steps to be made for improvements towards well-defined goals and specifications for device performance.*[24] Reduction of device dimensions, noise, offset charges, materials, fabrication and integration are addressed within this project divided over the different members including Delft University, Chalmers University, Centre d'Etudes de Saclay, Glasgow University and the Physikalisch Technische Bundesanstalt in Braunschweig. The work done under the denominator of SETTRON, presented in this thesis, is clustered around a subset of problems focussed on the integration and interfacing of SET devices. In chapter

2, a multilayer SET fabrication technique is introduced, yielding controllable SET devices, with improved device characteristics. Using this multilayer technique, a number of different applications are discussed. Furthermore, in chapter 3 and 4 hybrid SET circuits[16, 17] are introduced, in which SET devices are integrated on-chip with different types of technologies.

The purpose of the rest of this chapter is to give an introduction to the work presented in this thesis. In the next sections the basic working principles of SET devices is reviewed. We will show that the addition of superconductivity drastically changes the characteristics of a SET device. The relevance of filtering in connection with the extreme sensitivity of these devices to noise is stressed. Beside SET devices also large superconducting Josephson junctions (JJ) will be discussed, which will be used as local microwave oscillators for the use in spectroscopy experiments. Finally, in the last section the general framework of the work in which this thesis is presented, will be discussed in more detail.

### 1.3 The normal SET transistor

The simplest and most thoroughly studied three terminal SET device is called the SET transistor.[25] The most impressive characteristic of the SET transistor is its extreme sensitivity to charge. Sensitivities at low as  $7 \times 10^{-5} e/\sqrt{\text{Hz}}$ , have been measured and are still limited by the low frequency  $1/f$  noise.[26] This charge sensitivity is orders of magnitude better than the best commercially available electrometer. Therefore most of its applications are in the field of precision measurements and metrology. It has been used for measuring charge with sub-electron charge sensitivity.[8, 9] Furthermore, a SET transistor has been used to make a very sensitive photodetector.[27] Using one-dimensional arrays of tunnel junctions an accurate current standard[28, 29, 30] can be achieved, in which the current through the device is linearly related to the clock frequency. Presently, the operation of this current standard is close to metrological accuracy.[31] In addition to its sensitivity, the utility of a SET transistor as an amplifier depends on its voltage gain.[32] Voltage gain allows a SET transistor to drive another SET transistor, which is required in logic circuits and cascade amplifiers. Gain was measured experimentally for the first time by Zimmerli *et al.*[33] Furthermore, groups in mesoscopic physics have started to use the SET transistor as a standard charge measuring tool, similar to SQUID's. For instance, metal SET transistors are used in the study of edge channels in semiconductor heterostructures.[34] Moreover, fabricating a SET transistor on a tip of an scanning microscope the electrostatic distribution on a surface can be studied.[35]

Two tunnel junctions in series form a semi-isolated island which has a charging energy of  $e^2/2C_\Sigma$  and is biased with a voltage source  $V$ . Here  $C_\Sigma = C_1 + C_2 + C_g$  is the total island capacitance, where  $C_g$  is a capacitively coupled gate which can polarize the island with a continuous charge  $C_g U$ . The Coulomb blockade

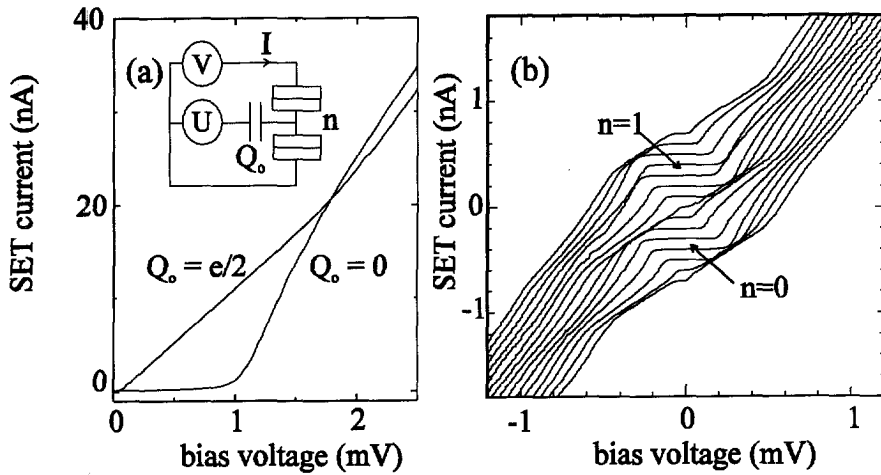


Figure 1.3: (a) Current-voltage ( $I-V$ ) characteristics of a normal SET transistor for the maximum ( $Q_0 = 0$ ) and minimum ( $Q_0 = e/2$ ) Coulomb blockade. (b) A set of  $I-V$  curves for different gate voltages. The plateaus indicate the Coulomb blockade for zero,  $n = 0$  and one,  $n = 1$  electron on the island.

suppresses current flow between the two output terminals for all voltages below a certain threshold voltage. This threshold voltage is a periodic function of the charge on the gate with a periodicity of the elementary charge of an electron,  $e$ . The electron transport in a SET circuit is described by the theory as a sequence of jumps of single electrons. For any given charge state ( $n, p$ ) of the system, where  $n$  is the number of excess electrons on the island and  $p$  is the number of electrons that passed the voltage source, one should calculate the tunneling rates for all junctions. In which particular junction and at what exact moment the next tunnel event will occur is a matter of the probabilities determined by the corresponding rates. In the theory developed by Likharev *et al.*[25] the change in the electrostatic energy  $\Delta E$  of the circuit associated with a particular tunnel process has to be considered. Furthermore, the change of the free energy of the voltage sources has to be taken into account. This approach is referred to as the global rule, and has experimentally been found to apply for circuits with low impedance leads, much smaller than the resistance quantum. For a given transition  $\Delta E$  the tunneling rate in the orthodox theory is calculated using the Golden Rule,

$$\Gamma = \frac{\Delta E}{e^2 R_T (1 - \exp(-\Delta E/k_B T))} \quad (1.1)$$



Transitions which increase the free energy of the system,  $\Delta E < 0$  are forbidden and therefore electron tunneling is blocked. This is the condition of the Coulomb blockade of tunneling. For a symmetrically biased SET transistor, the energy difference between the initial state  $n$  and the final state  $n \pm 1$ , where one electron either has tunneled on or off the island is given by,

$$\Delta E = \frac{e}{C_{\Sigma}} \left( \pm \frac{1}{2} e - Q_o \right) \mp \frac{eV}{2} \quad (1.2)$$

Here  $Q_o = C_1 V - C_g U + Q^*$  is the effective charge bias of the island. Here  $Q^*$  is an effective random offset in the range of  $[-e/2, e/2]$ , which can be caused by charge traps around the island or in the tunnel barrier. Although in theory often omitted, random offset charges will always be present in an experimental system. Due to their extreme charge sensitivity, complicated SET circuits will never operate properly if no solution is found for this problem. A more quantitative description on this subject is given by Lafarge *et al.*[37] Fig. 1.3 (a) and (b) show current-voltage ( $I - V$ ) characteristics for different gate voltages. In Fig. 1.3 (b) the periodic Coulomb blockade plateaus are clearly visible, corresponding to an integer number of electrons on the island. Current biasing the SET transistor such that the output voltage is larger than the threshold voltage, the input-output voltage curves,  $U - V$  form a sawtooth pattern which have slopes of  $C_g/(C_g + C_1)$  on one side and  $-C_g/C_2$  on the other, as shown in Fig.1.4. In this limit the voltage gain is  $K_V = C_g/C_2$ , and can be greater than unity if  $C_g > C_2$ . While in principle the voltage gain can be large, the practical realizable gain depends on the extent to which the temperature and junction capacitance can be reduced. Given a 100 mK operating temperature and a 0.1 fF junction capacitance the voltage gain is limited to about  $K_V = 8$ . Higher values of gain require either lower temperatures or smaller junction dimensions.

Even at zero temperature the Coulomb blockade will not block all charge transport. Taking into account second order tunneling processes, Averin and Odintsov[20] have pointed out that second order tunneling transitions always lead to a finite current in the presence of a voltage. In these co-tunneling events an electron tunnels onto the island while a second electron simultaneously leaves the island across the other junction. Since the charge on the island is only changed virtually, there is no Coulomb barrier for this process. The co-tunneling rate is proportional to  $(R_K/R_T)^2$  and hence smaller than the rate for first order processes. To study the dynamics of single-electron transport Eq. (1.2) and Eq. (1.1) can be implemented in a Monte-Carlo algorithm or master equation [25], which describes the evolution of the probability distribution among all possible charge configurations. The simple orthodox theory is sufficient to describe most experimental results on simple normal state SET devices quantitatively. Theories beyond the orthodox theory include the account of arbitrary electromagnetic environment [38, 39], the theory of co-tunneling [20] and the account of energy quantization.[40]

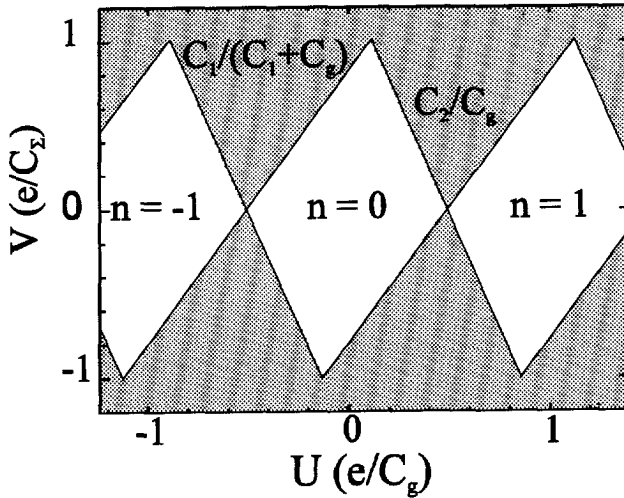


Figure 1.4: Stability diagram of a SET transistor. In the diamond shaped areas the charge on the island is an integer number of electrons. Outside these areas a tunnel current will flow through the device.

## 1.4 The superconducting SET transistor

Below 1.2 K, aluminium is a superconductor[41] in which the electrons form a condensate of Cooper pairs, carrying a charge of  $2e$ . The superconductor can be described by a macroscopic wave function with an amplitude and a phase. The superconducting phase difference  $\phi$  across a tunnel barrier will give rise to a dissipationless coherent transport of Cooper pairs through the barrier of,  $I = I_o \sin \phi$ . This remarkable discovery was made by Josephson[42] in 1960 and is referred to as the dc Josephson effect. The strength of this effect is given by the Josephson coupling energy  $E_J = I_o \Phi_o / 2\pi$ , where  $I_o$  is the supercurrent of the junction with a magnitude given by the Ambegaokar-Baratoff relation[43] and  $\Phi_o = h/2e$  is the superconducting flux quantum. Decreasing the capacitance of the junction, the charging energy and the Josephson coupling energy become comparable. Since the charge and the phase of the junction are non-commuting variables, this will give rise to some interesting quantum phenomena.

In the ground state all the electrons are paired if the island contains an even number of conduction electrons. However, if it is odd, one electron must be necessarily unpaired and leads to an elementary excitation known as a *quasiparticle*. Consequently, the ground state energy of the device with an odd number of elec-

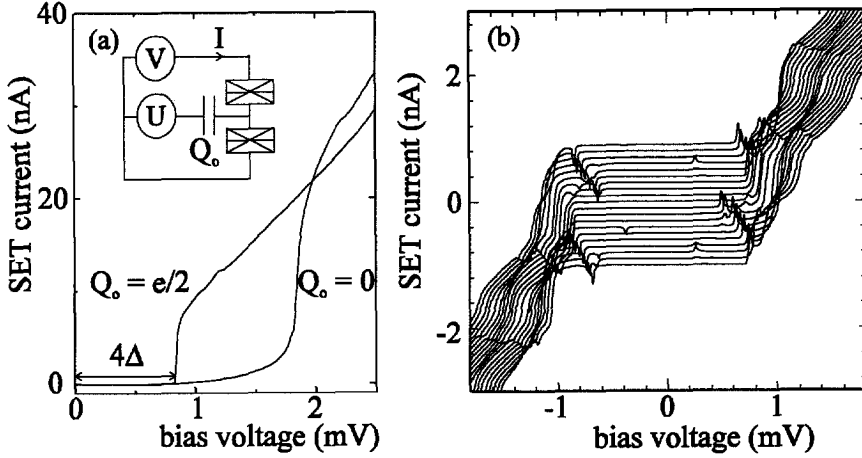


Figure 1.5: (a) Current-voltage characteristics for the maximum and minimum Coulomb blockade of a superconducting SET transistor. At  $Q_o = e/2$  quasiparticle conduction starts at a bias voltage of  $2\Delta$ . (b) Set of  $I-V$  curves for different gate voltages. The curves have an offset for clarity and exhibit a rich structure, illustrating the superconducting SET transistor fundamentally differs from its normal counterpart.

trons on the island is raised above that of an even number by the amount of the energy gap  $\Delta$ . Therefore the behavior of superconducting SET devices is strongly dependent of the parity of the island and is usually referred to as the even-odd effect. Based on this remarkable effect, superconducting SET transistors can be used as ultra-sensitive photon detectors.[44]

Furthermore, the supercurrent through the device depends on the competition between the Josephson effect and the charging effect. Since the supercurrent is a direct reflection of the ground state energy, it provides a direct way to probe the ground state properties of the system. Therefore superconductivity gives rise to a gate charge dependent  $2e$  periodic supercurrent in a S-SET. The sensitivity of the critical current on the charge can be used to operate the S-SET as a electrometer based on Cooper pair tunneling. At low temperatures, the energy resolution of this device approaches the fundamental quantum limit,  $\hbar/2$ . [45] Biased at finite voltages, the S-SET can be used as an electrometer similar to the normal SET transistor. However, due to the BCS density of states the device is able to resolve energy changes of order  $E_C$ , even when the thermal energy is larger than the charging energy.[46]

The tunneling of Cooper pairs is coherent and reversible, unlike the tunneling of electrons through a junction which is incoherent and reversible. These are two very severe requirements for basic elements in a quantum computer.[47] Quantum computation has recently gained great interests when Shor[48] showed that quantum mechanics can be used in an algorithm that factorizes large integers much faster than a classical computer. Although no proposal for quantum computation based on solid state devices has been made yet, Cooper pair electronics form an interesting option.

The orthodox theory does not provide a good starting point for calculating the tunnel rates, since this theory omits all coherent tunnel effects. Therefore a full non-perturbative quantum mechanical calculation is needed (the superconducting SET transistor is extensively discussed by Maassen van den Brink *et al.*[49] and Joyez[50]). Instead of the classical charge states  $(n, p)$ , now the device is described in terms of a set of eigenfunctions  $|n, p\rangle$ . Fig. 1.5 (a) shows the  $I - V$  curves of a superconducting SET transistor for the gate charges  $Q_o = 0$  and  $Q_o = e/2$ . The supercurrent is suppressed due the large charging energy,  $E_C \gg E_J$ . On a large scale the  $I - V$  looks similar to a normal SET transistor  $I - V$  shifted over  $4\Delta/e$ . However as will be described in chapter 5, in general at finite bias the tunnel processes can be much more complicated than its normal counterpart, and careful interpretation is required. At bias voltages larger than  $4\Delta/e$ , the current will increase rapidly due to the onset of quasiparticle conduction. At bias voltages smaller than  $4\Delta/e$  a number of different processes involving resonant Cooper pair tunneling, combined Cooper pair-quasiparticle processes and environmental resonances can occur. These processes start to become more pronounced when  $E_C$  is of the same order of  $E_J$ . Fig. 1.5 (b) shows an example of a superconducting SET transistor for  $E_C/E_J \sim 10$ , exhibiting a rich structure of resonances at finite bias. The supercurrent is still negligible.

## 1.5 The electromagnetic environment

The necessity of extremely good filtering in mesoscopic experiments has started to draw more and more attention. The electron transport in SET devices at low temperatures is strongly affected by electromagnetic fluctuations (noise) from the environment. This occurs via dynamic excitations of single particle states via uncontrolled photon exchange or photon-assisted tunneling (PAT).[52] This extreme sensitivity is due to the non-linear or quantum nature of the processes inducing errors. Recently, progress in the theory[51] and practical implications[53] has been made. Requirements for the filter characteristics of Coulomb blockade devices using a quantum spectral density formalism and the implementation of these requirements in a practical filter design is now understood in detail.

The first class of noise errors arises from unwanted activation over the Coulomb barrier  $\Delta E$ . The activation energy either comes from the thermal reservoir of

conduction electrons  $k_B T_o$  or from electromagnetic noise coming from the leads which are represented by an impedance  $Z_e(\omega)$ . This impedance can be described by some arbitrary quantum spectral density of voltage fluctuations  $S_V(\omega)$ . However, for convenience, usually the spectral density of the blackbody radiation of a resistor is taken. Photons radiated from this electromagnetic environment can be absorbed by tunneling electrons and will contribute to the escape from the Coulomb blockade state and will induce 'errors' in the device operation. On the other hand this extreme sensitivity can be used to detect single photons. Hergenrother *et al.*[44] proposed a photon-activated switch using a SET transistor with a superconducting island. The estimated sensitivity of this devices is approximately  $3 \times 10^{-22} \text{ W}/\sqrt{\text{Hz}}$ , about two orders of magnitude more sensitive than best existing bolometers operating at the same frequency range.[54] The uncontrolled photon-assisted tunneling processes not only depend on the device characteristics but also on the rest of the whole circuit. One must therefore reduce the electromagnetic noise to a level such that its contribution to the escape rate is of the same order of the rate one would observe if the entire circuit was at equilibrium at temperature  $T_o$ . Very high attenuations are required to obtain such effective thermalization of the junctions at low temperatures. For instance in order to thermalize a SET transistor at 50 mK which is anchored to a resistor of  $1 \text{ M}\Omega$  at 300 K the attenuation should be approximately 150 dB! In the recent years a number of very effective cryogenic microwave filters have been developed. The filters are either based on copper powder, lossy coaxial cable or micro fabricated  $RC$ -striplines, developed by different groups. There is however, due to the need for full experimental control of the electromagnetic environment in which the circuit is embedded, a general trend towards on-chip filtering very close to the actual circuit.[55]

## 1.6 A Josephson junction microwave generator

SET devices and quantum dots are examples of artificially fabricated quantum structures. They are sometimes referred to as artificial atoms because like atoms they exhibit discrete energy spectra. These artificial atoms have typical dimensions of tens to hundreds nanometers in size and are thus much larger than real atoms. One consequence of this is that the energy level spacing is much smaller than in real atoms. Typical energy spacings are on the order of  $0.1 - 1 \text{ meV}$ . The frequencies to probe these levels are tens to hundreds GHz. This is an inconvenient frequency range since there are few tunable microwave sources of radiation available in this range which can be coupled to the sample at low temperatures while isolating the sample from room temperature blackbody radiation. In many experimental studies an external microwave source is coupled via a coax to the sample. However, even when using carefully engineered microwave equipment, the coupling from the source to the system is strongly frequency dependent.

Moreover, an open microwave connection to the sample space in the cryostat is totally incompatible with the filtering requirements due to the extreme intrinsic sensitivity of mesoscopic systems to microwave noise. Therefore another approach can be chosen by using a superconducting Josephson junction (JJ) as local high frequency generator[56] close to the system under study.

Biasing a shunted Josephson junction above its critical current, the voltage across the junction starts to oscillate with a frequency described by the ac Josephson relation[42],  $f = 2eV/h$ , where  $V$  is the dc voltage across the junction. For (overdamped) junctions with a McCumber parameter[57] smaller than unity, the ac voltage signal generated by the JJ can be calculated analytically. Biased at a current above the critical current the junction oscillates, generating a time dependent ac voltage with an amplitude of approximately  $I_c R_s$ , where  $R_s$  is the shunt resistor. For low bias currents, the ac signal will contain a number of harmonics. At higher bias currents, the signal starts to become more and more sinusoidal. The frequency of the generated signal will be within the GHz range, depending on the magnitude of the superconducting gap of the material. Providing good coupling to the load and taking into account the higher harmonics at low bias voltages the JJ can be used as a local microwave generator. Fig. 1.6 shows (a) the physical multilayer layout, (b) the circuit schematic and (c) a photo micrograph of a SQUID generator coupled on-chip to a SET transistor. Prior to the development of JJ generator circuits, a new fabrication process had to be developed to fabricate high quality, controllable, aluminium shunted junctions. In chapter 4 the development and the experimental operation of the JJ generator is described.

## 1.7 Microwave spectroscopy on Josephson junction systems

Using the developed JJ generator described in the previous section, two high frequency experiments have been performed. The first experiment is described in chapter 4 and consists of a generator coupled to a single underdamped tunnel junction. The experiment was performed in what is known as the classical regime. In this regime, the tunnel rate in the tunnel junction is much greater than the frequency of the applied radiation,  $\Gamma \gg f$ . Here, the tunnel rate is the current divided by the charge of a Cooper pair,  $\Gamma = I/2e$ . Therefore in this regime the quantization of radiation in single photons is not relevant, hence the generator can be modelled as a rf current source. The current biased underdamped Josephson junction can be represented as a particle confined in a washboard potential[57]. Irradiating the underdamped Josephson junction with microwave radiation, the particle in the well can be resonantly activated out of the well.[58] The experiment provides more detailed insight in the generator signal and the coupling of the generator to the detector.

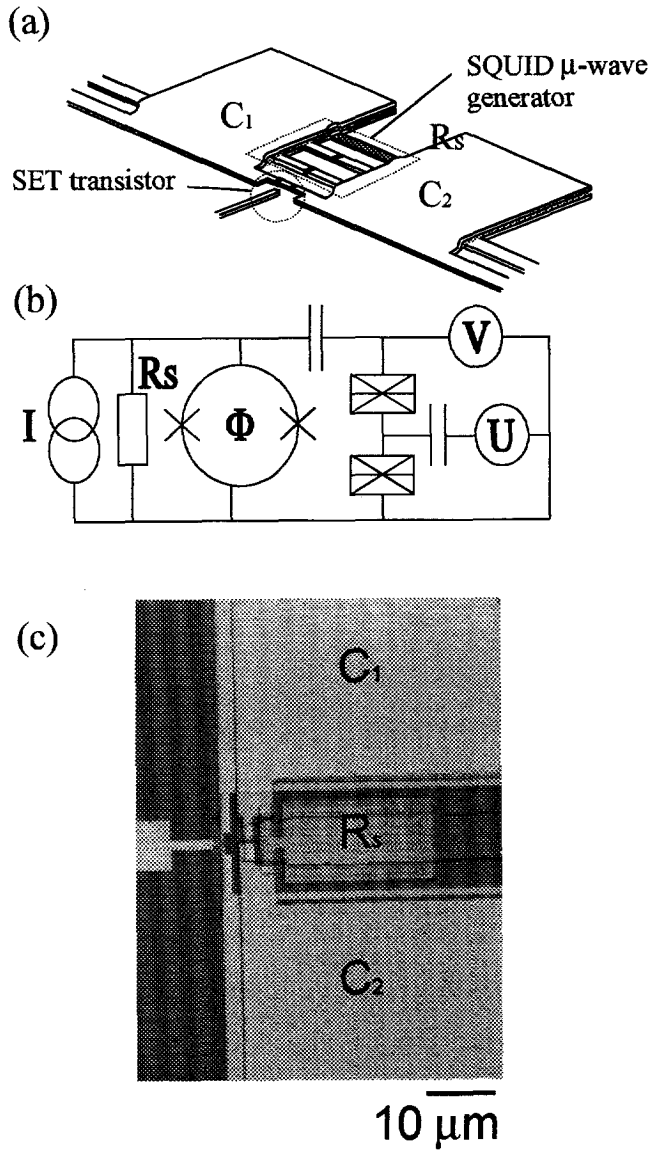


Figure 1.6: (a) multilayer fabricated SQUID generator coupled to a superconducting SET transistor. (b) Schematic of the coupled circuit. (c) Micro photograph of the fabricated circuit, showing the big overlap capacitors, the shunted SQUID generator and the SET transistor.

In a second experiment, described in chapter 5, a Josephson junction generator was coupled to a superconducting SET transistor. First of all, an analysis of the subgap tunnel processes in the S-SET without radiation is made. At subgap bias voltages the quasiparticle rate through the S-SET is much lower than the applied radiation i.e.  $\Gamma \ll f$ . Hence, when irradiated with microwave frequencies there are many rf cycles between each tunnel event. In this regime, which is known as the quantum regime, the quantization of the radiation in single photons is relevant. In the quantum regime, the electrons that tunnel can gain energy from or give energy to the electromagnetic field in units of  $hf$ . These tunnel processes are known as photon-assisted tunneling (PAT) and result in an enhanced tunnel current in a situation when the initial and final states of a tunneling electron differ by multiples of  $hf$ . We will show that even in the simplest limit of  $E_C \gg E_J$ , the photon response yields complex subgap structures. This is the first time microwave spectroscopy on a SET transistor was successfully shown using an on-chip microwave generator.

## 1.8 General framework and scope of this thesis

In chapter 2 the conventional SET technology first is improved by developing a multi-layer SET technology in which a better control over the device parameters is obtained. Using multilayer technology, in chapter 3 we present the coupling of a cryogenic high-electron mobility transistor (HEMT) on-chip to a metallic SET transistor [16]. This development is depicted in Fig.1.7. Due to the intrinsically large output impedance of the SET transistor, coupled to the capacitive load at the output, the bandwidth of SET devices is basically reduced to dc operation. The HEMT is used in a source follower configuration transforming the output of the SET transistor to a low output impedance. The experiment is the first demonstration of the direct integration and operation of a metallic SET device and a semiconductor HEMT. The results are used to propose SET experiments where a fast electrometer with sub-electron sensitivity is an essential element.

A similar line of reasoning can be given for driving the input of a SET device. The first demonstration of a single-electron device driven by an externally generated ac input signal was performed by Geerligs *et al.* [28]. The dc characteristics of an ac driven four junction array, normally referred to as the turnstile, exhibits current plateaus at exactly  $I = ef$ . In this regime the SET device responds approximately adiabatically to the time dependent gate drive. At frequencies higher than a few tens of MHz, the coupling becomes frequency dependent destroying the proper device operation. Using a similar philosophy as in the SET - HEMT circuit, a Josephson junction (JJ) generator is used as an on-chip tunable local microwave generator driving a superconducting SET transistor from a few to approximately 190 GHz. This work is described in chapters 4 and 5 of this thesis. In chapter 4, the new developed technology for the fabrication of shunted junctions



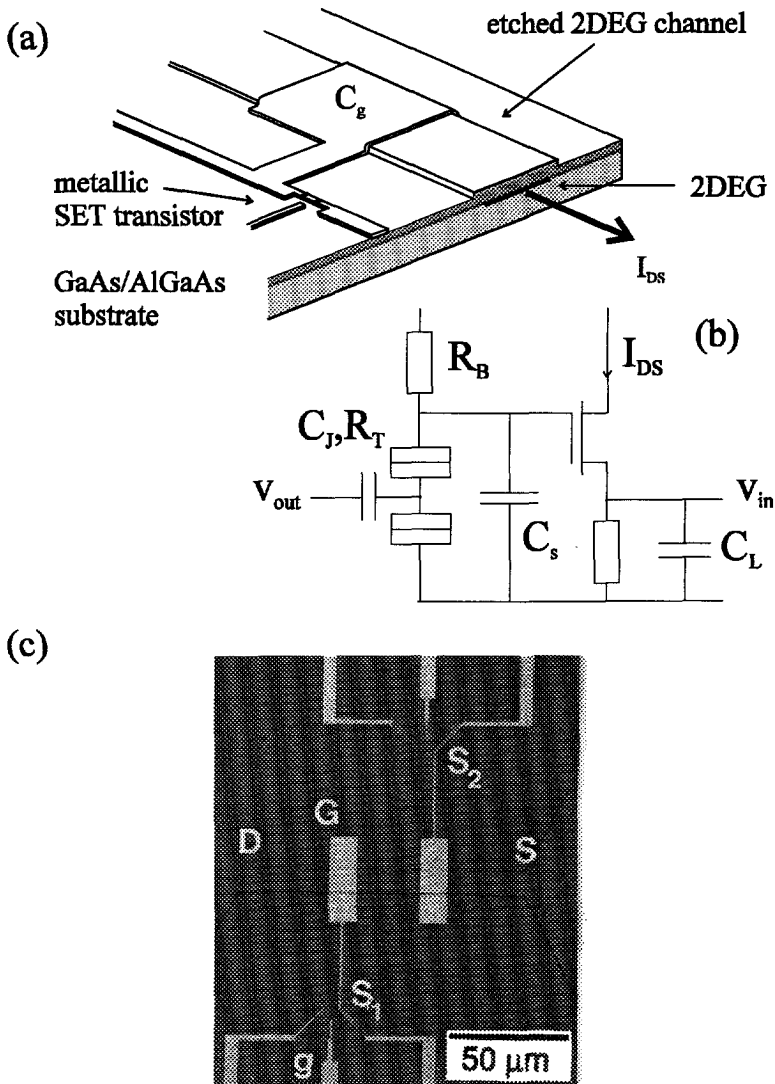


Figure 1.7: (a) Schematic layout of the integrated SET - HEMT circuit. The metallic SET is fabricated on a GaAs/AlGaAs heterostructure. The output of the SET is directly coupled to the input of the HEMT. In (b) the schematic of the circuit is sketched. (c) Shows a photo micrograph of the total circuit. Two SET transistors S<sub>1</sub> and S<sub>2</sub> are coupled to a 2DEG channel, which connects the source (S) to the drain (D) of the HEMT.

is described. Furthermore, the designed JJ generator first was characterized by measuring its response using an unshunted JJ as a threshold detector. Driving a SET transistor instead of a large JJ with microwave frequencies, it will respond non-adiabatically. This results in photon-assisted tunneling processes (PAT), in which tunneling electrons can absorb an integer number of photons resulting in an enhancement of the tunnel current. Using the JJ generator, these PAT processes in a superconducting SET transistor are studied in chapter 5. Again the coupled JJ generator - SET transistor circuits forms a hybrid circuit combining to different type of technologies. Furthermore, it is the first successfully proven experiment using a Josephson junction as a microwave generator for the high frequency study of SET circuits. It opens the possibility of numerous different experiments involving microwave spectroscopy.

Ultimately all the developments described in this thesis should lead to fully integrated SET experiments and devices. Filtering, oscillators, and output buffering all can be integrated on one chip, leading to a mature SET technology, in which more complicated SET circuits can be implemented.

## References

- [1] R. A. Millikan, *Phys. Rev.* **32**, 349 (1911).
- [2] See for reviews: D.V. Averin and K.K. Likharev in *Single-electronics: A Correlated Transfer of Single Electrons and Cooper Pairs in Systems of Small Tunnel Junctions in Mesoscopic Phenomena in Solids*, edited by B.L. Altshuler, P.A. Lee and R.A. Webb; *Single Charge Tunneling, Coulomb Blockade Phenomena in Nanostructures*, edited by M.H. Devoret and H. Grabert, NATO ASI Series B: Physics **294**, (Plenum, New York, 1991).
- [3] H. Birk, M. J. M. de Jong, and C. Schonenberger, *Phys. Rev. Lett.* **75**, 1610 (1995).
- [4] C. J. Gorter, *Physica* **17**, 777, (1951).
- [5] I. Giaever and H. R. Zeller, *Phys. Rev. Lett.* **20**, 1504 (1968).
- [6] J. Lambe and R. C. Jaklevic, *Phys. Rev. Lett.* **22**, 1371 (1969).
- [7] T. A. Fulton and G. J. Dolan, *Phys. Rev. Lett.* **59**, 109 (1987).
- [8] T. A. Fulton, P. J. Gammel, and L. N. Dunkleberger, *Phys. Rev. Lett.* **67**, 3148 (1991).
- [9] P. Lafarge, H. Pothier, E. R. Williams, D. Esteve, C. Urbina and M. H. Devoret, *Z. Phys. B* **85**, 327 (1991).
- [10] C.T. Foxon, in: *Interfaces, Quantum Wells and Superlattices*, edited by C. Richard Leavens and Roger Taylor (Plenum Publishing Corporation, 1988).

- [11] For a review on quantum dots, see: L. P. Kouwenhoven and P. L. McEuen in *Nanoscience and technology* edited by G. Timp (AIP press, New York, to be published).
- [12] M. Kastner, *Physics today* **46**, 24 (1993).
- [13] G. J. Dolan, *Appl. Phys. Lett.* **31**, 337 (1977).
- [14] D. C. Ralph, C. T. Black, and M. Tinkham, *Phys. Rev. Lett.* **74**, 3241 (1995).
- [15] See for example: L. J. Geerligs, V. F. Anderegg, J. Romijn, and J. E. Mooij, *Phys. Rev. Lett.* **65**, 377 (1990); M. T. Tuominen, J. M. Hergenrother, T. S. Tighe, and M. Tinkham, *Phys. Rev. Lett.* **69**, 1997 (1992); P. Joyez, P. Lafarge, A. Filipe, D. Esteve, *Phys. Rev. Lett.* **72**, 2458 (1994); T. M. Eiles and J. M. Martinis, *Phys. Rev. B* **42**, 627 (1994); M. Matters, W. J. Elion, and J. E. Mooij, *Phys. Rev. Lett.* **75**, 721 (1995).
- [16] E. H. Visscher, J. Lindeman, S. M. Verbrugh, P. Hadley, and J. E. Mooij, *Appl. Phys. Lett.* **68**, 2016 (1996).
- [17] submitted to *Appl. Phys. Lett.* 1996.
- [18] R. Wilkins, E. Ben-Jacob, and R. D. Jaklevic, *Phys. Rev. Lett.* **63**, 801 (1989).
- [19] Y. Takahashi *et al.*, *Elec. Lett.* **31**, 136 (1995).
- [20] D.V. Averin and Yu.V. Nazarov, *Phys. Rev. Lett.* **65**, 2446 (1990).
- [21] R. C. Ashoori, *Nature* **379**, 413 (1996).
- [22] S. Tarucha, D. G. Austing, T. Honda, R. J. van der Hage, and L. P. Kouwenhoven, submitted to *Phys. Rev. Lett.* (1996).
- [23] W. J. Elion, M. Matters, U. Geigenmuller and J. E. Mooij, *Nature* **371**, 594 (1994).
- [24] see ESPRIT Settron basic research project 9005.
- [25] K. K. Likharev, *IEEE Trans. Mag.* **23**, 1142 (1987).
- [26] See for example L. S. Kuzmin, P. Delsing, T. Cleason, and K. K. Likharev, *Phys. Rev. Lett.* **62**, 2539 (1989); L. J. Geerligs, V. F. Anderegg, and J. E. Mooij, *Physica B* **165**, 937 (1990).
- [27] A. N. Cleland, D. Esteve, C. Urbina, and M. H. Devoret, *Appl. Phys. Lett.* **61**, 2820 (1992).
- [28] L.J. Geerligs, V.F. Anderegg, P. Holweg, J.E. Mooij, H. Pothier, D. Esteve, C. Urbina, and M.H. Devoret, *Phys. Rev. Lett.* **64**, 2691 (1990).
- [29] H. Pothier, P. Lafarge, P. F. Orfila, C. Urbina, D. Esteve, and M. H. Devoret, *Physica B* **169**, 573 (1991); H. Pothier, P. Lafarge, C. Urbina, D. Esteve, and M. H. Devoret, *Europhys. Lett.* **17**, 249 (1992).

- [30] S. M. Verbrugh, Ph.D. Thesis, Delft (1995).
- [31] H. Dalsgaard Jensen and J. M. Martinis, *Phys. Rev. B* **46**, 13407 (1992); presently an electron pump with metrological accuracy has been demonstrated by Martinis, to be published.
- [32] K. K. Likharev, *IBM J. Res. Develop.* **31**, 144 (1988).
- [33] G. Zimmerli, R. L. Kautz, and John M. Martinis, *Appl. Phys. Lett.* **61**, 2616 (1992).
- [34] R. C. Ashoori, unpublished.
- [35] Bell laboratories, unpublished.
- [36] see P. Lafarge Ph.D. thesis, University of Paris, 1993.
- [37] P. Lafarge *et al.*, submitted to *Phys. Rev. B*.
- [38] M. H. Devort, D. Esteve, H. Grabert, G. -L. Ingold, H. Pothier, and C. Urbina, *Phys. Rev. Lett.* **64**, 1824 (1990);
- [39] G. -L. Ingold and Yu. V. Nazarov, in *Single Charge Tunneling*, edited by H. Grabert and M. H. Devoret (Plenum, New York, 1992), Chap. 2.
- [40] For a review, see: H. van Houten, C. W. J. Beenakker, A. A. M. Staring, in *Single Charge Tunneling*, edited by H. Grabert and M. H. Devoret (Plenum, New York, 1992), Chap. 5.
- [41] For a good review on superconductivity, see: M. Tinkham, *Introduction into superconductivity*, (McGraw-Hill, New York, 1996).
- [42] B. D. Josephson, *Phys. Lett.* **1**, 251 (1962).
- [43] V. Ambegaokar and A. Baratoff, *Phys. Rev. Lett.* **10**, 486 (1963).
- [44] J. M. Hergenrother, J. G. Lu, M. T. Tuominen, D. C. Ralph, and M. Tinkham, *Phys. Rev. B* **51**, 9407 (1995).
- [45] A. B. Zorin, accepted for *Phys. Rev. Lett.* (1996).
- [46] A. N. Korotkov, submitted to *Appl. Phys. Lett.* (1996).
- [47] For a good review article see: C. H. Bennet, *Physics Today*, October 1995.
- [48] P. Shor, in *Proceedings of the 35th Annual Symposium on Foundations of Computer Science* (IEEE Pres, Piscataway, NJ, 1994).
- [49] A. Maassen van den Brink, A. A. Odintsov, P. A. Bobbert, and G. Schön, *Z. Phys. B* **85**, 327 (1991).
- [50] P. Joyez, Ph.D. thesis, University of Paris (1995).
- [51] J. Martinis and M. Nahum, *Phys. Rev. B* **48**, 18316 (1993).
- [52] P. K. Tien and J. R. Gordon, *Phys. Rev.* **129**, 647 (1963).

- [53] D. Vion, P. F. Orfila, P. Joyez, D. Esteve, and M. H. Devoret, submitted to *J. Appl. Phys.*
- [54] M. Nahum, and J. M. Martinis, *Appl. Phys. Lett.* **63**, 3075 (1993).
- [55] D. Vion, private communications.
- [56] See experimental references on Josephson junction generators: S. P. Benz and C. H. Burroughs, *Appl. Phys. Lett.* **58**, 2162 (1991); B. Bi, S. Han, and J. Lukens, *Appl. Phys. Lett.* **64**, 1424 (1994); P. A. A. Booij and S. P. Benz, *Appl. Phys. Lett.* **68**, 3799 (1996).
- [57] W. C. Stewart, *Appl. Phys. Lett.* **12**, 277 (1968); D. E. McCumber, *J. Appl. Phys.* **39**, 3133 (1968).
- [58] M. H. Devoret, J. M. Martinis, D. Esteve, and J. Clarke, *Phys. Rev. Lett.* **53**, 1260 (1984).



## Chapter 2

# Multilayer single-electron tunneling devices

### 2.1 Introduction

Control of the fabrication of SET devices is of great importance for practical design. When optimizing SET devices, one should be able to fabricate their parameters within certain specifications. Furthermore when increasing the complexity of the devices, electrostatic cross-capacitances will hinder the practical operation. The robustness of SET devices against fabrication handling, such as metal evaporation or resist baking will eventually determine what is possible. Surprisingly little research has been carried out on these technological aspects of SET devices. In this chapter we will focus on a specific set of these technological issues, which include multilayer fabrication, robustness, cross-capacitances and filtering. A multilayer fabrication technique [1] for SET devices was developed, which is based on metal insulator multilayer structures. As we will show, the technique is applied to SET devices of various complexity. We have successfully fabricated SET transistors with voltage gain[2], electron box circuits[3] and six junction turnstiles[4], each in which capacitor design is an important issue. The observation that the SET devices can withstand further fabrication cycles has lead to the integration of SET circuits in different layers in the same circuit. Furthermore, a proposal based on a very simple extension of the existing shadow evaporation technique is made for a controlled down sizing of the junctions *without* degrading the yield of the circuit fabrication.

### 2.2 Multilayer fabrication

Until now, SET devices have been fabricated in one single lithographic step, using a shadow evaporation technique [6], in which tunnel junctions, coplanar or overlap capacitors [2], and resistors [5] have to be formed. In this chapter a multilayer fabrication process is presented, in which different layers dimensions can

be aligned on top of each other. We have applied this process to the fabrication of SET devices with overlap capacitors, in which the metallic base electrodes, the dielectric, and metallic islands with tunnel junctions can be processed independently. The fabricated SET transistors exhibit voltage gain and low charge noise [10] characteristics, despite the more complicated device structure. The use of the compact geometry of the overlap capacitors results in a considerable reduction of cross-capacitances from gate electrodes to neighboring metallic islands, which can considerably influence the device operation.

SET devices with either Au-SiO-Al or Al-AlO<sub>x</sub>-SiO-Al thin film overlap capacitors have been fabricated, here referred to as the SiO SET and the AlO<sub>x</sub>-SiO SET. The circuits were fabricated on Si substrates which have a 0.5 μm thermally oxidized SiO<sub>2</sub> top layer to reduce stray capacitances to ground. Each layer requires four basic fabrication steps of resist baking, e-beam writing, material deposition and lift-off. The layers were aligned on top of each other with a set of Au markers within an accuracy of 20-30 nm, using a Philips EBPG HR-5 e-beam writer. The first layer of the SiO SET was 40 nm thick Au pattern which defines the base electrodes of the gates and the coupling capacitors. On top of the Au pattern we deposited a 100 nm thick amorphous SiO layer, forming the dielectric of the overlap capacitor. The dielectric was deposited using e-beam evaporation or a K-cell at a rate of 10 Å/s, a substrate temperature of 10 °C and a base pressure of 10<sup>-7</sup> Torr. SiO has a relatively low deposition temperature, which can be used in combination with lift-off. Recently Bouchait *et al.*[7] reported the use of a thin polyamide layer as a dielectric. The third layer forms the Al island and the two Al-AlO<sub>x</sub>-Al tunnel junctions of the SET, obtained by two angle shadow evaporation, as shown in Fig. 2.1. The evaporation mask is written in a double layer PMMA/MAA (100 g/l in acetic acid)-PMMA (1% 950 K in ClB) double-layer resist with a high-resolution Electron Beam Pattern Generator (EBPG-5) at 100 kV. After exposure, the resist is developed in a 1:3 solution of MIBK and 2-propanol for 1 min. and rinsed in pure 2-propanol. The development transforms the written pattern in the resist by dissolving the exposed areas. Due to the higher energy sensitivity of the bottom layer, it will develop more rapidly creating an undercut mask profile. After the creation of the mask, a 30 nm aluminum layer was evaporated under an angle  $\theta$ , varying from 10 to 18 degrees with respect to the normal of the substrate surface, using e-beam evaporation in high vacuum. After the first evaporation, the aluminum surface is exposed to oxygen at a controlled pressure of 0.01 to 0.3 mbar. During oxidation a aluminum-oxide layer is formed, with a thickness depending on the O<sub>2</sub> pressure. In a second step, a 60 nm metal layer is evaporated under an angle  $-\theta$  and an Al-AlO<sub>x</sub>-Al tunnel junction is formed at the overlap of the two metal layers. The oxidation pressure  $p$  and oxidation time  $t$  sets the resistance of the junction via  $R_n \propto (pt)^\alpha / A$ , [8] where  $A$  is the junction area and  $\alpha$  is some experimental constant. The capacitance can be estimated using the parallel plate formula,  $C_J \sim \epsilon_0 \epsilon_r A / d$ , where  $d$  is the thickness of the barrier. For very low oxidation



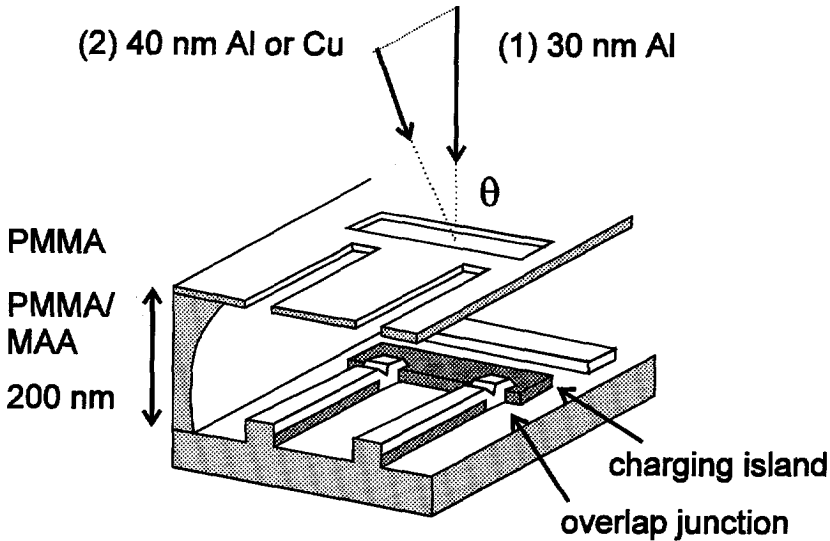


Figure 2.1: Schematic of the two-angle shadow evaporation technique. Cross-sectional view showing where the metal is deposited in the first evaporation, illustrated by the gray metallic pattern. Note that because of the suspended resist bridge, in the first layer the leads are not connected to the island. After oxidation, the second evaporation step is performed at an angle  $\theta$ . Because of the angle of this evaporation, metal deposited through the lead channel overlaps the (previously oxidized) island and forms a tunnel junction. The island is now connected via two tunnel junctions to the two leads.

pressures deviations from this value occur. Especially for barrier thicknesses of the order of a monolayer, modeling the tunnel barrier with a single, continuously variable thickness is an oversimplification.[9]

The  $\text{AlO}_x\text{-SiO}$  SET was fabricated using the same process except that an *aluminum* base electrode was used which was thermally oxidized for 3 hours at a temperature of 300 °C. Afterwards a 50 nm SiO layer was deposited resulting in a larger gate capacitance without changing the SET geometry. Fig. 2.2 (a) and (b) show scanning electron micrographs of two capacitively coupled SETs and a six junction series array with overlap capacitors.

We deduced the device parameters by fitting the experimental data to the theoretical  $V - V_g$  curves derived from the orthodox theory [12] without taking into account co-tunneling [14]. All measurements were performed in a dilution refrigerator with a base temperature of 10 mK. Special care was taken to reduce

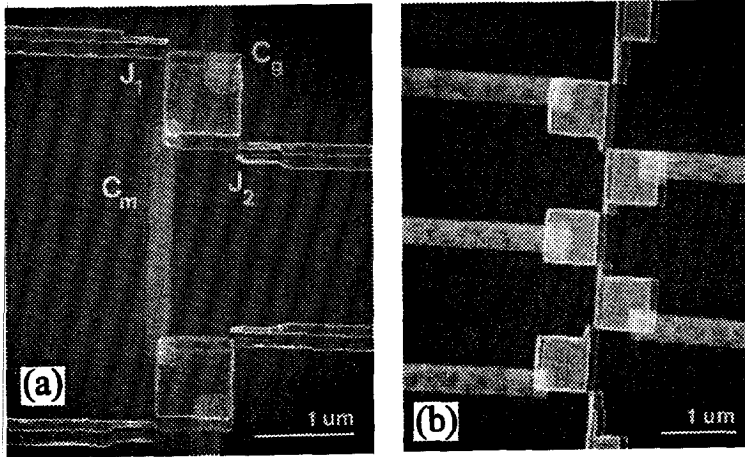


Figure 2.2: (a) Scanning electron micrograph of two capacitively coupled SiO SET transistors. The tunnel junctions  $J_1$  and  $J_2$  are defined by the overlap of the horizontal leads and the square metallic island. Both island have a overlap gate,  $C_g$ , and are coupled to each other by a vertical coupling capacitor  $C_m$ . In (b) a six junction series array is shown. Each square metallic island is coupled to a horizontal overlap gate via a SiO dielectric. The schematic circuit of a current-biased SET is shown in (c). The junctions are indicated by boxes.

the noise reaching the SET device. In particular all leads down to the sample have special high frequency copper powder filters [15]. A magnetic field of 2 T was applied to keep the aluminum in the non-superconducting state. In Fig. 2.3 the results of the  $\text{AlO}_x\text{-SiO}$  SET are shown. By fitting the data we obtain  $R_1 = 210 \text{ k}\Omega$ ,  $R_2 = 200 \text{ k}\Omega$ ,  $C_1 = 0.21 \text{ fF}$ ,  $C_2 = 0.20 \text{ fF}$  and a device temperature of 60 mK. The  $200 \times 200 \text{ nm}^2$   $\text{AlO}_x\text{-SiO}$  gate capacitor has a capacitance of 0.36 fF. The experimental voltage gain is  $K_V = 1.5$  as indicated by the dashed line in Fig. 2.3 and is slightly less than the theoretical maximum obtainable voltage gain  $K_V = 1.8$ , using the calculated device parameters. This can be attributed to thermal heating of the device due to power dissipation and insufficient filtering of the leads. The SiO SET has similar device parameters except for a gate capacitance of 0.12 fF. Using the parallel-plate formula we estimate a geometrical capacitance of 0.03 fF for the 100 nm thick SiO overlap gate, using  $\epsilon_r = 4$  for the SiO dielectric. The discrepancy between the geometrical estimation and the measured value is most likely due to the edges and SiO step coverage of the gate which consequently results in an increased effective capacitance. Later results by Matters *et al.*[22] show that an  $\text{AlO}_x\text{-SiO}$  coupling capacitors using a SiO layer

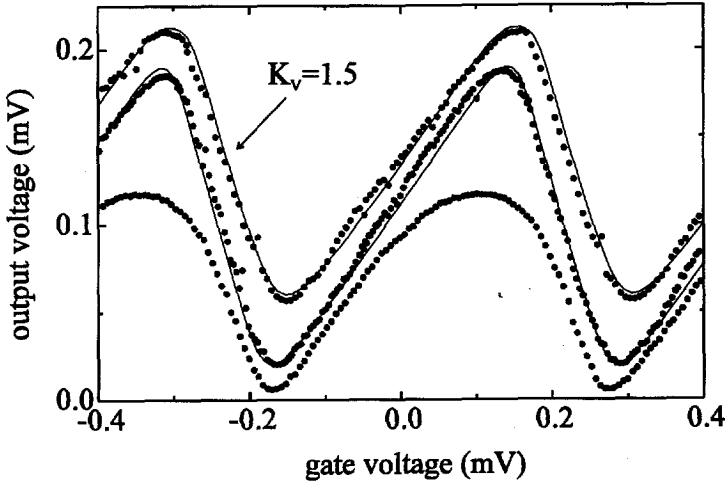


Figure 2.3: Output voltage as a function of the gate voltage at fixed bias currents of a Al-AlO<sub>x</sub>-SiO-Al SET transistor. The bias currents are 1 pA, 26 pA, and 50 pA. The solid lines indicate the best fits to the experimental data at moderately high bias currents. A maximum attainable voltage gain of 1.5 is indicated by the dashed line.

as thin as 10 nm could be used to obtain very a large coupling capacitance up to 4 fF.

We have also tested whether a SET device could withstand a full fourth fabrication cycle in which we locally deposited a 100 nm thick SiO layer on top of the Au-SiO-Al SET transistor. The device did not show any significant parameter change or degradation after processing. This opens the possibility that SET devices can be integrated in different layers in the same circuit.

### 2.3 Applications of multilayer SET devices

The first practical use of the extreme charge sensitivity of the SET transistor have been used to demonstrate the quantization of the charge on a metallic electrode connected to an electron reservoir by a tunnel junction. This experiment, usually referred to as the electron box [17, 3] is the solid state analog of Millikan's famous experiment performed in 1911. Such measurements would be impossible with commercial electrometers which have a charge resolution of a few  $e/\sqrt{\text{Hz}}$ . Due to this extreme charge sensitivity the leakage resistance of the capacitors should be extremely low. Any electron leakage through the capacitor will destroys any

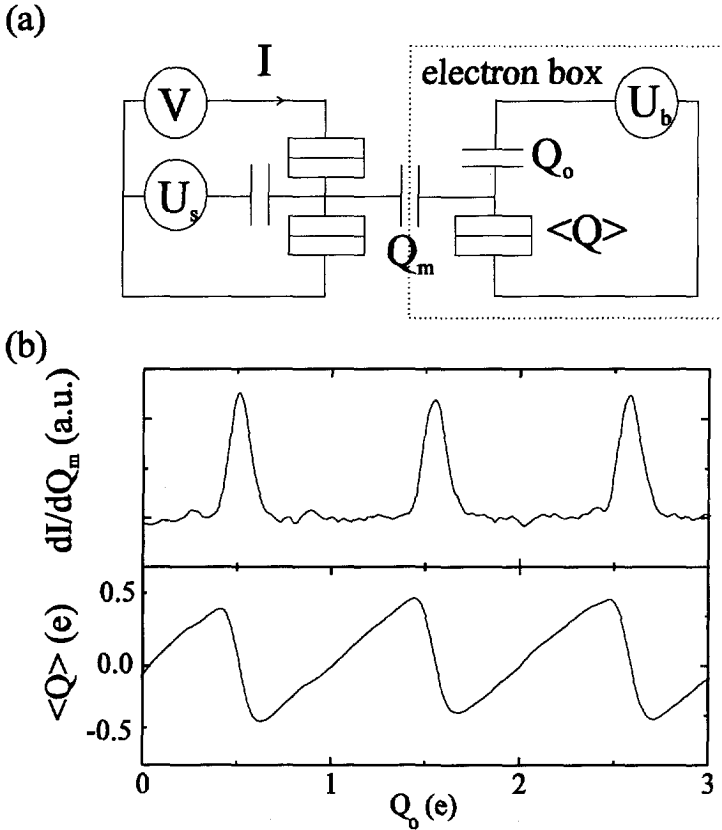


Figure 2.4: Schematic of the electron box experiment. A metallic island is coupled via a single tunnel junction to a charge reservoir. The charge on the box-junction  $\langle Q \rangle$  can be measured as a function of the gate charge  $Q_0$  by a SET electrometer, which is coupled to the island via a capacitance  $C_m$ . In (b) the measured SET transistor signal due to the entrance of electrons onto the box-island is shown. From this signal the charge oscillations on the box junction are obtained.

practical use of the SET transistor. Its therefore of importance to determine the leakage resistance of the capacitors carefully. In this section we will determine the leakage of electrons through the overlap capacitors by using a electron box configuration, fabricated with the multilayer fabrication technique. At the same time the electron box is a very elegant experiment demonstrating the practical use of the SET transistor in a typical mesoscopic experiment.

The electron box consists of a small tunnel junction of capacitance  $C$  and a capacitor  $C_i$  placed in series with a voltage source  $U$ , as shown in Fig. 2.4 (a). The tunnel junction has a tunnel resistance,  $R_T$ , much larger than the resistance quantum  $R_K = h/e^2 \cong 25.8 \text{ k}\Omega$ . Under this condition the number of electron on the island  $n$  is a good quantum number. The average charge on the junction capacitor as a function of the gate is given by  $\langle Q \rangle = [-e \langle n \rangle + Q_g] C/C_i$  and is a directly measurable quantity. The SET transistor is coupled to the electron box island via a coupling capacitor  $C_c$ . The charge on the coupling capacitor is simply  $(C_m/C) \langle Q \rangle$ . As a consequence, a change in the electrometer current  $I$  will be induced due to a change of the thermally averaged junction charge  $\langle Q \rangle$ . The electrometer was biased at its optimum gain point, which is approximately at the threshold voltage 0.2 mV. Small excursions of the charge on  $C_c$  induced an approximately linear response in the electrometer current. Fig. 2.4 (b) shows the measured average charge  $\langle Q \rangle / e$  oscillations on the junction capacitance as a function of the gate voltage of the box. These oscillations are analogous to the SET oscillations of the average charge  $Q$  versus  $It$  for a small tunnel junction biased with a current  $I$ . Any leakage of electrons through the dielectric of the overlap capacitor would destroy the oscillation period. Therefore we can conclude there is no measurable leakage current through the overlap capacitor.

Other SET devices take advantage of the discreteness of charge to perform digital functions. The electron turnstile [4] and the electron pump [18], are used to establish precise currents where single electrons are transferred one by one through the device. By doing this repeatedly with frequency  $f$ , a constant current can be generated with a value,  $I = ef$ . This led to extensive research on the use of SET devices as a current standard. The use of a turnstile for metrological applications is a very illustrative example in which one needs to be able to control and engineer the device parameters very accurately. External and intrinsic error sources can contribute to a deviations from this precise current value. Using co-tunneling as the dominant intrinsic error source a turnstile for metrological applications should have at least six junctions. Fig. 2.5 (a) shows a schematic circuit of the turnstile. It comprises one-dimensional array of six small tunnel junctions forming five charging islands. Each island needs an individual gate to tune away offset charges. The middle gate which is driven by an external ac frequency should have a value of approximately  $C_j/6$  and at the same time as little cross-capacitance to neighboring islands possible. Driving the middle gate with an ac frequency, plateaus will appear in the I-V curve at specific values of the current. Fig. 2.5 (b) showed the best obtained plateaus of the 6 junction turnstile with overlap gates at 10, 20, 30 and 40 MHz.

An important reason for using overlap capacitors is the possibility to reduce cross-capacitances. The cross-capacitance was derived from  $I - V_g$  curves of a four junction series array with overlap gates, similar to the one shown in Fig. 2.2 (b). The middle gate polarizes the middle island but will influence also the neighboring island via an unwanted cross-capacitance  $C_c$ . The outer gates and are

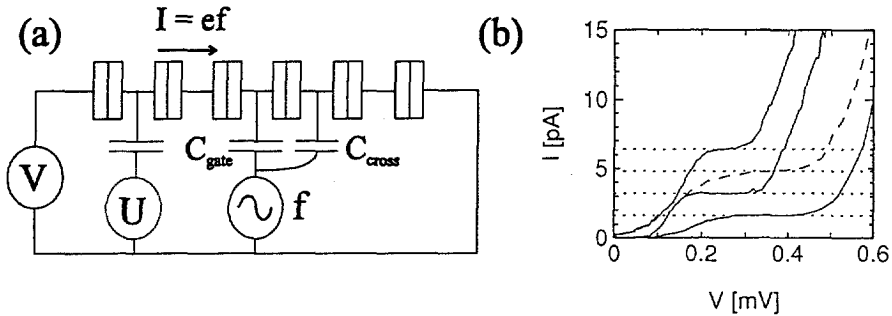


Figure 2.5: (a) Schematic of a 6 junction turnstile. The dc offset charges which are present on the islands can be tuned away by dc gates. A rf gate is coupled to the middle island of the array. The rf gate controls the clocking of the electrons through the array. The cross-talk problem is illustrated by a cross-capacitance  $C_{cross}$  to the neighbouring islands. (b) The best measured plateaus exhibiting controlled charge transfer of  $I = ef$  through the device. The curves correspond to 10, 20, 30 and 40 MHz.

tuned such that the Coulomb blockade gap of the device is maximum. Then the middle gate is swept recording the  $I - V_g$  trace. We have compared traces of an earlier planar design with the overlap design, shown in Fig 2.6 (a). From Fourier analysis of the  $I - V_g$  trace of the overlap array a gate capacitance of 0.10 fF and a cross-capacitance of 8 aF is obtained (Fig 2.6 (b)). This results in a cross-talk of the middle gate of only 8%. Similar analysis on the array with planar gates is not possible because the large cross-capacitances blur the spectrum. The reduced cross-talk to the neighboring island due to use of overlap capacitors allows the use of Fourier analysis as a very versatile tool for estimating the capacitances in more complex SET circuits. Difficult optimization processes for canceling the cross-talk by tuning the gates individually [19] can thus be avoided this way.

Once determined, the fabrication parameters of the fabrication it can be easily extended to related fields of research, yielding results which were previously inaccessible due to technological problems. For example, in the study of transport of two-dimensional (2D) networks of small tunnel junctions[20] information on the distribution of offset charges can be extracted. It is important in these experiments that one can change the distribution of these offset charges experimentally. Fabricating a gate over the whole array, a charge frustration can be applied to the array similar to a magnetic field frustration in superconducting 2D arrays. An other illustrative example in which the results of the multilayer technique is the electron transport in strongly coupled one-dimensional arrays.[21, 22] If the coupling capacitor  $C_C$  is large enough an electron which enters the first island of the top array can induce a hole in the bottom array due to Coulomb interac-

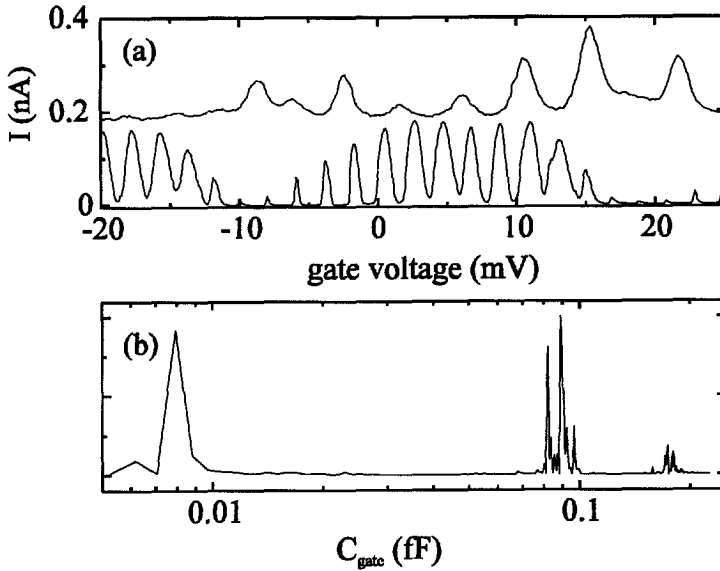


Figure 2.6: (a)  $I - V_g$  traces of an old turnstile design compared with the new overlap design. Fourier analysis (b) shows the overlap design has only 8% cross-talk of the middle gate to neighbouring islands.

tion. The electron-hole pair can be considered as an charge exciton which can move through the array. The description of the exciton transport is only valid for  $C_C \gg C_J$ . One can only realize this applying the multilayer fabrication technique, which enables us to make strong capacitively coupled devices fabricated in different layers.

## 2.4 Noise and offset charges in a SET transistor

Like all electronic devices, SET devices exhibit noise. First of all, shot noise arising from the discrete nature of the random tunneling electrons is intrinsic to the SET transistor and sets the ultimate noise floor of the device. As Korotkov *et al.*[23] have shown, the spectral density of the output current noise at low frequencies is given approximately by the Schottky formula  $2eI$ . Referred to the input charge using the transfer function  $dI/dQ$ , the shot noise yields a charge noise  $Q_{SN} = 2eI / (dI/dQ)^2$ . When the thermal fluctuations are smaller than the quantum fluctuations the energy sensitivity  $E_{SN} = Q_{SN}^2 / 2C_\Sigma$  approaches the

quantum limit  $\hbar$ .

Furthermore, at low frequencies the main source of noise is the  $1/f$  noise. It is believed that the main contribution arises from sources that induce a time dependent charge on the island. These sources can be attributed to moving charge traps close to the island or in the tunnel barrier. The switching act as two-level fluctuators (TLF), which sometimes can be observed very clearly, due to the extreme charge sensitivity of the transistor.[24] One single TLF will have a Lorentzian spectrum. If many TLF's with different switching times are present and the trapping energies are uniformly distributed, the spectrum will yield a  $1/f$  character. Rogers *et al.*[25] have shown that several charge traps in the tunnel barrier of a small junction can produce a  $1/f$  noise spectrum. Localization and modeling of these noise sources in a SET transistor is difficult, as was shown by Zorin *et al.*[26], who used a dual spectrum method to measure the noise. However, qualitatively we support the reasoning by Song *et al.*[27], who argued the system is the most sensitive to charge motion in regions where the electric field is high. In a SET transistor the electric field is mainly concentrated in the tunnel junctions and in region of the dielectric of the gate capacitor. Moreover, the fact that SET transistors fabricated on various substrates (Si, SiO<sub>2</sub>, Al<sub>2</sub>O<sub>3</sub> and SiN<sub>3</sub>) exhibit the same noise figures, strongly suggest the main contribution is due to traps in the tunnel barrier region.

Charge traps with a very long time constants compared to the measuring time, effectively can be considered as a constant offset charge. Furthermore, experiments on tunnel junctions[28] showed that an internal work function difference  $\Delta\phi$  is present even if the material of the electrodes is the same, yielding a frozen in extra charge on each junction capacitance of  $Q^* = C\Delta\phi$ . This work function difference can be explained by the asymmetric growth of the tunnel barrier during thermal oxidation. In a SET transistor it can introduce a constant zero-bias offset charge  $Q^* = (C_1\Delta\phi_1 + C_2\Delta\phi_2)/e$  on the island.[12] A more systematic study of different tunnel barrier systems is needed. For instance, beside the Al-AlO<sub>x</sub>-Al, also Al-AlN<sub>x</sub>-Al[29] and Cr-CrO<sub>x</sub>-Cr[30] tunnel junctions have been reported. Moreover a theoretical model for quantitative analysis, incorporating defects and work function offsets in the tunnel barriers of a Coulomb blockade system[31] is still lacking.

Since the noise can be related to charge traps and defects in the island and the tunnel barrier it directly reflects the quality of the fabricated sample, similar to semiconductor devices. Therefore here we will compare the noise figure with other measured data to see whether the more complex fabrication influences the noise figure in a negative way. For instance, traps in the SiO layers can deteriorate the device characteristics. Measuring the  $1/f$  noise will therefore provide us with important extra information on the fabrication quality. We determined the quality of the multilayer SETs by measuring its low frequency  $1/f$  noise spectrum.[23] The charge noise of the SiO SET was measured, operating the device in a charge-locked loop similar to the flux-locked loop of a dc SQUID



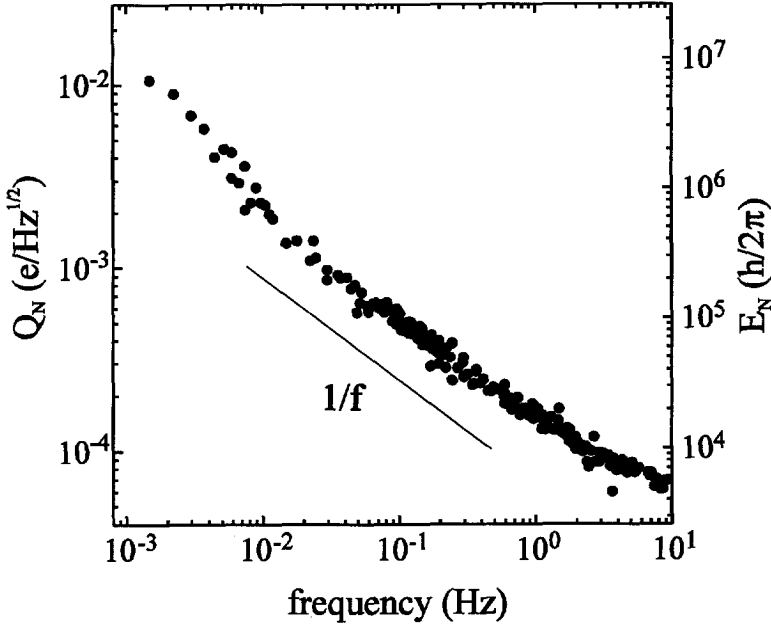


Figure 2.7: Measured charge noise referred to the input of the SET transistor as a function of frequency. The axis on the right hand side gives the equivalent energy sensitivity. The dashed line indicates the  $1/f$  character of the noise.

[16]. Fig. 2.7 shows the measured input charge noise  $Q_N$  and the related energy sensitivity  $E_N = Q_N^2/2C_\Sigma$  as a function of the frequency. The energy sensitivity shows the clear  $1/f$  character of the low frequency noise. The gate was modulated with a square wave at a frequency of 100 Hz and an amplitude of about half of the gate periodicity  $\Delta V_g/2$ . The output of the SET was synchronously detected with a lock-in amplifier such that the output was only sensitive to dc changes in the gate voltage, measuring directly the input charge noise  $Q_N = C_g V_N$ . At 10 Hz the charge noise was  $7 \times 10^{-5} e/\sqrt{\text{Hz}}$  corresponding to an energy sensitivity of  $1000 \hbar$ , which is better than earlier reported values for *planar interdigital* SETs [10]. Although the amorphous SiO is known to contain a relatively high density of traps and defects, which one would expect to increase the charge noise of the device. The noise is *not* increased by the use of evaporated SiO as a dielectric. The  $\text{AlO}_x\text{-SiO}$  SET was biased in the gain region and an input charge noise  $Q_N$  of  $4 \times 10^{-4} e/\sqrt{\text{Hz}}$  was measured. This is at least an order of magnitude improvement compared to previous experimental results *overlap* SETs with voltage gain. [2].

## 2.5 Filtering and shielding

The dynamics of SET circuits is very sensitive to noise generated by the external circuitry it is connected to. This external circuitry, which is usually denoted by the electromagnetic environment, includes impedance of the leads, filtering, current and voltage sources, which in practice can have an extremely complicated behavior at high frequencies and is hard to control. This can be particularly critical in schemes which are used in metrology, e.g., the quantum standard of current, or for digital applications, where almost errorless operation is needed. Therefore, reduction of the noise by using cryogenic microwave filtering in the leads is necessary. Reflective filters are very sensitive to impedance mismatches in the rest of the line, thereby affecting the behavior of the circuit. Therefore dissipative wide-band cryogenic microwave filters are needed. In chapter 1 it was already shown that the requirements on these filters are particularly severe, resulting in required attenuations larger than 100 dB. Dissipative filters with such specifications are not commercially available.

Since the relevance of the microwave filtering has been recognized, three types of dissipative filters are currently used by various groups. The first type of filter was developed in the group of Clarke[15], and is known as a copper powder filter. This filter has been proved successfully in a number of experiments in different groups. An improved version is now in use in Delft. The filter consists of a 2 meter manganin wire wound in a cylindrical copper casing filled with fine irregularly shaped copper powder (1 – 5  $\mu\text{m}$  grain size). Since each grain appears to be insulated from its neighbor by a natural oxide, the effective surface area is enormous, and the skin-effect damping produces a substantial attenuation at microwave frequencies. The copper powder is thermalized by injecting Stycast providing good thermal contact. A one meter prototype measured an attenuation of 90 dB from 1 to 20 GHz. Assuming the attenuation scales with the wire length, the filter provides at least 180 dB attenuation. The filters serve as an electrical feedthrough from an outer microwave tight can to an inner microwave tight can. The cans serve as radiation shields and are essential in the design. In the cryostat the 4 K black body radiation photons[32] can induce uncontrolled photon-assisted tunneling processes, strongly affecting the transport properties of the device. An additional 3-pole  $RC$  rf-filter[33] made from surface mount devices (SMD) 1 nF capacitors and 100  $\Omega$  small metal films resistors was put in series with the copper powder filter, providing an attenuation of more than 90 dB at frequencies larger than 100 MHz up to 1 GHz. Using this configuration a maximum of 24 filtered dc lines are available.

Within the SETTRON project a new interesting filter design was put forward by Zorin *et al.*[34] and Glattli[35], both based on resistive lossy coaxial cables. Here the attenuation properties of a thin coaxial cable is exploited, which arise in the line due to skin-effects in its conductor. The coaxial cables can be home-made tailoring the lines to the desired specifications or can be bought commercially as

Thermocoax made by Philips. Analyzing the propagation modes in the coaxial line, it can be estimated that a length of approximately 50 cm is needed to meet the desired specifications. The lossy coaxial cable option is especially interesting for top loading dilution refrigerators, which have only limited available space.

The last type recently developed by Vion *et al.*[36] is based on a distributed *LCR* meandering line microfabricated on a chip. Using optical lithography and etching a on-chip miniature coax line was fabricated using a resistive copper-gold alloy as the inner conductor. The whole chip then was mounted in small copper casing with SMA connectors, providing approximately 60 – 70 dB attenuation starting from 100 MHz to 40 GHz. To obtain the required attenuation of 200 dB approximately would require 3 filters in series in each line. Recently the Saclay group has chosen for a combination of both a lossy coaxial line with the microfabricated filter at the end as close as possible to the sample.

More recent developments are leading towards on-chip filtering, thereby fully controlling the electromagnetic circuitry in which the SET circuit is embedded. This philosophy was first experimentally realized by Haviland *et al.*[5] fabricating high resistive leads close to the circuit in order to study the effect of a high impedance environment. Also Joyez *et al.*[37] and more recently Vion *et al.*[38] used this concept in the study of the switching current of superconducting SET transistors and single junctions. Also in chapter 4 and 5 this aspect is of relevance. By engineering a controlled electrical circuit around the SET circuit its dynamics at high frequencies can be totally controlled. For instance Zorin[39] proposed to shunt a superconducting SET transistor, resulting in a quantum limited Cooper pair electrometer. Therefore, it is our belief that in the future filtering will become part of the chip layout, which is fully consistent with the trend towards the on-chip integration of all functional circuitry.

## 2.6 Operation temperature

Looking to the present status of nano fabrication, on the one hand devices to approximately 50 nm can be made with standard e-beam techniques, on the other hand we have very tempting but very difficult experiments manipulating single atoms on the scale of a few nanometers, using STM techniques.[40] Within the dimensions of 50-5 nm a 'gap' is apparent, where still a lot of research can be done using normal e-beam lithography. Only recently more effort is put in techniques to reduce the dimensions of the devices to tens of nanometers, thereby increasing the operation temperature to higher temperatures.

A first step was made by Ralph *et al.*[41], who was able to fabricate SET transistors with 10 nm islands, using nanoscale holes in SiN membranes. However, this process is not suitable for more complex multi junction circuits. An important result was shown recently by Nakamura *et al.*[42] in which they pushed shadow evaporation to its limits, yielding charging energies of approximately 20

meV. This shows the potential of shadow evaporation is still not fully exploited. The same group developed a very interesting dimension reduction technique of the tunnel junctions based on controlled anodization of the aluminium, anodization controlled miniaturization enhancement (ACME).[43] The final charging energy they obtained was 3.2 mV equivalent to a island capacitance of 50 aF, which is an order of magnitude larger obtained by normal shadow evaporation. The process was limited by the asymmetry in the devices initially induced by the shadow evaporation, showing a scattering in junctions size of  $\sim 20\%$ .

Although a number of innovative techniques have shown blockades up to 20 meV, it will be increasingly hard to meet the desired specifications. For instance pushing the shadow evaporation to its limits one is limited by a combination of the resolution of the e-beam resist, the grain size of the aluminium and the reliability and reproducibility of the shadow evaporation process. Adding up these constraints, dimension reduction always leads to very asymmetric devices and an unacceptable low yield. Therefore different approaches are needed in order to have more control on the nanoscale devices. A first approach in this direction was done by Fujita *et al.* developing a new resist called Calixarene[45], which has a resolution of less than 10 nm. Another approach is to use simple tricks to control the fabrication. We propose a simple technique which could be used in the fabrication of ultra-small SET devices without degrading the yield. It is based on an almost trivial but very essential addition to the already used shadow evaporation. Using shadow evaporation the junctions are defined by an overlap of two different layers evaporated under two different angles. Decreasing this angle will result in a smaller overlap junction, however the yield and variation will increase rapidly. A more controlled reduction of the overlap, which does not include the use of a critical evaporation angle, can be accomplished by using an additional SiO step in the process. Fig. 2.8 is a schematic illustration the idea. First a 15 nm base electrode is deposited perpendicular to the sample. The next step is a 10 nm isolating SiO layer on top of the Al base layer. This layer will insulate the top of the island from the counter electrode. Only the 15 nm high Al edge of the pillar will be exposed to the oxygen and will form the barrier for the junction. The counter electrode is evaporated under angle finishing the tunnel junctions. Looking at the cross section of the junction one can see the junction is formed perpendicular to the substrate and size is defined by the height of the island deposited in the first evaporation step and the width of the junction is determined by the counter electrode. The use of a critical angle is eliminated and is partly substituted by the height of the island, which can be controlled on sub-nanometer level during evaporation. Estimations based on the smallest junctions fabricated in our group, using this technique it should be possible to fabricate multi junction circuits with standard 50 aF tunnel junctions.

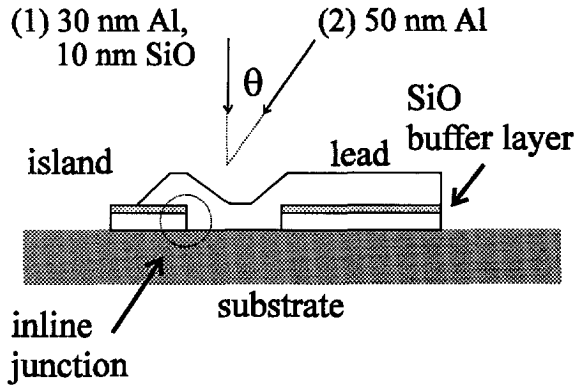


Figure 2.8: Schematic of the improved shadow evaporation technique for the fabrication of inline junctions instead of overlap junctions. This technique leads a reduction of the tunnel junction dimensions without reduction of the fabrication yield.

## 2.7 Conclusions and future prospects

Although the multilayer technique has led to a more 'mature' SET fabrication technology it is only the first step towards a technology which can offer all the fabrication features which are needed in a modern submicron IC technology. The multilayer technique can easily be extended to include the fabrication of high-ohmic resistors and submicron interconnects.

Submicron interconnects can be made by using a thick positive two layer e-beam resist to define the holes in the SiO. After the realization of the holes an additional cleaning step as described above is needed in order to guarantee good low-ohmic contact. This can be realized by introducing a simple in-situ ion-milling step before the metal evaporation. Moreover, once vertical interconnects can be realized, it is only a simple step to extend this process to fabricate controllable vertical tunnel structures, thereby eliminating the in-line shadow evaporation process.

In the discussion, material issues were totally neglected although they play an important role especially in the noise performance. Since the SET devices are ultra sensitive to any moving charge, any moving charge defect will induce time dependent offset charges on the island thereby deteriorating its performance. Reducing the number of material defects can be realized by using low energy processes such as high quality low pressure chemical vapor deposition (LPCVD) dielectrics and molecular beam epitaxy (MBE) thin film growth techniques. A

new, preferably self-aligning, fabrication technique still has to be developed in order to fabricate tunnel structures.

## References

- [1] E. H. Visscher, S. M. Verbrugh, J. Lindeman, P. Hadley, and J. E. Mooij, *Appl. Phys. Lett.* **66**, 305 (1995).
- [2] G. Zimmerli, R. L. Kautz, and John M. Martinis, *Appl. Phys. Lett.* **61**, 2616 (1992).
- [3] P. Lafarge, H. Pothier, E. R. Williams, D. Esteve, C. Urbina, and M. H. Devoret, *Z. Phys. B* **85**, 327 (1991).
- [4] L. J. Geerligs, V. F. Anddereg, P. Holweg, J. E. Mooij, H. Pothier, D. Esteve, C. Urbina, and M. H. Devoret, *Phys. Rev. Lett.* **64**, 2691 (1990).
- [5] D. B. Haviland, L. S. Kuzmin, P. Delsing, and T. Claeson, *Z. Phys. B* **85**, 339 (1991).
- [6] G. J. Dolan, *Appl. Phys. Lett.* **31**, 337 (1977).
- [7] V. Bouchait, private communications.
- [8] R. E. Miller, W. H. Mallison, A. W. Kleinsasser, K. A. Delin, and E. M. Macedo, *Appl. Phys. Lett.* **63**, 1423 (1993).
- [9] H. S. J. van der Zant, R. A. M. Reuveur, and T. P. Orlando, *Appl. Phys. Lett.* **65**, 2102 (1994).
- [10] See for example L. S. Kuzmin, P. Delsing, T. Cleason, and K. K. Likharev, *Phys. Rev. Lett.* **62**, 2539 (1989); L. J. Geerligs, V. F. Anddereg, and J. E. Mooij, *Physica B* **165**, 937 (1990).
- [11] T. A. Fulton and G. J. Dolan, *Phys. Rev. Lett.* **59**, 109 (1987).
- [12] K. K. Likharev, *IEEE Trans. Magn.* **23**, 1142 (1987).
- [13] K. K. Likharev, *IBM J. Res. Develop.* **31**, 144 (1988).
- [14] D. V. Averin and Yu. V. Nazarov, *Phys. Rev. Lett.* **65**, 2446 (1990).
- [15] J. M. Martinis, M. H. Devoret, and J. Clarke, *Phys. Rev. B* **35**, 4682 (1987).
- [16] J. Clarke, W. M. Goubau, and M. B. Ketchen, *Journal of Low Temp. Phys* **25**, 99 (1976).
- [17] T. A. Fulton, P. L. Gammel and L. N. Dunkleberger, *Phys. Rev. Lett.* **67**, 3148 (1991).
- [18] H. Pothier, P. Lafarge, P.F. Orfila, C. Urbina, D. Esteve, and M. H. Devoret, *Physica B*, **169**, 573 (1991).
- [19] John M. Martinis and M. Nahum, *Phys. Rev. Lett.* **72**, 904 (1994).

- [20] P. Lafarge *et al.*, submitted to Phys. Rev. B (1996).
- [21] D. V. Averin, A. N. Korotkov, and Yu. V. Nazarov, Phys. Rev. Lett. **66**, 2818 (1991).
- [22] M. Matters, Ph.D. thesis, Delft University of Technology, 1995.
- [23] A. N. Korotkov, D. V. Averin, K. K. Likharev, and S. A. Vasenko, in *Single Electron Tunneling and Mesoscopic Devices*, edited by H. Koch (Springer, New York, 1992), p. 45.
- [24] S. M. Verbrugh, Ph.D. thesis 1995.
- [25] C. T. Rogers, and R. A. Buhrman, Phys. Rev. Lett. **53**, 1272 (1984).
- [26] A. B. Zorin, F. -J. Ahlbers, J. Niemeyer, T. Weimann, H. Wolf, V. A. Krupenin, and S. V. Lotkhov, to be published in Phys. Rev. B (1996).
- [27] D. Song, A. Amar, C. J. Lobb, and F. C. Wellstood, IEEE trans. Appl. Supercond. **5**, 3085 (1995).
- [28] See for instance: J. G. Simmons, J. Appl. Phys. **35**, 2472 (1964); G. Lewicki, C. A. Mead, Phys. Rev. Lett. **16**, 939 (1966); D. J. Adelerhof, E. P. Houwman, D. Veldhuis, J. Flokstra, and H. Rogalla, Physica B **165**, 1581 (1990).
- [29] E. H. Visscher, unpublished.
- [30] L. S. Kuzmin, Yu. A. Pashkin, A. N. Tavkhelidze, F. -J. Ahlers, T. Weimann, D. Quenter, and J. Niemeyer, Appl. Phys. Lett. **68**, 2902 (1996).
- [31] For small MOS structures, the Coulomb energy of traps in semiconductor space-charge regions was modeled: M. Schulz, J. Appl. Phys. **74**, 2649 (1993).
- [32] J. M. Hergenrother, J. G. Lu, M. T. Tuominen, D. C. Ralph, and M. Tinkham, Phys. Rev. B **51**, 9407 (1995).
- [33] M. M. Freud *et al.*, Rev. Sci Instrum. **66**, 2638 (1995).
- [34] A. B. Zorin, Rev. Sci. Instrum. **66**, 4296 (1995).
- [35] Glattli, private communication.
- [36] D. Vion, P. F. Orfila, P. Joyez, D. Esteve, and M. H. Devoret, submitted to J. Appl. Phys.
- [37] P. Joyez, Ph.D thesis, University of Paris, 1995.
- [38] D. Vion, M. Götz, P. Joyez, D. Esteve, and M. H. Devoret, submitted to Phys. Rev. Lett. (1996).
- [39] A. B. Zorin, submitted to Phys. Rev. Lett. (1996).
- [40] D. M. Eigler and E. K. Schweitzer, Nature **344**, 524 (1990).
- [41] D. Ralph, C. T. Black, and M. Tinkham, Phys. Rev. Lett. **74**, 3241 (1995).

- [42] Y. Nakamura, private communication.
- [43] Y. Nakamura, D. L. Klein, and J. S. Tsai, *Appl. Phys. Lett.* **68**, 275 (1996).
- [44] K. Matsumoto, M. Ishii, K. Segawa, Y. Oka, B. J. Vartanian, and J. S. Harris, *Appl. Phys. Lett.* **68**, 34 (1996).
- [45] J. Fujita, Y. Ohnishi, Y. Ochiai, and S. Matsui, *Appl. Phys. Lett.* **68**, 1297 (1996).



## Chapter 3

# High frequency operation of SET devices

### 3.1 Introduction

Although the intrinsic speed of a SET transistor is approximately limited by its  $RC$  response time to 10 – 100 ps, it is impossible to make measurements at high speed in a typical measurement set-up. The intrinsically large output impedance of the tunnel junctions ( $R_T \gg R_K = 25.8 \text{ k}\Omega$ ) coupled with the inevitable capacitances of the filtering [1] and the leads ( $C_L \simeq 100 \text{ pF/m}$ ), reduces the bandwidth of SET devices to a few hundred Hertz. There are, however, applications where one would like to make very fast charge measurements. For instance, in SET devices the shot noise can be suppressed below the Schottky value due to electron correlations.[2, 3] Furthermore, it is the shot noise which sets the ultimate sensitivity of the SET transistor. To directly probe this intrinsic shot noise one needs to measure at high frequencies where the shot noise dominates over the  $1/f$  noise.[4]

In order to perform high frequency charge measurements, the bandwidth of the SET transistor must be increased by placing an impedance matching circuit close to the SET transistor, which has a high input resistance and is able to drive high capacitance leads. A cryogenic field effect transistor based on a GaAs/AlGaAs heterostructure [5] and usually referred to as a high electron mobility transistor (HEMT) satisfies both requirements. At low temperatures it has a very high input resistance as well as a low output impedance. These devices can without any problem be operated up to hundreds of MHz. To increase the operation frequency even further the SET device should be matched with HEMTs specially optimized for microwave frequencies.

## 3.2 Experimental considerations

Electron tunneling devices such as metallic or semiconductor SET circuits, and also scanning tunneling microscopes (STM), have some common characteristics. First of all, the sensitivity of tunnel devices to the external electromagnetic environment is extremely high, requiring very efficient microwave filtering. When operated inside cryostats, the intrinsically large output impedance of the tunnel junctions is coupled to the inevitable capacitances of the long leads. This not only reduces the bandwidth of the devices, but also makes the set-up very sensitive to radio frequency interference and mechanical vibrations. Very efficient dedicated filters and shielding has been developed in the last few years. However, surprisingly in the field of SET devices, the operation improvement of SET devices by the use of cryogenic amplifiers has only gained recent interest.[6, 7, 8] A cryogenic low noise preamplifier close to the circuit not only improves the bandwidth and but also decreases the effect of electromagnetic and vibration pick-up. Depending on the bandwidth requirements of an experiment, the amplifier should be placed close the circuit. The low temperature operation imposes both limitations on the power dissipated by the active devices and the type of active device used in the amplifier. A proper place to mount an amplifier would be the 1 K stage of the cryostat. At that stage refrigerators can maintain the proper operation temperature with  $\sim 10$  mW dissipated by the amplifier. The power dissipation will limit the amplifier design to only a few active commercially available components. Positioning an amplifier at the 10 mK cold finger drastically increases the power dissipation requirements due to the limited cooling power of refrigerator, which is limited to only  $\sim 10$   $\mu$ W. Therefore the amplifier is reduced to a one-component circuit, which has to be specially designed for low power operation [9]. This illustrates the necessity of defining the bandwidth requirements of the particular experiment in advance, thereby choosing for the most suitable and simplest solution. In this chapter we will propose a possible experiment in which single-electron motion in a long array of small tunnel junction is detected, using a broadband SET transistor. We will refer to this circuit as the electron counter. The circuit has potential for possible applications as a current standard in metrology. It will be shown that in order to realize this experiment, the operation frequency of the SET transistor needs to be extended to higher frequency. Although the electron counting experiment is only a proposal, the first experimental realization of the SET-HEMT circuit is considered to be an essential technological achievement in the development towards this experiment.

## 3.3 On-chip HEMT impedance matching

Within the SETTRON project the impedance matching project was approached via two complementary paths. This was done intentionally due to the large

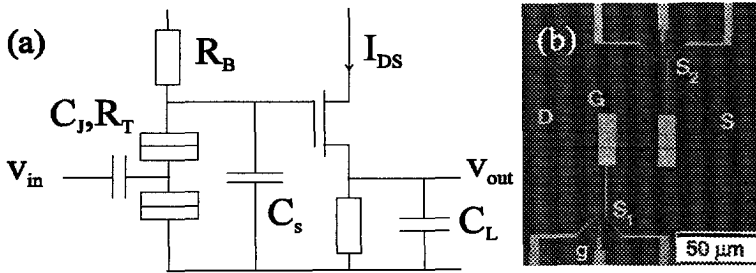


Figure 3.1: (a) Schematic circuit of the integrated circuit. The circuit is comprised of a directly coupled SET transistor as a charge sensitive input stage. The tunnel junctions are indicated by the boxes. The voltage output of the SET transistor is directly coupled to the input gate of the HEMT, which buffers the output signal of the SET transistor. (b) Photomicrograph of the device. Two SET transistor  $S_1$  and  $S_2$  are coupled to a horizontal 2DEG channel, connecting the source (S) to the drain (D) of the HEMT. Note that the SET transistor is much smaller than the dimensions of the HEMT. A small signal to the gate of the SET transistor (g) is transferred to the gate of the HEMT (G).

number of technological issues involved in the project. First of all the Delft group with its multi-layer SET fabrication and 2DEG experience, integrated a metallic SET transistor directly on-chip to a simple 2DEG HEMT. Petterson *et al.*[7] collaborated with the department of microwave technology of Chalmers university to couple an InP microwave HEMT via a bonding wire to a SET transistor, which was fabricated on a separated chip. Both groups were able to extend the high frequency limit of a SET transistor.

The direct integration of the SET transistor on-chip next to a GaAs-AlGaAs HEMT is shown schematically in Fig. 3.1 (a) and (b). The voltage output of the current-biased SET transistor was directly connected to the gate of the HEMT. The on-chip HEMT was optimized for megahertz operation in a dilution refrigerator.[10] The design is a trade-off between a large signal response i.e. transconductance and low power dissipation ( $\sim \mu\text{W}$ ). For a saturated source-drain current,  $I_{DS}$ , the HEMT response is determined by its transconductance,  $g_m = (\partial I_{DS} / \partial V_{GS})_{V_{DS}}$ , and can be controlled by the ratio of the channel width,  $W$ , and the active layer thickness,  $d$ . Here  $V_{GS}$  is the gate-source voltage and  $V_{DS}$  is the drain-source voltage. Beside parasitics, its high frequency operation is determined by the transit time,  $1/\tau \simeq g_m / C_G$ , which is the time spend by the electrons under the gate capacitor,  $C_G$ .

The HEMT structures were fabricated using a GaAs/ $\text{Al}_{0.3}\text{Ga}_{0.7}\text{As}$  heterostructure

ture grown by molecular beam epitaxy. The two-dimensional electron gas (2DEG) had a sheet density of  $n_s = 4 \times 10^{11} \text{ cm}^{-2}$  and a mobility of  $\mu = 9 \times 10^5 \text{ cm}^2/\text{Vs}$  and was situated at a depth  $d = 75 \text{ nm}$  below the surface. The source-drain channel was  $60 \text{ }\mu\text{m}$  long and  $10 \text{ }\mu\text{m}$  wide and was defined by electron-beam lithography and a mesa-etch. The ohmic contacts to the 2DEG were made by thermal diffusion of Ni-AuGe.

The SET transistor was fabricated directly next to the 2DEG channel using accurate alignment. The SET transistor consisted of a small metallic island weakly coupled to the leads by two ultra-small tunnel junctions, as shown in Fig. 3.1 (a). The tunneling of electrons through the junctions was strongly affected by the Coulomb blockade, which inhibits tunneling below a certain threshold voltage. The threshold voltage was controlled by an input gate, which was capacitively coupled to the island. The Al-AlO<sub>x</sub>-Al junctions were fabricated using a two-angle shadow evaporation technique. [11] The gate of the HEMT was directly coupled to the output voltage of the SET transistor as shown in photograph of Fig. 3.1 (b). The SET transistor was situated  $40 \text{ }\mu\text{m}$  away from the 2DEG channel. Beside the integrated circuits, the chip also contained single HEMTs and SET transistors for detailed device characterization.

The dc characteristics of a single HEMT is shown in Fig. 3.2. The measurements were performed in a dilution refrigerator with a base temperature of 10 mK. The HEMT was biased using low noise mercury cells. The gate was defined by the channel width,  $W = 10 \text{ }\mu\text{m}$ , the gate length,  $L = 10 \text{ }\mu\text{m}$ , and had a nominal area of  $100 \text{ }\mu\text{m}^2$ . The gate length was larger than the elastic scattering length of the electrons so the transport along the channel was diffusive. Typical source-drain characteristics are shown in Fig. 2. At source-drain voltages larger than 100 mV, the source-drain current saturates. The channel pinches off smoothly, at a gate threshold voltage of  $-450 \text{ mV}$ . The experimentally measured gate-capacitance of  $0.13 \text{ pF}$  agrees well with the value of  $0.15 \text{ pF}$ , estimated for the geometrical capacitance.

To measure the characteristics of the SET transistor, a magnetic field of 0.2 T was applied to keep the aluminum in the normal state. The circuit parameters of the current biased SET transistor were obtained by fitting the experimentally measured transfer characteristics,  $V_o - V_g$ , to the theoretical calculated curves using the orthodox theory.[12] The SET transistor had junction capacitances of  $C_1 = 0.24 \text{ fF}$ ,  $C_2 = 0.29 \text{ fF}$ ; tunnel resistances of  $R_1 = 720 \text{ k}\Omega$ ,  $R_2 = 700 \text{ k}\Omega$ ; and a gate capacitance of  $C_g = 80 \text{ aF}$ . Consequently, the gain of the SET transistor was less than unity  $K_V = (\partial V_o / \partial V_g)_{I_b} = C_g / C_2 \simeq 0.3$  and the total output impedance was  $1.4 \text{ M}\Omega$ . The maximum output voltage swing of the SET transistor is set by the threshold voltage,  $V_T = e / C_\Sigma \simeq 0.25 \text{ mV}$ , where  $C_\Sigma = C_1 + C_2 + C_g$  is the total island capacitance.

The SET transistor and the HEMT were put in their optimal working points by setting the dc bias voltages of each device. The current bias of the SET transistor was realized by putting a  $20 \text{ M}\Omega$  metal film resistor in series with the

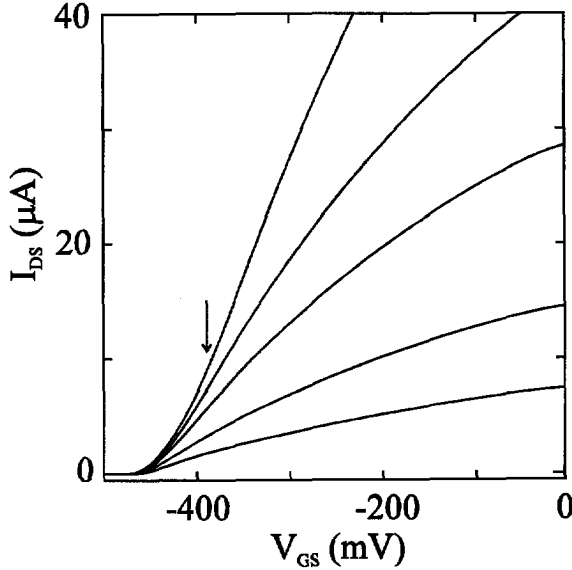


Figure 3.2: Gate-source characteristics taken at a base temperature of 10 mK and a magnetic field of 0.2 T for different values of the drain-source voltage:  $V_{DS} = 20, 40, 60, 80,$  and  $100$  mV. The arrow indicates the working point of the HEMT at a gate-source voltage of  $-390$  mV. At this point the transconductance is  $g_m = 0.2$  mS.

device and was about 25 pA. The HEMT was used in a source-follower configuration with a gain close to unity. The channel was biased at a source-drain voltage  $V_{DS} = 100$  mV, just in its saturation region. Then the gate-source voltage was set to  $V_{GS} = -390$  mV by means of a cold 46 k $\Omega$  source resistor,  $R_S$ . At this point, the drain current was 8.5  $\mu$ A and the transconductance was 0.2 mS. The settings were such that the total power dissipation in the HEMT was 0.8  $\mu$ W and did not seriously affect the SET transistor characteristics. The total output impedance and the gain of the circuit were then calculated using simulations, yielding an output impedance of  $Z_{out} \simeq 1/g_m = 5$  k $\Omega$  and a gain of  $G_H = 0.74$ . The experimentally measured gain of the HEMT in the source-follower configuration was  $G_H = 0.72$  and thus in good agreement with the simulations.

The frequency response of the integrated circuit was then determined by applying a small ac signal  $v_{in} = \Delta V_g/2 \simeq 1.5$  mV p-p to the gate of the SET transistor. The response  $v_{out}$  at the output of the HEMT was then measured using a low noise differential amplifier. Fig. 3.3 (a) schematically shows the response of the circuit. For frequencies up to 50 kHz, the gain of the total circuit,

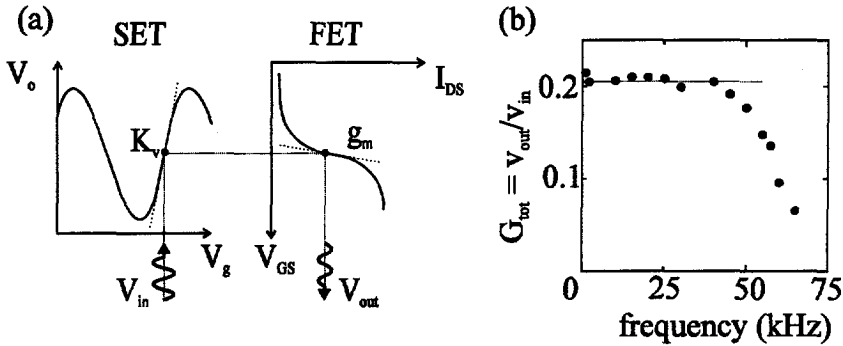


Figure 3.3: (a) Schematic of the device operation. The SET transistor and the HEMT are set in their optimal working points, denoted by the black dots in their transfer characteristics. A small ac voltage signal is transferred via the voltage transfer coefficient  $K_V$ , and the transconductance  $g_m$ , to the output of the HEMT. The experimental response of the circuit is shown in (b). The gain of the circuit is 0.21. At a corner frequency of 50 kHz the response decreases rapidly due to stray capacitances.

$G_{tot} = v_{out}/v_{in} \simeq 0.21$ , is shown in Fig. 3.3 (b). This agrees well with what one would expect from the gain parameters of the individual circuits,  $G_{tot} \simeq K_V G_H$ . The signal-to-noise ratio at 50 kHz was approximately 10 dB, and decreased rapidly above the corner frequency due to stray capacitances. In order to reduce the stray capacitance of the bias resistor, shown Fig. 1 (a), a high ohmic, low capacitance thin-film resistor [13] of about 1-10  $k\Omega/\square$  must be fabricated on-chip close to the circuit. The development of high ohmic resistors for SET devices is in progress and can be implemented in our multi-layer fabrication approach.[14] Alternatively, one could use an array of small junctions close to the SET transistor as a (non-linear) bias resistor.[15]

An interesting application for the use of the SET-HEMT circuit was recently proposed by Likharev.[16] In his proposal, he considered a non-volatile dynamic RAM combining SET-based cells and HEMT sense amplifiers, where the bits are stored in the form of a few electrons. The interesting feature of these memory cells is that they are offset charge independent. The source-drain current through the SET transistor is an  $e$ -periodic function of the polarization charge on the island,  $Q_o = Q^* + C_g U$ , and an amplitude  $\Delta I \sim e/R_T C_J$ . The randomness of the background charge  $Q^*$ , makes the response to small input signal  $\Delta U$  unpre-

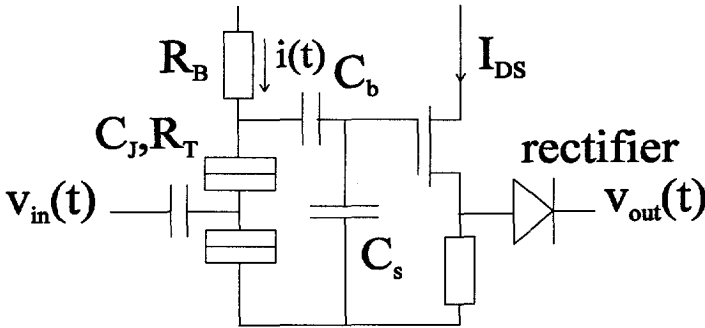


Figure 3.4: Schematic of the proposed SET-HEMT circuit. The output signal is insensitive to a random background charge  $Q^*$ . Except from the blocking capacitor  $C_b$  and the rectifier, the circuit is equivalent to the measured SET-HEMT circuit.

dictable. However, for a large input signal  $\Delta U > e/C_g$ , the transistor response will be an oscillation of the current  $I$  with the full swing equal to  $\Delta I$ , regardless of  $Q_o$ . After amplification of the output signal by the HEMT this response can be rectified and serve as an output signal, as shown in Fig. 3.4. Apart from the blocking capacitor and the rectifier the circuit is similar to the SET-HEMT described above.

Optimizing the SET-HEMT structures for microwave operation the HEMT structures will more and more resemble commercially available HEMTs. This means the HEMTs will have a very short gate length and will be designed such that its internal stray capacitances are minimized. This requires true microwave engineering of the HEMTs. At such high frequencies a simple impedance matching buffer will not be able to drive the large output capacitance. Therefore an additional amplification stage in the design is needed. At this point the GaAs/AlGaAs circuits will start to resemble to microwave monolithic integrated circuits (MMICs). All input and outputs have to be matched to  $50 \Omega$  striplines. Still the operation of the HEMT will be limited by its power consumption. Therefore in parallel to the development of the GaAs/AlGaAs HEMT structures, the charging energy should be increased via reduction of the tunnel junction dimensions.

In conclusion, we have transformed the impedance of a SET transistor by two orders of magnitude down to  $5 \text{ k}\Omega$ , increasing its bandwidth to  $50 \text{ kHz}$ . It is the first demonstration of the direct integration and operation of a metallic SET device with a semiconductor HEMT. Optimization of the on-chip design suggests

operation in the MHz range will be possible.

### 3.4 The electron counter

The SET electrometer can measure charge with a precision of about  $10^6$  times better than that possible with commercially available electrometers. At higher frequencies, the charge noise is limited by shot noise to a value of  $10^{-6} e/\sqrt{\text{Hz}}$ . These devices have been used to detect the motion of individual electrons.[17] Likharev [18] proposed that a current could be measured simply counting the number of electrons that pass a certain point in a circuit. In order to be able to perform such experiment, a wide-band SET transistor [6] as described above is an essential element.

There have been a number of attempts to use both semiconductor and metallic single electron tunneling circuits to produce a current standard. One possibility is to phase lock single electrons moving correlated in a one dimensional array of tunnel junctions to external rf driven, analogous to the Josephson voltage standard. Putting several SET transistors in series, electrons can be controlled by an external rf source one by one through a circuit called the electron turnstile.[19] Alternatively, individual electrons can be pulled one by one through a circuit called an electron pump.[20] By doing this repeatedly with frequency  $f$ , a constant current was generated with a value,  $I = ef$ . The turnstile produces a current of a few picoamps with an accuracy of 1 part in 1000. The feasibility of using the turnstile as a current standard and its limitations in its accuracy have been thoroughly investigated by Verbrugh.[21]

In order to be able to count the electrons that pass by a single point it is necessary to have spatially correlated electron motion.[22] Such correlated electron motion occurs in a series arrays of small tunnel junctions. The voltage profile induced by an electron in the array extends over an characteristic length scale extending over several islands. When more electrons are induced in the array, the repulsive Coulomb interaction between the electrons assures that they are evenly spaced along the array. At low currents this spatial correlation between the electrons remains, resulting in narrowband SET oscillations. The longer the array, the narrower the peak of the SET oscillations are. Korotkov[23] calculated that the 1D array should at least consist of 20-30 tunnel junctions in order to exhibit pronounced SET oscillations. Each time one electron passes by at a certain point in the array there is a voltage oscillation. The frequency of the SET oscillations is related to the dc current flowing through the array as,  $I = ef$ . A wideband electrometer can monitor the charge on one of the islands similar to the electron box experiments. Here we propose to use SET transistors to count the number of electrons that pass through an array of tunnel junctions. This design for a current standard is better than a turnstile, because co-tunneling events, the dominant error source in the turnstile are suppressed due to the Coulomb



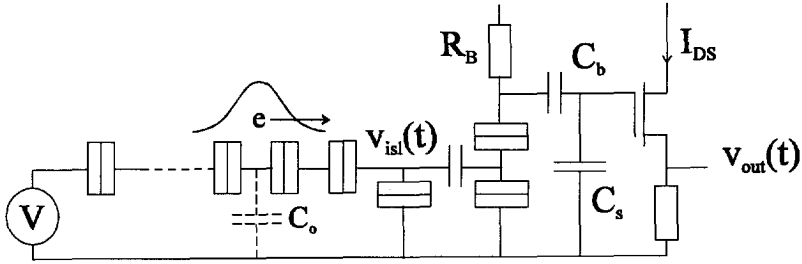


Figure 3.5: Schematic of the proposed electron counter circuit. Electrons which move correlated through the one dimensional array of tunnel junctions. The passing electrons can be detected with a broadband SET transistor.

interactions in the long 1D array. An estimation of the precision of the electron counter is described below and would be on the order of 1 part in  $10^{10}$  for a current of 1 fA.

Fig. 3.5 shows the circuit of the proposed experiment. The input signal generated by SET oscillations will be between 1 kHz and 10 MHz, depending on the current through the array. The precision of the electron counter can be estimated from the measured charge noise of the SET transistor. The contribution from the noise will be a random signal with a Gaussian distribution,

$$\sqrt{\frac{\tau_m}{Q_N^2}} \exp\left(-\frac{q^2 \tau_m}{2Q_N^2}\right) \quad (3.1)$$

where  $\tau_m$  is the duration of the measurement,  $q$  is the measured charge, and  $Q_N$  is the charge noise of the SET transistor. If we assume that the measurement time is 10 times shorter than the period of the SET oscillations, then the probability of erroneously recording a measurement greater than  $q_c$  is

$$P(q > q_c) = \sqrt{\frac{e}{10\pi I Q_N^2}} \int_{q_c}^{\infty} \exp\left(-\frac{eq^2}{20I Q_N^2}\right) dq = \frac{1}{\sqrt{2}} \operatorname{erfc}\left(\sqrt{\frac{e}{20I Q_N^2}} q_c\right) \quad (3.2)$$

Using typical parameters for the SET transistor,  $Q_N = 10^{-4} e/\sqrt{\text{Hz}}$  and  $q_c = 0.1 e$ , we find that the electron counter should have a precision of one part in  $10^{10}$  for a current of 1 fA. The theoretical estimate for the quantum limited charge noise is  $Q_N = \sqrt{\hbar C}$  [2], therefore lowest charge noise SET transistor is  $Q_N \approx 10^{-6} e/\sqrt{\text{Hz}}$ . If this limit can be realized, then it will be possible to measure 10 pA with a precision of one part in  $10^{10}$ . By passing the same current through two counters one could test the precision of the electron counters. The output of many counters in parallel could be summed to measure larger currents.

### 3.5 Further developments

The success of the proposed experiments described above relies heavily on the control of the required technology, like the integration of GaAs/AlGaAs and metallic SET technology. Furthermore increasing the charging energy of the SET transistor will reduce the power dissipation requirements of the design. However, not all interesting high frequency experiments have such severe bandwidth requirements. In those cases a much simpler solution can be chosen.

Here we will take the example of shot noise measurement, which was already mentioned in the introduction. In SET circuits and other mesoscopic structures the shot noise can be suppressed below the classical Poisson shot noise due to the correlations in the transfer of electrons imposed by Coulomb interaction. Although the suppression of the shot noise has been theoretically investigated quite extensively, experimentally it is difficult to probe this noise due to the high intrinsic impedance of these devices. From a practical point of view, the shot noise magnitude in a SET transistor is important since it sets the ultimate charge sensitivity. The observation of the shot noise requires that the  $1/f$  noise spectral density,  $S_{1/f} = \alpha \langle I \rangle^2 / f$ , be much smaller than the (Poisson) shot noise spectral density,  $S_{SN} = 2e \langle I \rangle$ . The parameter  $\alpha$  is system dependent and for a SET transistor with a  $1/f$  charge noise magnitude of  $10^{-4} e / \sqrt{\text{Hz}}$  at 10 Hz,  $\alpha \simeq 10^{-5}$ . Hence to measure the shot noise of a SET transistor with a bias current of 100 pA, would require a bandwidth of at least 100 kHz. The bandwidth requirement of 100 kHz can be met by choosing for an cold amplifier at the 1 K stage. At the 1 K stage a heat load of approximately 10 mW can be tolerated, therefore commercial GaAs Metal-semiconductor field-effect transistors (MESFET) can be chosen as the active components of the amplifier. MESFETS have proven successful operation at 1 K [24], have a good low-frequency noise performance and are stable against oscillations. This approach was recently successfully shown by Birk *et al.* [3] who measured the suppression of the shot noise in a SET transistor realized with an STM setup.

We have started to develop cold amplifiers for the use in a dilution refrigerator. The current biased SET transistor is connected via a short shielded twisted pair to the input of the amplifier, which is mounted on the 1 K pot of the fridge. The material of the twisted pair is manganin and is chosen for its poor thermal conductivity, thus minimizing heating of the SET transistor. The amplifier is built on a special double sided Cu-plated PC board. Special care was taken in designing the layout to minimize stray capacitances. All components were surface mount devices (SMD) components. The resistors were NiCr thin metal film resistors and the capacitors had NPO dielectrics. Both had very small temperature coefficients. The SMA output of the amplifier was connected to a 1 m stainless steel coax cable. Active devices made from GaAs operate at cryogenic temperatures without carrier freeze out. The amplifier circuit comprises a two stage voltage sensitive amplifier with capacitively coupled differential input. The

dissipation in each stage was about 1 mW, so the total circuit only dissipated 2 mW. The amplifier has a flat gain of 20 in the desired frequency range from 100 kHz to 1 Mhz. The noise referred to the input is  $2 \text{ nV}/\sqrt{\text{Hz}}$ . Although no results are obtained yet, this example show that by analyzing each experiment individually in terms of bandwidth requirements easier solutions can be chosen.

## References

- [1] J. M. Martinis, M. H. Devoret, and J. Clarke, *Phys. Rev. B* **35**, 4682 (1987).
- [2] A. N. Korotkov, *Phys. Rev. B* **49**, 10381 (1994).
- [3] H. Birk, M. J. M. de Jong, and C. Schöenberger, submitted to *Phys. Rev. Lett.*
- [4] G. Zimmerli, T. M. Eiles, R. L. Kautz, and John M. Martinis, *Appl. Phys. Lett.* **61**, 237 (1992).
- [5] D. J. Mar and R. M. Westerveld, P. F. Hopkins, *Appl. Phys. Lett.* **64** (5), 631 (1994).
- [6] E. H. Visscher, J. Lindeman, S. M. Verbrugh, P. Hadley, and J.E. Mooij, *Appl. Phys. Lett.* **68**, 2014 (1996).
- [7] J. Pettersson, P. Wahlgren, P. Delsing, N. Rorsman, D. B. Haviland, H. Zirath and T. Claesson, to be published in *Phys. Rev. B*.
- [8] D.Berman and R. Ashoori, proceedings of the ICQDC, Alexandria, 1996.
- [9] D. J. Mar, R. M. Westervelt and P. F. Hopkins, *Appl. Phys. Lett.* **64**, 631 (1994); D. J. Mar, Ph.D. thesis, Harvard University, 1994.
- [10] For a detailed review on HEMTs, see: *HEMTs and HBTs: Devices, Fabrication, and Circuits*, edited by F. Ali and A. Gupta, (Artech House, 1991).
- [11] G.J. Dolan, *Appl. Phys. Lett.* **31**, 337 (1977).
- [12] K. K. Likharev, *IEEE Trans. Magn.* **23**, 1142 (1987).
- [13] D. B. Haviland, L. S. Kuzmin, P. Delsing, K. K. Likharev, and T. Claesson, *Z. Phys. B* **85**, 339 (1991).
- [14] E. H. Visscher, S. M. Verbrugh, J. Lindeman, P. Hadley, and J.E. Mooij, *Appl. Phys. Lett.* **66** 305 (1995).
- [15] P. Delsing, K. K. Likharev, L. S. Kuzmin and T. Claesson, *Phys. Rev. Lett.* **63**, 1180 (1989).
- [16] K. K. Likharev, and A. N. Korotkov, ISDR Charlottesville, 1995.
- [17] P. Lafarge, H. Pothier, E.R. Williams, D. Esteve, C. Urbina, and M.H. Devoret, *Z. Phys. B* **85**, 327 (1991).

- [18] K. K. Likharev, Single-Electronics: Correlated Transfer of Single Electrons in Ultrasmall Junctions, Arrays and Systems in *Granular Nanoelectronics*, edited by D. Ferry, NATO ASI Series B: Physics 251, (Plenum, New York, 1990).
- [19] L. J. Geerligs, V. F. Anderegg, P. A. M. Holweg, J. E. Mooij, H. Pothier, D. Esteve, C. Urbina, and M. H. Devoret, *Phys. Rev. Lett.* **64**, 2691 (1990).
- [20] H. Pothier,
- [21] S. M. Vergrugh, Ph.D. thesis, Delft University of Technology, 1995; S. M. Verbrugh and J. E. Mooij, *Proceedings of Metrologie in Physik und Technik*, Sept. 1994.
- [22] K. K. Likharev, N. S. Bakhvalov, G. S. Kazacha, and S. I. Serdyukova, *IEEE Trans. Magn.* **25**, 1436 (1989).
- [23] A. N. Korotkov, *Phys. Rev. B* **50**, 17674 (1994).
- [24] For references to cold amplifiers, see for example: A. T. Lee, *Rev. Sci. Instrum.* **60**, 3315 (1989); A. T. Lee, *Rev. Sci. Instrum.* **64**, 2373 (1973);

## Chapter 4

# Josephson junction microwave generators

### 4.1 Introduction

In recent years, other measuring techniques beside dc transport measurement have been applied to mesoscopic systems. Techniques such as capacitance spectroscopy[1] and microwave spectroscopy[2] have been successfully demonstrated. In this chapter we will focus on the use of microwaves to study high frequency dynamics in superconducting tunnel junction systems. In analogy to spectroscopy on atoms, it is interesting to study the interactions between light (photons) and electrons in quantum devices. Moreover, in a superconducting SET transistor coherent resonant Cooper pair tunneling is possible, comparable to the resonant tunneling of electrons through a 0D state in a quantum dot. The energy level spacing in these devices is much smaller than in real atoms. Typical energy spacings are on the order of 0.1 – 1 meV. The frequencies to probe these levels by means of spectroscopic techniques are within the microwave range from tens to hundreds GHz. In contrast to the light transmission or luminescence measurements used in atomic spectroscopy, the photo response is measured in the dc current. Using microwave spectroscopy the complex junction impedance can be measured *in-situ*. [3] Moreover, it is an essential tool in studying macroscopic quantum tunneling (MQT) and coherence effects in quantum devices. [4, 5]

The microwave regime however is an inconvenient frequency range experimentally, since there are few tunable microwave sources of radiation available, which can be coupled to the sample at low temperatures while isolating the sample from room temperature blackbody radiation. Therefore the approach of using a superconducting Josephson junction (JJ) as local high frequency generator [6] close to the system under study has been chosen. The concept to use Josephson junction devices as a local microwave source in mesoscopic and SET experiments has already been around for a long time, however mainly due to technological barriers such experiments have never been demonstrated successfully. In this chapter we

will demonstrate the operation of an on-chip superconducting JJ SQUID as a local microwave generator.

## 4.2 A tunable SQUID microwave source

When a junction shunted with a resistor  $R_s$  is biased at a constant voltage, its supercurrent oscillations at a well-defined fundamental frequency,  $f = V/\Phi_o$ , where  $\Phi_o \approx 2.07$  mV/THz and  $V$  is the time-averaged voltage across the junction. For junctions with a McCumber parameter  $\beta_c = 2\pi I_o R_s^2 C_J / \Phi_o < 1$ , the ac voltage signal  $\tilde{V}(t)$  generated by the JJ can be calculated analytically within the resistively shunted junction (RSJ) model,

$$\tilde{V}(t) = R_s \sqrt{i^2 - 1} \left\{ 1 + 2 \sum_{n=1}^{\infty} \left( \sqrt{i^2 - 1} - i \right)^n \cos(n\omega t) \right\} \quad (4.1)$$

where  $i = I_B/I_o$  is the normalized bias current. Eq. (4.1) shows that if the system is biased at a current above the critical current the junction will start to oscillate, generating an ac voltage with an amplitude of approximately  $I_o R_s$ . For low bias currents the ac signal will contain a number of harmonics. At higher bias currents the signal starts to become more and more sinusoidal. The characteristic frequency of the generated signal will be within the GHz range depending on the magnitude of the superconducting gap of the material,  $f \sim 4\Delta/h$ .

When coupled to a load  $R_L$ , the transmitted power will be approximately  $V^2 R_L / (2(R_s + R_L)^2)$ . Hence, for a matched load the maximum transmitted power is  $P_{\max} \approx I_o^2 R_s / 8$ , whereas for a large impedance mismatch,  $R_s \ll R_L$ , the transmitted power will be  $P_{\max} (R_s / R_L)$ . In general, the load will be a complex frequency dependent impedance  $Z_L(\omega)$ . We will show this can complicate a more quantitative analysis. The transmitted power scales with  $I_o^2$ , therefore the generator has a SQUID layout[8]. By applying an external flux through the SQUID loop, the critical current and thus the power can be tuned *independently* from the frequency. Therefore the SQUID acts as microwave source with two 'knobs' for tuning both the frequency and the generated power. Providing good coupling to the load and taking into account the higher harmonics at low bias voltages the JJ can be used as a local microwave generator with a tunable power output of 0.01 – 1 nW. Note that due to the high energy sensitivity of most mesoscopic systems the power requirements are orders of magnitude lower from generator requirements in metrology, astronomy and high-speed electronics where power levels of mW are preferable.

The main requirement for making JJ microwave generators is the controlled fabrication of resistively shunted junctions with a McCumber parameter smaller than unity. An external normal metal resistor parallel to the junction makes the  $I - V$  curve of the JJ non-hysteretic and therefore the junction can be biased at any voltage. Thus far, only high quality JJs made in the niobium technology

were able to meet these requirements. However, niobium trilayer technology[9] requires an expensive fabrication line and is not accessible for a low budget academic environment. We therefore have developed shunted junctions in aluminum technology. The aluminum fabrication technique produces high quality over-damped Josephson junctions with typical critical currents from 5 up to 20  $\mu\text{A}$ . The junctions show excellent stability against thermal cycling.

The generator circuit is shown in Fig. 4.1 (a) and consists of two Josephson junctions in a low inductance SQUID configuration. The SQUID microwave source is fabricated by aluminum Josephson junctions shunted by a platinum thin film resistor. The total circuit was made on oxidized Si wafers, using a four-level fabrication process[10]. Fig. 4.1 (b) shows the multilayer structure. The first layer defined the shunt resistors of the junctions and the markers to align all the following layers and was made of platinum. The next layer determines the Al-AlO<sub>x</sub>-Al junctions by means of the shadow evaporation technique. The junctions have a critical current densities of typically 1 kA/cm<sup>2</sup> and are shunted by the 3.5  $\Omega$  platinum resistor,  $R_s$ . The platinum resistor has an additional coolingfin which helps preventing heating effects[11] at low temperatures. No extra cleaning of the platinum contacts was needed to obtain nice RSJ-type junction behavior. The shunted junctions were designed to be non-hysteretic by choosing,  $\beta_c = 2\pi I_c R_s^2 C_J / \Phi_0 \leq 1$ , where  $C_J$  is the junction capacitance. Both leads of the junctions defined the first layer of the large square coupling capacitors,  $L^2 = 100 \times 100 \mu\text{m}^2$ . In the next step a 75 nm thick SiO layer formed the dielectric of the capacitors. The final step both defines the counter electrodes of the capacitors and the detector, which can be any object under study. This way, both a single junction and a SET transistor have been coupled to a SQUID generator.

The dc-blocking capacitor,  $C_B = 10$  pF realized by the two overlap capacitors should be large in order to have good coupling. The impedance of the capacitor is in the order of a few ohms for microwave frequencies. The resonant modes in the capacitor are of the form  $f_{n,m} = c/2Ln_e\sqrt{m^2 + n^2}$ , where  $c$  is the speed of light,  $n_e$  is the effective refraction index and is a function of the penetration depth and the thicknesses of the superconducting aluminum capacitor electrodes. The total device dimensions are smaller than one quarter of the wavelength of the generated frequencies,  $f \ll f_{1,1}$ . The capacitors can thus be considered as lumped element circuits for the relevant frequencies. This ensures a reasonably constant coupling at every frequency and considerable simplification in the circuit analysis.

The measurements were taken in a dilution refrigerator with a base temperature of 10 mK. All leads were filtered with copper powder filters[5], attenuating gigahertz frequencies by at least 200 dB. Additionally, the samples were shielded by various microwave tight metal shields, preventing uncontrolled photon processes due to black body radiation of the 1 K environment[6]. Fig. 4.2 shows the  $I - V$  curves of the SQUID at various external fluxes from  $\Phi = 0$  to  $\Phi = \Phi_0/2$ . The  $I - V$  curves show RSJ-like behavior[12]. The junctions have critical currents of tens of  $\mu\text{A}$ , which is comparable to standard JJs in Nb technology. The SQUID

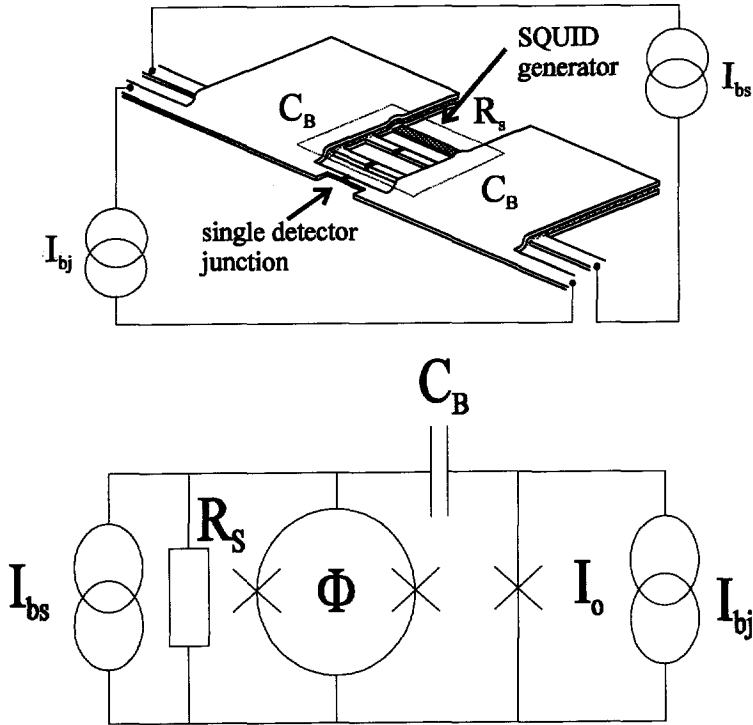


Figure 4.1: (a) Photomicrograph of the fabricated generator circuit. A Josephson junction (G) is shunted by a platinum resistor (R), which has a cooling fin attached. The generator is coupled via two big dc blocking capacitors to a detector (D), which in this case is a superconducting SET transistor. In (b) the multilayer circuit is shown schematically. The single detector junction is fabricated on top of the SQUID generator, separated by a SiO dielectric. A circuit equivalent is given in (c), the crosses indicate the Josephson junctions. A flux  $\Phi$  can be applied to the generator, controlling the generated power in the circuit.

has a McCumber parameter of  $\beta_c = 0.7$ . The inductance is kept as low as possible by fabricating the SQUID ring as close as possible to the detectors, which is usually approximately  $10 \mu\text{m}$ . By varying the externally applied flux through the SQUID generator the critical current can be varied from 6 to  $20 \mu\text{A}$  tuning



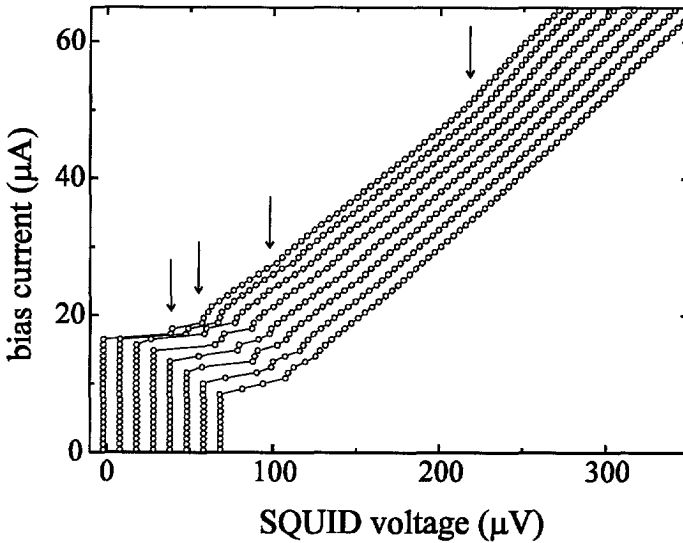


Figure 4.2: Typical RSJ type current-voltage characteristics of the SQUID for different values of the flux through the loop. The curves have an offset in the current direction for clarity. At low biases small hysteretic parts are visible. The arrows indicate the subharmonic structure in the  $I - V$ 's.

the power from approximately 0.1 to 1.1 nW. From the  $I - V$  curves resonant structure is visible. The structure arises from the resonant circuit formed by the shunt inductance  $L_s$  and the junction capacitance  $C_J$ . The resonant circuit pulls the Josephson frequency slightly so that it will become more closely a subharmonic of the resonant frequency. Hence, the dynamic resistance of the generator will be affected as the Josephson frequency passes through each subharmonic of the resonator.[7] Note that the inductance introduces a third degree of freedom to the circuits and therefore can behave chaotically. By designing two shunts close to the junctions the effect of the inductance can be reduced.

### 4.3 Microwave interaction between a JJ generator and a single Josephson junction

In the first experiment performed with the JJ generator we have looked at the response of a single unshunted Josephson junction, as shown in Fig. 4.1 (a) and (b). A single unshunted JJ is ac coupled to a SQUID generator. First of all, it is

important to establish the nature of the response of the junction to GHz radiation. The tunnel rate of the Cooper pairs is equal to the supercurrent divided by the charge of a Cooper pair:  $\Gamma = I_o/2e \approx 10^{14}$ , assuming a critical current of the order of 10  $\mu\text{A}$ . This rate is much larger than the generator frequency, hence many charge carriers tunnel per cycle of the applied radiation. This regime is known as the classical regime in which the photonic (quantum) nature of the radiation does not play a role. Therefore the dynamics of the single Josephson junction detector biased at a current  $I$  can be very well described by the resistively and capacitively shunted junction (RCSJ) model[12] including the ac current source  $\tilde{I}_{rf}(t)$ ,

$$\beta_c \ddot{\phi} + \dot{\phi} + \sin \phi = \tilde{I}_{rf}(t) + I_{bj} \quad (4.2)$$

where  $\phi$  is the phase difference across the junction and the McCumber parameter  $\beta_c$  of the detector, representing the effective damping of the system. Considerable insight into the non-linear dynamics of the junction is obtained by realizing that Eq. (4.2) describes the motion of a particle in a tilted washboard potential,  $U(I, \phi) = -(I\phi + I_o \cos \phi) \Phi_o/2\pi$ . Biased at a bias current,  $I < I_o$ , the particle oscillates at the bottom of the potential well with the plasma frequency,  $\omega_p = (2\pi I_o/\Phi_o C_J)^{1/2} [1 - (I/I_o)^2]^{1/4}$ , schematically shown in Fig. 4.3 (a). At the critical tilt,  $I = I_o$ , the particle will run down the potential, and a voltage will develop across the junction (Fig. 4.3 (b)). Depending on the McCumber parameter, the dynamics of the junction can be either overdamped,  $\beta_c < 1$ , or underdamped  $\beta_c > 1$ . Unlike an overdamped junction, an underdamped junction will exhibit a hysteretic  $I - V$  curve. Applying an ac current source tilts the washboard potential back and forth. At certain frequencies motion of the ball locks with the external frequency (Fig. 4.3 (c)).

Radiation effects can be studied in two distinct states of the junction: the zero-voltage or superconducting state of the junction and the finite voltage or resistive state of the junction. The latter case features the well-known Shapiro steps, which are due to phase locking of the external signal and the Josephson frequency. In this section, we will focus on the effect of radiation in the zero voltage state of the junction. Considering the washboard model biased below the critical current as in Fig. 4.3 (a), this is equivalent to exciting the particle out of the well by radiation. Application of a small enough rf signal will result in small oscillations  $\eta(t)$  of the phase around a constant phase difference  $\phi(t) = \phi + \eta(t)$ . Note that this approximation is only valid in the small microwave limit. The ac current amplitude should be significantly smaller than the critical current. In case of a large amplitude signal the critical current varies with the microwave amplitude according to a 0-th order Bessel function. In the small microwave

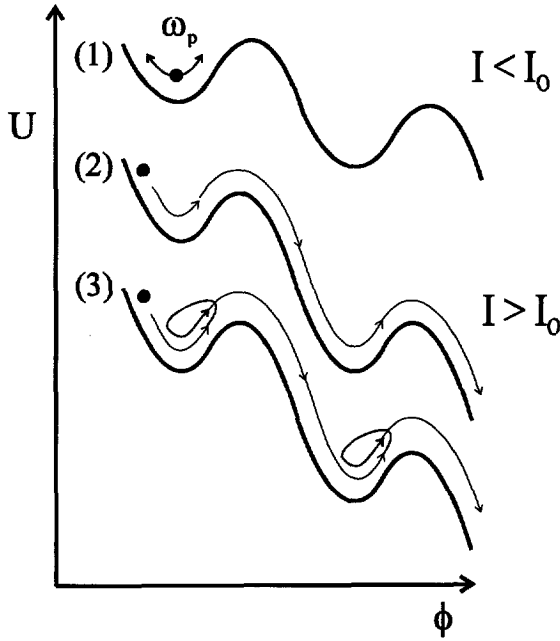


Figure 4.3: Schematic of the particle in the washboard potential. The bias current determines the tilt of the washboard potential. For a bias current smaller than the critical current (1), the particle oscillates with the plasma frequency in a local minimum. If the bias current exceeds the critical current (2) the particle runs down the potential generating an average voltage across the junction. If an additional ac signal is added to the bias current (3) the dynamics of the particle can lock with the external signal.

approximation Eq. (4.2) be linearized around  $\phi$ , yielding,

$$|\eta| \approx \frac{\tilde{I}_r/I_0 \cos \phi}{\sqrt{[1 - (\omega/\omega_p)^2]^2 + [\omega/\omega_p Q]^2}} \quad (4.3)$$

Here  $Q = \omega_p R_e C_J$  is the quality factor of the plasma resonance of the junction, which is determined by the effective damping resistor  $R_e$  of the total circuit and the junction capacitance  $C_J$ . This expression shows that the single JJ behaves as a *LCR* resonant circuit.[13, 12] Switching from the superconducting to the resistive state will occur whenever the inequality  $\phi + |\eta| > \pi/2$  is satisfied. At the resonant condition  $\omega = \omega_p$ , the particle will be resonantly activated out of the

well.[14] Hence, recalling that Eq. (4.3) applies for all harmonics of the Josephson frequency, it is expected that a series of resonances occur at  $\omega = \omega_p/n$ . Using Eq. (4.2) and Eq. (4.3) a connection is established between the switching current of the JJ detector, the plasma frequency, and the amplitude of the generator signal. Recalling that subharmonic structure can also occur in the generator due the resonant circuit formed by the shunt inductance and generator capacitance, it is clear care should be taken interpreting the data. The first is a signature of the dynamics of the generator, the latter is determined by the detector junction.

The bias current through the detector junction was swept from zero to the current value  $I_{sw}$  were it switches to the finite voltage state. Since it has been shown that the plasma frequency is a function of the bias current, this is equivalent to sweeping the plasma frequency of the detector junction from  $\omega_{p0}$  to zero. The junction detector switches whenever the total current through the junction exceeds the critical current. The value of this switching current was then recorded for different values of the generator current bias. The result is presented in Fig. 4.4, which shows the response of the switching current of the detector,  $I_{sw} \approx I_{bj} + I_{rf}$ , as a function of the frequency (voltage) across the junction from 5 to 175 GHz. First of all, the switching current exhibits a number

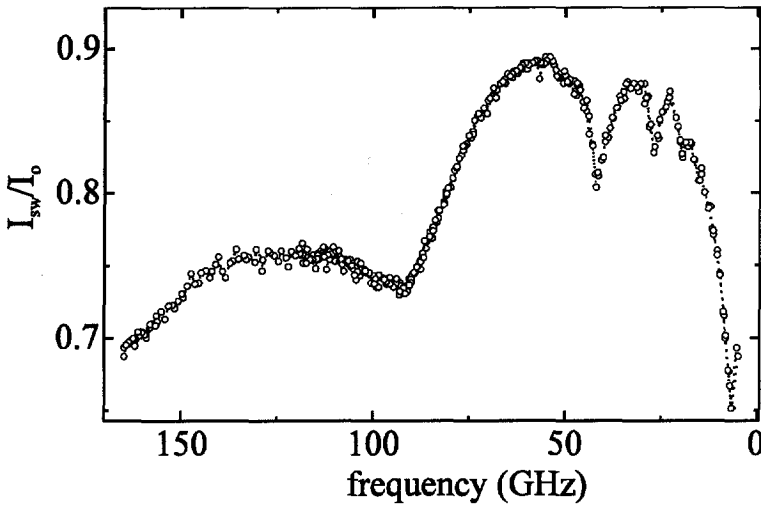


Figure 4.4: The response of the switching current of the detector as a function of the generator frequency over the whole frequency range. Cusps with a subharmonic structure are visible in the response.

of very sharp cusps, spaced further apart as the frequency increases. Since experimental measured spacing scales with  $1/n$ , we can attribute these dips to the

occurrence of resonant activation of either the internal junction plasma frequency of the detector junction or the  $L_s C_J$  resonant circuit of the generator.

In order to obtain some more insight in the dynamics of the detector circuit, we take the rather naive assumption that the generator can be modeled as a set of time-dependent current sources  $\tilde{I}_{rf}(t) = \sum_n \tilde{I}_{n,rf} \sin(n\omega t)$ , where the amplitudes of the harmonics is given by expression Eq. (4.1). The switching current of the junction is simulated using Eq. (4.3) up to ten harmonics of the radiation frequency and for different amplitudes of the rf source. Fig. 4.5 (a) and (b) show both the simulated and the experimental data. The plasma frequency is plotted for several harmonics as a function of the detector current, using the capacitance of the detector a fit parameter. For a detector capacitance of 140 fF, it is found that these resonant dips are situated quite accurately on the plasma frequency curves. If the power of the generator is increased, the resonant dips are shifted to higher frequencies and the switching current is decreased. This can be understood by noting from Eq. (4.3), that a higher generator critical current will result in a larger  $\tilde{I}_{rf}$ , leading to a lower switching current. Comparing the experimental data with the simulations, we can make four important observations. First of all, by looking at the low frequency side of the experimental data a sharp decrease of the switching current is noticeable. This can be understood in terms of noise, which is fully omitted in the simple model. The non linearity of the junction mixes the noise generated at the Josephson frequency to the measurement frequency. In the limit of  $eV \geq k_B T$ , quantum corrections to the noise generated in the shunt resistor[15] become important and scales for low biases with the dynamic resistance in the bias point of the  $I - V$ . Therefore at low biases, the switching of the detector junction is totally determined by noise. Secondly, at the high frequencies the switching current shows a tendency to decrease. This could be attributed to the increase of the amplitude of the Josephson oscillations as the voltage across the junction approaches  $2\Delta/e$ . As a result of the BCS theory, the amplitude of the Josephson oscillations shows a singularity at the gap frequency, which is normally referred to as the Riedel peak.[16] The third and most important observation is that at the resonant frequencies the shape of the measured cusps differ substantially from the simple model described above. This can be understood that noting that at the resonant frequency the linear approximation used in Eq. (4.3) is not valid. At resonance, the generator and the detector cannot be treated independently. A fully consistent description of this problem can be given using the harmonic balance method developed by Likharev.[12]

In order to obtain some more physical insight in the complex dynamics of the system, we apply the same approach Joyez *et al.* used for the analysis of the switching current of a superconducting SET transistor. In the high frequency limit,  $V \gg I_o R_s$ , the generator signal is almost sinusoidal and therefore can be regarded as an ac current source  $I_o \sin(Vt/\Phi_o)$  in parallel with the resonant circuit as shown schematically in Fig. 4.6. Now, since the junction is a

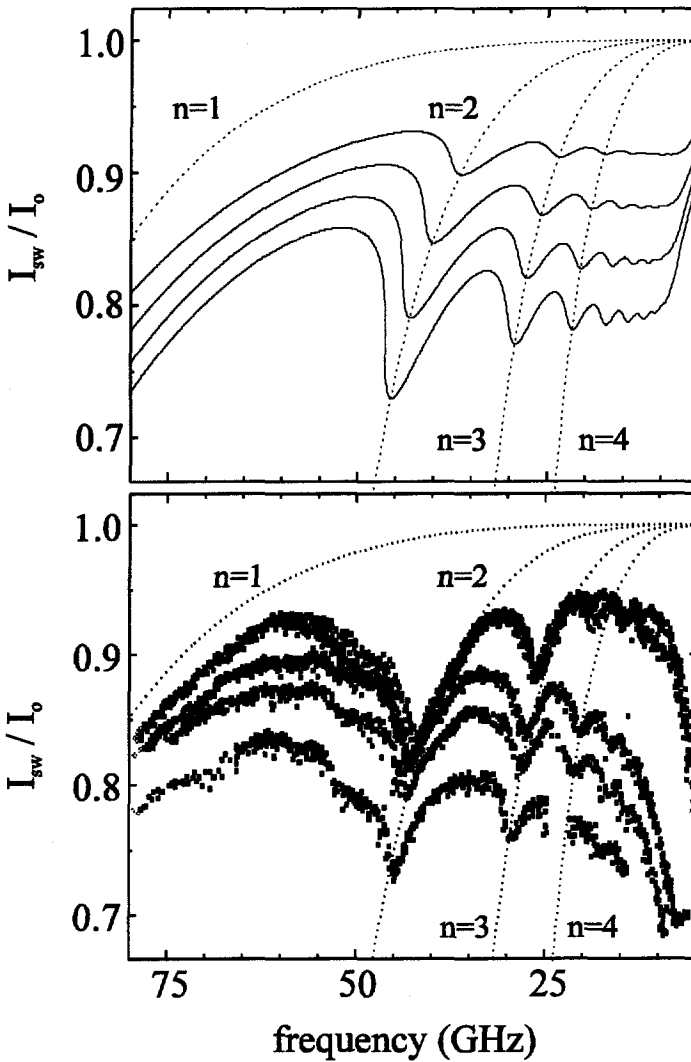


Figure 4.5: Simulated (a) and measured (b) responses of the detector switching current for increasing power settings of the generator. The dashed lines are the plasma resonances for the first for harmonics  $n = 1, 2, 3$  and 4. Although qualitatively simulation and measured data follow the same trend, clear differences are seen in the shape of the cusps and the magnitude of the switching current at low frequencies.

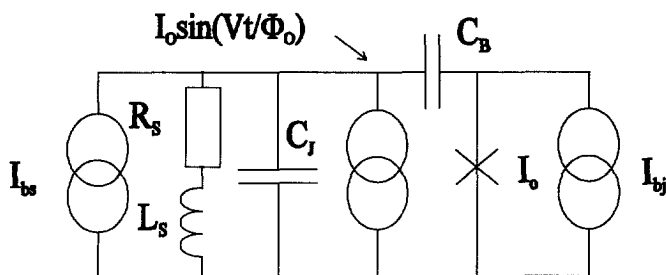


Figure 4.6: (a) Schematic of the circuit in the high frequency approximation. The junction can be replaced by a voltage dependent ac current source. The inductance of the shunt resistor and the capacitance of the junction form a resonant circuit.

non-dissipative element, the power dissipated in the electromagnetic environment  $P_{ac} = \frac{1}{2} I_0^2 \text{Re } Z(Vt/\Phi_0)$  is equal to the applied dc power  $P_{dc} = IV - V^2 Y(0)$ . Here  $\text{Re } Z(Vt/\Phi_0)$  is the total impedance of the circuit at the Josephson frequency. At a certain bias current  $I$  stable solutions for  $V$  can be obtained self-consistently by solving

$$I - \frac{V}{R} = \frac{1}{2} I_0^2 \text{Re } Z(Vt/\Phi_0) \quad (4.4)$$

In Fig. 4.7 (a) this equation is solved graphically and shows that the stable solutions are parts of the resonant curve. At a certain bias current the voltage switches from one stable branch to the other. This mechanism explains the cusp structure seen in the experimental data and is reminiscent to coupled nonlinear oscillators.[17] In Fig. 4.7 (b) the experimental data of cusp measured at the highest frequency is plotted. The drawn line is a hypothetical resonant curve of the circuit. Thermal averaging can wash out the switching between both branches, resulting in the special cusp structure. Although the cusp is a reminiscence of a resonance, it is not possible to determine its quality factor directly. In this picture, the features measured by the detector junction are a direct cause of the change in the dynamic resistance of the generator. Since the power received by the detector junction is a direct function of the source (generator) impedance, the detector junction can be regarded as a local spectrum analyzer. The plasma frequency of the detector is much larger than the plasma frequency of the generator, there will occur no large back-action effects of the detector on the generator. However, due to the fact that both the generator and detector are intrinsic nonlinear devices, one should be very careful making such statements. For instance, careful examination of the response in Fig. 4.5 (b) shows smaller,

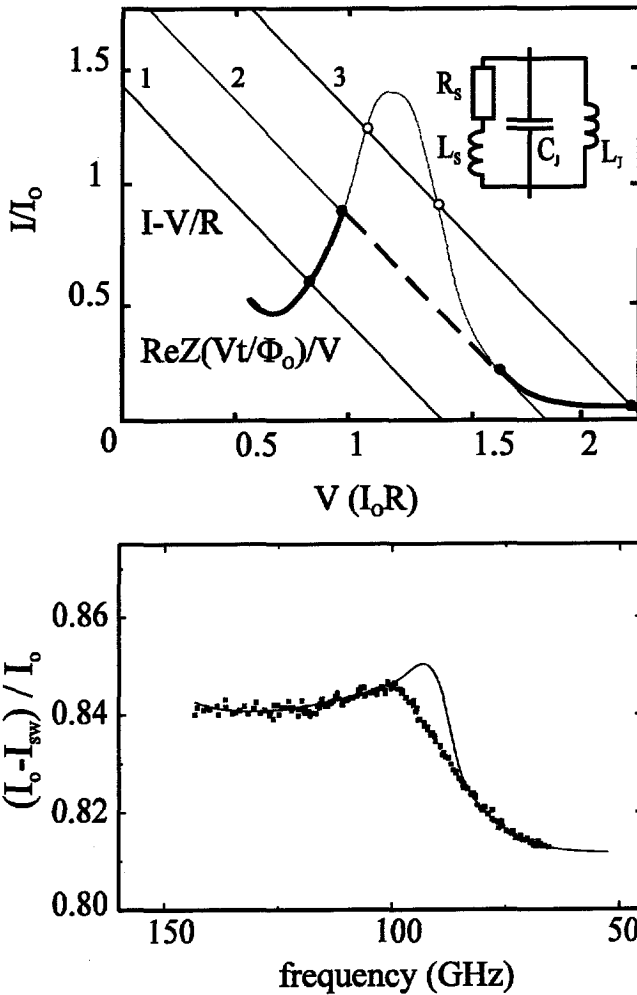


Figure 4.7: (a) Graphical solution of the power balance. Intersections of the load line and the real part of the frequency dependent impedance seen by the junction, will give the solutions to the equation. At low bias (1) the load line intersects the curve at one point forming a stable solution indicated by the solid dot. Increasing the bias current two solution appear. At that point the system can switch between two stable states. At higher bias currents the system will choose for the solution with the lowest dynamical resistance. The other solutions indicated by the open dots are inaccessible for the measurements. Fig. 7 (b) shows the interpretation of the experimentally measured cusp at 100 GHz, denoted by the black dots. The drawn line indicates a possible resonant curve.



additional structure beside the subharmonic cusps is apparent. This could indicate combined effects of both generator and detector effects. The back action of the detector on the generator should be analyzed more carefully, measuring the dynamic resistance of the generator as a function of the bias current through the detector. More thorough analysis of the whole circuit using computer simulations is needed in order to make more quantitative statements.

The single junction detector supercurrent is never completely suppressed. We would expect this to occur on the grounds that the generator supercurrent is larger than the detector supercurrent. This suggests only a fraction of the signal amplitude is coupled into the detector. As a rough measure, it can be estimated that the maximum fraction of the amplitude which is coupled into the detector is given by the ratio of the difference  $\Delta I$  between the detector critical current and the minimum switching current, and the generator critical current,  $\Delta I/I_c \approx 0.1$ . In the simulations we also have to use a coupling parameter of approximately 0.1. Part of these losses can be attributed to the losses in the SiO overlap capacitors. The SiO dielectric at microwave frequencies can have substantial ac losses.

In conclusion, we qualitatively analyzed a coupled SQUID generator - JJ circuit, which revealed a wealth of interesting nonlinear dynamics. Possible explanations for the measured subharmonic response can be given in terms of the plasma resonance of the detector or a  $L_s C_J$  resonance of the generator. We have tried to give a qualitative analysis for the shape of the measured cusps in terms of a Josephson junction coupled to a resonant circuit. Because both circuits are intrinsically nonlinear, therefore a full simulation of the whole circuit is needed to give some more quantitative discussion of the measurements. In principle, we have shown that radiation can be coupled into the detector continuously from 5 to 175 GHz. Only a fraction of the generated signal effectively couples to the detector, probably due to ac losses in the SiO capacitors. The single detector junction can be used as a sensitive bistable threshold detector, responding to the change in the dynamic resistance of the generator. In that case the junction acts as a sort of local spectrum analyzer. Furthermore, in combination with noise and a subthreshold driving signal the dynamics of this system can be mapped on stochastic resonance dynamics, which has wide interest from neural networks to sensory systems. Taking into account the nonlinear aspects of the generator, it can easily be used in a number of high frequency applications in mesoscopic physics.

## References

- [1] R. C. Ashoori, *Nature* **379**, 413 (1996).
- [2] T. H. Oosterkamp, L. P. Kouwenhoven, A. E. A. Koolen, N. C. van der Vaart, and C. J. P. M. Harmans, submitted to *Phys. Rev. Lett.* (1996).

- [3] M. H. Devoret, J. M. Martinis, D. Esteve, and John Clarke, *Phys. Rev. Lett.* **53**, 1260 (1984).
- [4] M. H. Devoret, J. M. Martinis, and J. Clarke, *Phys. Rev. Lett.* **55**, 1908 (1985).
- [5] J. M. Martinis, M. H. Devoret, and J. Clarke, *Phys. Rev. B* **35**, 4682 (1987).
- [6] See experimental references on Josephson junction generators: S. P. Benz and C. H. Burroughs, *Appl. Phys. Lett.* **58**, 2162 (1991); B. Bi, S. Han, and J. Lukens, *Appl. Phys. Lett.* **64**, 1424 (1994); P. A. A. Booij and S. P. Benz, *Appl. Phys. Lett.* **68**, 3799 (1996).
- [7] R. H. Koch, D. J. van Harlingen, and J. Clarke, *Phys. Rev. B* **26**, 74 (1982).
- [8] J. Clarke, in *Superconducting electronics* edited by H. Weinstock and M. Nisenzon, NATO ASI Series, Vol. F-59, 1989.
- [9] Nowadays high quality niobium circuits can be bought commercially at Hypress Inc.
- [10] E. H. Visscher, S. M. Verbrugh, J. Lindeman, P. Hadley, and J. E. Mooij, *Appl. Phys. Lett.* **66**, 305 (1995).
- [11] F. C. Wellstood, Ph.D. thesis, Lawrence Berkeley Laboratory, 1988.
- [12] K. K. Likharev, *Dynamics of Josephson junction and circuits*, Gordon and Breach, Paris, 1986.
- [13] J. M. Martinis, Ph.D. thesis, Lawrence Berkeley Laboratory, 1985.
- [14] M. H. Devoret, J. M. Martinis, D. Esteve, and J. Clarke, *Phys. Rev. Lett.* **53**, 1260 (1984).
- [15] R. H. Koch, D. J. van Harlingen, and J. Clarke, *Phys. Rev. Lett.* **45**, 2132 (1980).
- [16] E. Riedel, *Z. Naturforsch.* **A19**, 1634 (1964).
- [17] A. B. Pippard, *Response and stability*, Cambridge University Press, Cambridge (1985).

## Chapter 5

# Microwave spectroscopy on a superconducting SET transistor

### 5.1 Introduction

In this chapter we focus on measurement of a superconducting SET (S-SET) transistor, coupled to a similar SQUID generator as described in chapter 4. We will show that contrary to the response of a single Josephson junction, the S-SET will respond in a non-classical way. At bias voltages smaller than  $4\Delta/e$ , a quasiparticle current can flow through the S-SET on the order of tens of pA. If GHz radiation is applied to this system the Tucker criterion [1],  $f > \Gamma$ , applies and many rf cycles will occur between each tunnel event. In this regime, referred to as the quantum regime, the tunneling electrons can absorb or emit photons from the electromagnetic field. This process is usually referred to as photon-assisted tunneling (PAT) and was first explained in single SIS junctions by Tien *et al.*[2]. PAT results in an enhanced tunnel current in a situation when the initial and final states of a tunneling electron differs by an integer number of energy quanta  $hf$ .

PAT processes are of particular interest in the study of the interactions between electromagnetic radiation and tunnel processes in semiconductor, metallic and superconducting [3] structures and can be used as a spectroscopy tool to probe excited states [4] in mesoscopic systems. PAT is also of importance in the analysis of applications of SET circuits. For example when a Cooper pair absorbs a photon with a frequency larger than the its pairing energy,  $2\Delta/h > 100$  GHz, two quasiparticles can be excited. If one of the quasiparticles is able to tunnel onto the superconducting island before it recombines, it can switch the device from a non-conducting to a conducting state. The superconducting SET transistor thus acts as an ultra-sensitive photon detector [5] in the far-infra red. Its estimated noise equivalent power (NEP) is in the order of  $10^{-20}$  W/ $\sqrt{\text{Hz}}$ , which is two orders of magnitude better than existing bolometers, operating in the same frequency regime [6]. Uncontrolled PAT processes is also an important

source for errors in SET circuits used in metrological applications [7], since it can excite electrons across Coulomb barriers. Utilizing SET circuits in practical circuits such as charge sensors or metrological and logic circuits, PAT events can destroy the proper operation the device. A more fundamental issue involves the ultimate speed of the SET transistor which can be estimated by its internal  $RC$  time, which is typically in the 100 GHz range. To study these high frequency processes in detail one would like to have a microwave generator which can be tuned continuously over a wide range of frequencies without considerable change in coupling. The SQUID generator opens an area of new possibilities in high frequency experiments.

## 5.2 Quasiparticle tunneling and parity effects in a superconducting SET transistor

Before we describe the results of the coupled generator-SET circuit, we first focus on the characteristic properties of a superconducting SET transistor (S-SET). A S-SET significantly differs from its normal counterpart, because the ground state of the superconducting SET transistor depends on the electron number parity of the island.[8] If there are an even number of electrons are on the island, it is in the even state and all electrons near the Fermi energy are paired. If one extra electron tunnels onto the island, it stays in an excited state above the gap energy. Therefore the ground state energy of the S-SET in the odd state is shifted by the value of the superconducting gap. At finite temperatures, the free energy change between the odd and even state not only includes the gap but also an entropy term. Therefore the odd-even effect can only be observed below a certain critical temperature  $T^* \approx \Delta/k_B \ln N_{eff}$ , where  $N_{eff}$  is the number of electrons involved in the pairing. This parity effect is reflected both in experiments on the modulation of the Cooper pair super current as a function of the gate charge [9, 10, 11], as well as the average charge of a superconducting electron box.[12] Both types of experiments probe the thermal equilibrium properties of the system. In these experiments it is crucial that the devices are in the limit that  $\Delta \geq E_C$ . In that limit the transition between two even ground states in the grain is possible. For  $\Delta < E_C$ , only transitions between different parities are possible. As a result, the processes of Cooper pair tunneling are strongly suppressed by the Coulomb blockade. This leads to both a drastic decrease of the critical Josephson current and a  $e$ -periodic modulation of the supercurrent, i.e. the supercurrent is 'poisoned' by quasiparticles. If the S-SET has a very large charging energy,  $\Delta \ll E_C$ , any  $2e$ -tunneling events hardly occur. Zaikin and Schön[13] showed that the odd-even asymmetry is not only reflected in the Cooper pair processes, but also by the quasiparticle current at finite bias. This effect was recently observed by Nakamura *et al.*[20] in very small 20 nm superconducting grains.

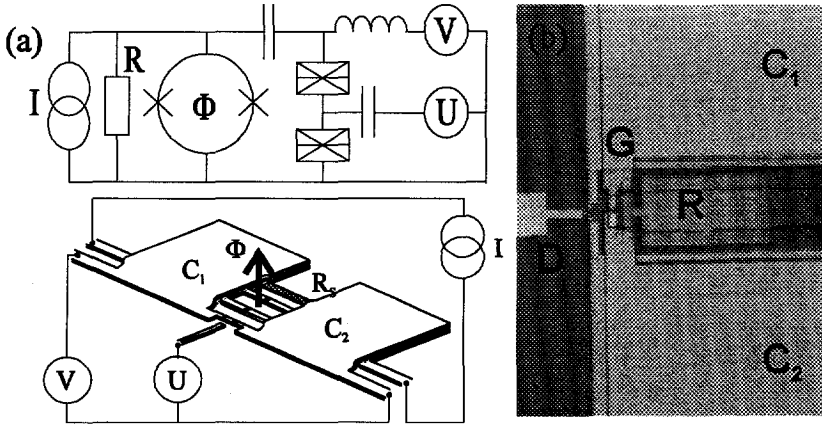


Figure 5.1: (a) Schematic of the electrical and physical layout of the SQUID generator coupled to the SET transistor. The frequency can be tuned by the bias current  $I$ . The power is controlled via the externally applied magnetic field,  $\Phi$ . (b) Photo micrograph of the SQUID generator (G) coupled via big overlap capacitors  $C_1$  and  $C_2$  to the SET transistor (D). The SQUID is resistively shunted by a resistor  $R$ .

Using standard two-angle shadow evaporation, the S-SET was fabricated on top of the SQUID generator, as shown in Fig. 5.1 (a). The SET transistor was fabricated using the standard two-angle shadow evaporation technique. The barriers were formed by oxidizing for 5 minutes in a 0.02 mBar oxygen atmosphere. The SQUID generator was capacitively coupled via the leads to the voltage biased S-SET transistor as shown in the schematic of Fig 5.1 (b). In Fig. 5.2 (a) the energy diagram of the S-SET is shown in the semiconductor representation and illustrates the quasiparticle density of states with a gap energy  $\Delta$  as well as the Fermi energy of the electrodes of both leads and island. Due to the odd-even energy symmetry caution should be taken using this model in illustrating tunneling cycles in the device. However, since the charging energy of the sample was much larger than the gap energy, only the state with one electron occupation is relevant largely simplifying the model.

The measured  $I - Q_0$  curves for the high bias regime,  $V_b > 4\Delta$ , and low bias regime,  $V_b < 4\Delta$ , are shown in Fig. 5.2 (b) and (c). The high bias curves exhibit the usual  $e$ -periodic current modulation. Superimposed on the curves a small resonance is visible. The curves in Fig. 5.2 (c) exhibit a linearly rising background quasiparticle current. This might be explained by the fact that heating effects will increase the quasiparticle subgap conduction as  $R_{sg}/R_T = \exp[\Delta/k_B T - 1.76]$ ,

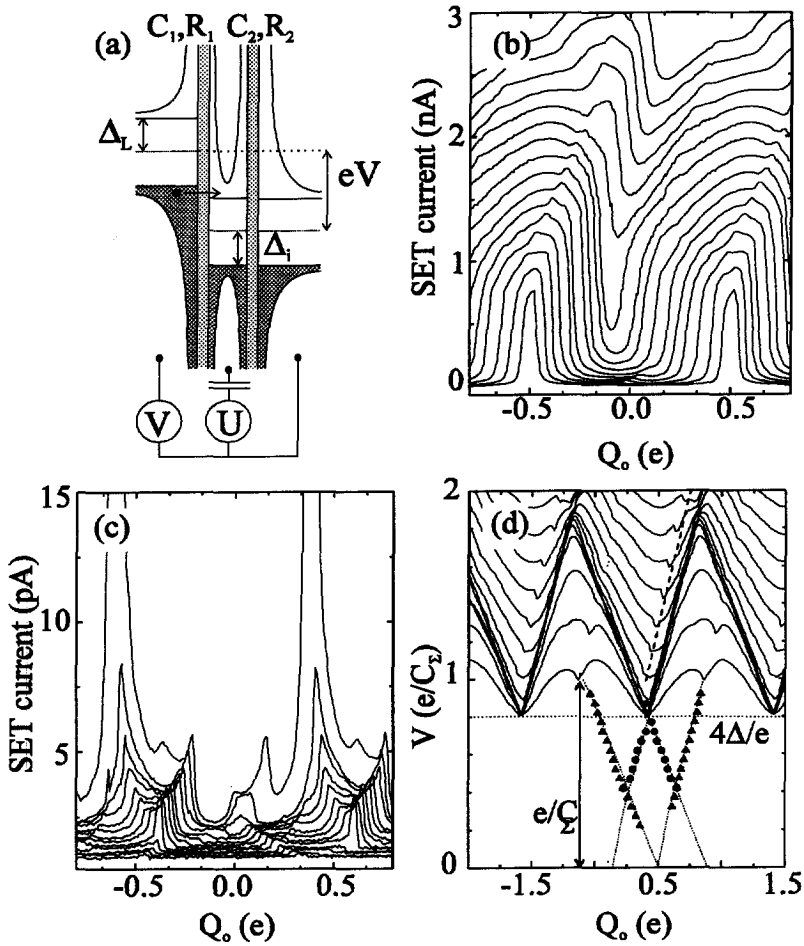


Figure 5.2: (a) Schematic energy diagram of the voltage biased S-SET, using the semiconductor model. At bias voltages  $V$  larger than  $2\Delta$  quasiparticles can tunnel through the device. The gate voltage  $U$  can tune the potential of the middle island continuously. (b)  $I - Q_0$  curves for the high bias regime  $V > 4\Delta$ . On top of the  $e$ -periodic current modulation a small resonant structure is visible. (c) The  $I - Q_0$  curves for the low bias regime  $V < 4\Delta$  exhibiting  $e$ -periodic current plateaus centered around  $Q_0 = e/2$ . In the measured  $V - Q_0$  curves for the S-SET (d) the different conductance areas in which are marked.

which is an approximate result from the BCS theory. To clarify the measured resonant structures, we have plotted the onset of these conductance plateaus in a measured  $V_b - Q_o$  diagram as shown in Fig. 5.2 (d). From the quasiparticle threshold voltages at

$$V_1^{th} = \frac{e}{C_1} \left( \frac{1}{2} - n - \frac{Q_o}{e} + \frac{2\Delta C_\Sigma}{e^2} \right) \quad (5.1)$$

$$V_2^{th} = \frac{e}{C_2 + C_g} \left( \frac{1}{2} + n + \frac{Q_o}{e} + \frac{2\Delta C_\Sigma}{e^2} \right) \quad (5.2)$$

capacitances of  $C_1 = 57$  aF,  $C_2 = 96$  aF and  $C_g = 7$  aF were deduced, yielding a charging energy  $E_C = e/2C_\Sigma \approx 2.5\Delta \approx 0.5$  meV. The tunnel resistances are  $R_1 = 88$  k $\Omega$  and  $R_2 = 397$  k $\Omega$ , therefore the device is in the regime where the charging energy is much larger than the Josephson energy,  $E_J/E_C \approx 3 \times 10^{-3}$ . In this regime, the supercurrent and low bias coherent Cooper pair resonances are suppressed. Secondly, the combined Cooper pair-quasiparticle process, usually referred to as the 'Josephson quasiparticle cycle'[16, 17, 18, 19] will not be observed within the subgap region. The subgap conductance is therefore totally dominated by quasiparticle tunneling. The low bias regime exhibits an  $e$ -periodic pattern of small conductance plateaus centered around  $Q_o = e/2$  and are marked by the solid triangles and dots. The solid triangles mark the threshold voltages for quasiparticles to tunnel. The shape of the quasiparticle current onset reflects the characteristic singularity in the BCS density of states in the leads. Within this region quasiparticle tunneling can occur at two different rates governed either by the normal state conductance or the subgap conductance of the tunnel junctions. The solid dots in Fig. 5.2 (d) are situated on the quasiparticle threshold curves extended to bias voltages between  $2\Delta < V_b < 4\Delta$ . They mark the boundaries of the two triangular areas, in which current is governed by single electron tunnel processes in which an energy gain of  $2\Delta$  can be obtained. The tunnel rate in these regions are proportional to the normal state conductance of one of the junctions. At zero temperature this yields  $\Gamma_{1,2} = -(\Delta E + 2\Delta)/e^2 R_{1,2}$ . The observed asymmetry in the height of both plateaus can be explained by the asymmetry in the tunnel resistances of the S-SET. The area denoted by the diamond shaped area is governed by quasiparticle tunneling with a rate proportional to the subgap conductance  $\Gamma_{sg} = -\Delta E/e^2 R_{sg}$ . The two triangular areas can be associated with the entrance of a quasiparticle on the island when the island contains either an even or odd number of electrons. In the experimental measurements we do not observe a  $2e$ -periodic even-odd asymmetry as measured by Nakamura *et al.*[20] We attribute this due to the fact that the effective temperature of the island is larger than the critical temperature  $T^*$  below which the odd-even effects are visible. A comparison between the measured data and a simulation at various biases yields an effective temperature of 336 mK. This is quite high compared to the base temperature of 10 mK and heavy filtering and shielding. [21] A

plausible explanation for the elevated temperature can be given by studying the environment, in this case the coupled generator, in which the S-SET is embedded. The generator provides an very low impedance environment of  $\text{Re } Z(\omega) = 3.5 \Omega$ . Tunneling Cooper pairs and quasiparticles can release their energy to the environment via photon emission. The coupling strength the environment is given by  $\alpha_{env} = \text{Re } Z(\omega)/R_K \sim 10^{-4}$ . [17] The generator is shunting the S-SET with an effective impedance lower than vacuum, effectively decoupling the S-SET from its environment. Therefore, the power dissipated due to quasiparticle tunneling is dumped into the island effectively heating it to an elevated temperature. This could explain why no even-odd asymmetry was observed in the measurements. A way to circumvent this problem is to couple the microwave radiation via the gate onto the island. In fact, these samples have been fabricated on the same chip.

In conclusion, we have described the subgap conductance of the S-SET in terms of quasiparticle tunneling processes. No  $2e$ -periodic parity effects could be measured. This probably can be attributed to the fact that heating, arising from the decoupling of the S-SET from its environment by the generator. Due to this effect the effective temperature of the island will be above the even-odd critical temperature. In the future, this effect can be circumvented by coupling the generator via the gate of the S-SET or by the inclusion of an resistor in the leads of the SET transistor.

### 5.3 Photon-assisted tunneling in a superconducting SET transistor

When the transistor is exposed to high frequency radiation by biasing the SQUID above its critical current, we expect to see a clear influence of the radiation on the quasiparticle current through the devices. Due to the magnitude of the quasiparticle current, the Tucker criterion applies and the response of the system to the radiation will be photonic. Therefore the oscillating electric field has to be modelled as an extra time-varying part in the Hamiltonian of the system. If an ac signal is applied, an ac voltage drop of  $\tilde{V} \cos(\omega t)$  will develop across the junction, where  $\tilde{V}$  and  $\omega$  are the amplitude and angular frequency of the signal. The influence of an ac signal is that parts of the electron wave function start to occupy sidebands with energies  $E \pm nhf$ . Physically speaking, the tunneling electron can absorb or emit photons in units of  $hf$ . The probability of going from an occupied state with energy  $E$  to an unoccupied state  $E + nhf$  is governed by the distribution function  $P(n) = J_n^2(e \tilde{V}/hf)$ , where  $J_n^2$  is the  $n$ -th order Bessel function. Based on this idea, Tucker *et al.*[1] was able to calculate the dc current  $\tilde{I}_{dc}$  under microwave radiation as a function of the dc bias voltage  $V_{sd}$

$$\tilde{I}_{dc}(V_{sd}) = \sum J_n^2(e \tilde{V}/hf) I_{dc}(V_{sd} + nhf/e) \quad (5.3)$$



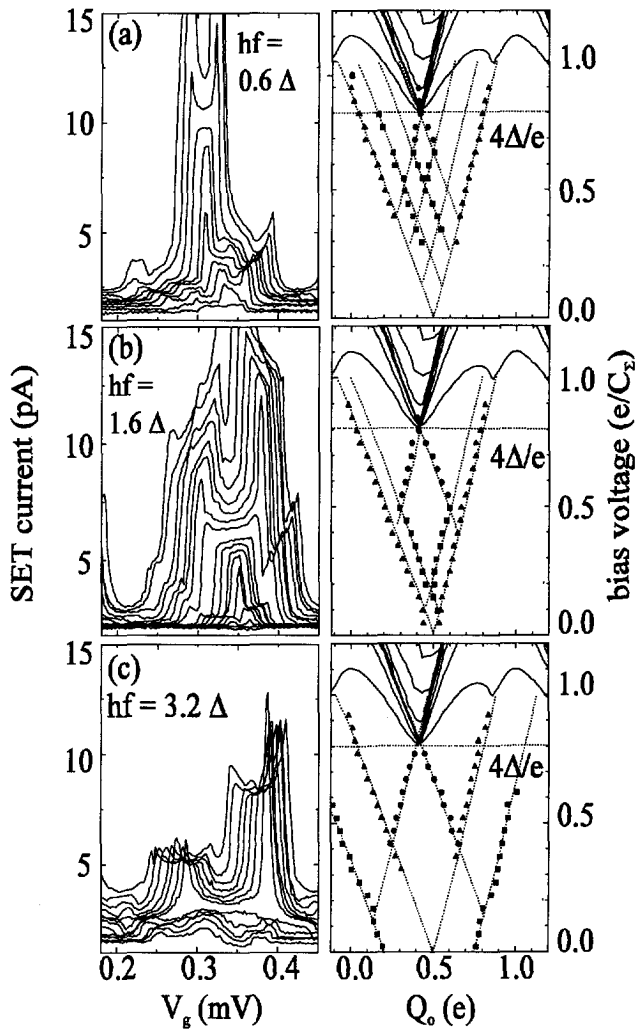


Figure 5.3: Current through the SET transistor as a function of the gate voltages for different bias voltages in the gap  $\Delta V_b = 0.5$  mV. The measurement was done for different settings of the generator (a)  $f = 0.6\Delta/h = 29$  GHz, (b)  $f = 1.6\Delta/h = 79$  GHz, and (c)  $f = 3.2\Delta/h = 160$  GHz. The current plateaus are mapped into the  $V - Q_0$  plane. The black triangles and dots mark the regular threshold voltages for quasiparticle tunneling and  $2\Delta$ -tunneling processes. The photon-assisted plateaus are marked by the black squares.

in which  $I_{dc}$  is the current in absence of an oscillating field. In a SET transistor the model by Tien *et al.*[2] must be extended to include the sequential tunneling of single electrons through the charging device. This is quite different from the one junction picture, where no correlation exists between tunneling electrons. PAT processes can easily be incorporated in the master equation of a double junction system, which was shown by Bruder *et al.*[14]

The dc response of the tunnel current through the S-SET was studied for different frequency settings of the generator. Three of them are shown in Fig. 5.3 a – c (29 GHz, 79 GHz, and 160 GHz respectively). Beside the current plateaus which were also present at zero frequency, extra current steps are observed for the first two frequencies for which the photon energy is  $hf < 2\Delta$ . The extra steps are marked in the  $V - Q_o$  plane by the black squares. The positions are parallel to the current steps as observed in the characteristics without rf, again indicated by the black triangles and dots. Since their relative shift is found to be  $hf$ , we attribute these steps to the photon-assisted tunneling of quasiparticles through either barrier where the condition  $hf = 2\Delta - eV_i$  ( $i = 1, 2$ ) is satisfied. Here  $V_i$  is the voltage difference across one of the junctions. The radiation is effectively shifting the threshold for  $2\Delta$  processes to lower voltages. As a consequence the shifted points in the sub threshold region corresponds to much higher bias voltages in the zero radiation case and can even correspond to points above  $4\Delta$ . This effect is clearly visible in Fig. 5.3 (a) and (b). The intersection point of the one-photon threshold lines at both junctions corresponds to photon-assisted  $2\Delta$ -processes occurring at both junctions. This point is equivalent to threshold point at  $Q_o = e/2$  for the zero radiation case, with the exception that the rate is not determined by the normal state conductance of the junctions but by the absorption rate of the tunneling quasiparticles. Increasing the bias voltage the one-phonon lines intersect the 'regular'  $2\Delta$ -threshold line. At these two intersections, at one barrier photon-assisted tunneling occurs, while at the other the quasiparticles tunnel directly. Hence the quasiparticle current increases rapidly above these points. For the case of 29 GHz radiation also two-photon processes are observed. Therefore following the same reasoning as above, current plateaus can be distinguished which exhibit both two-photon tunneling at both barriers, two-photon at the first and one-photon at the other barrier or two-photon tunneling and direct tunneling. In Fig. 5.4 the effect of the photon-assisted tunneling is illustrated very clearly in a 3-D plot of the  $I - V$  curves for different gate charge at 55 GHz. The same diamond-shaped current plateaus are formed. Each plateau can be assigned to a specific tunnel process, which is illustrated using the semiconductor model. This way we can analyze all the current plateaus very easily, as illustrated in Fig. 5.5 for the case of 29 GHz radiation. Each region defined by the threshold lines can be assigned to a certain transport mode ( $l, r$ ) of the current through the S-SET, where  $l$  and  $r$  are the left and right junction. The possibility to map the threshold lines this way is a direct consequence of the shape of the BCS density of states in the leads. At the third frequency shown in

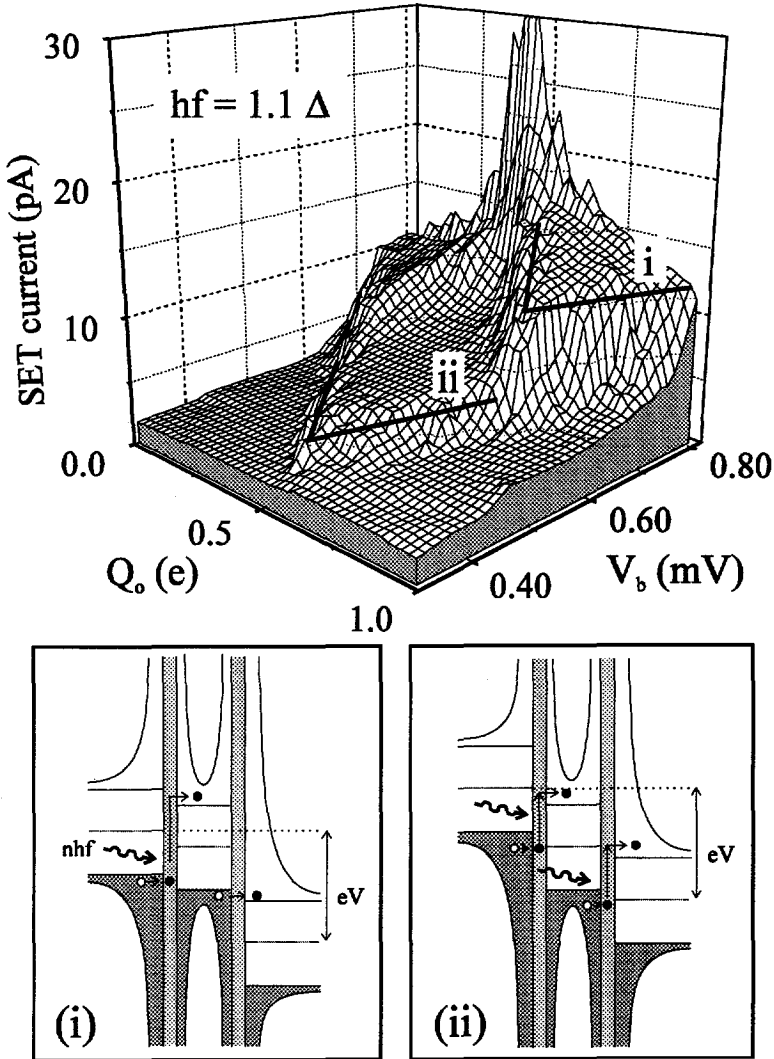


Figure 5.4: 3-D plot of the current-voltage characteristics for different gate voltages at a constant radiation frequency of 55 GHz. Each current plateau can be assigned to a specific tunnel process, as illustrated by the schematic energy diagram (i) and (ii).

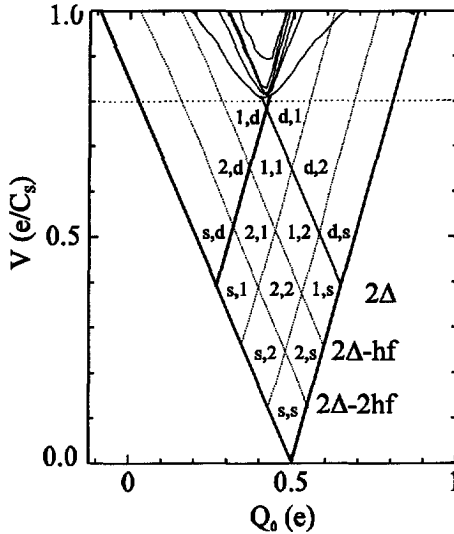


Figure 5.5: Positions of the different current plateaus for  $f = 29$  GHz. The solid lines indicate the threshold for quasiparticles, which are either determined by the normal or the subgap conductance of the tunnel junctions. The dotted lines are the one and two photon-assisted tunneling threshold voltages. Across each junction 4 different type of tunnel processes are possible:  $d$  (irect tunneling),  $1$  (-photon tunneling process),  $2$  (-photon tunneling process) and  $s$  (ubgap quasiparticle tunneling).

Fig. 5.3 (c), where  $hf > 2\Delta$ , the effect is less pronounced. Instead, all existing peaks and plateaus are increased in magnitude with respect to the case without rf. This is a consequence of the ability of the photon-assisted electrons to bridge the entire energy gap  $2\Delta$ . Again, current steps denoted by the black squares are formed at a distance  $hf$ , and are now within the regions of Coulomb blockade for quasiparticles. Only photon-assisted tunneling is possible, since direct tunneling of quasiparticles is blocked. Therefore the current is significantly lower.

In conclusion, multiple PAT processes have been observed in the subgap quasiparticle current of a superconducting SET transistor. Due to the superconducting leads all the different photon-assisted processes can be mapped out in detail. This shows the generator can be a very powerful tool in microwave spectroscopy. A number of interesting experiments are now accessible. First of all, if the radia-

tion is applied to the gate instead of the leads the low impedance shunting of the S-SET can be avoided. In principle it would be possible to observe the even-odd symmetry at finite bias voltages, as discussed above. Using photon-assisted tunneling parity changes can be induced, switching the system from an even to an odd state. Moreover, the application of the generator to a superconducting SET transistor with a supercurrent, opens the possibility to probe the excited states away from its ground state. Also the interplay between radiation and Andreev processes in NSN circuits can be studied, which was recently studied theoretically by Hanke *et al.*[23] The generator can be a useful tool to study all the possible Cooper pair processes by means of spectroscopy. Moreover, because of the simple fabrication process the SQUIDs can easily be fabricated on different substrates opening the possibility for combining semiconductor quantum dots and local oscillators.

## References

- [1] J. R. Tucker and M. J. Feldman, *Rev. Mod. Phys.* **57**, 1077 (1985).
- [2] P. K. Tien and J. R. Gordon, *Phys. Rev. Lett.* **129**, 647 (1993).
- [3] L.P. Kouwenhoven, S. Jauhar, K. McCromick, D. Dixon, and P.L. McEuen, *Phys. Rev. B* **50**, 2019 (1994).
- [4] T. H. Oosterkam, L. P. Kouwenhoven, A. E. A. Koolen, N. C. van der Vaart, and C. J. P. M. Harmans, submitted to *Phys. Rev. Lett.*
- [5] J. M. Hergenrother, J. G. Lu, M. Tuominen, D. C. Ralph, and M. Tinkham, *Phys. Rev. B* **51**, 9407 (1995).
- [6] M. Nahum and John. M. Martinis, *Appl. Phys. Lett.* **63**, 3075 (1993).
- [7] John M. Martinis and M. Nahum, *Phys. Rev. Lett.* **72**, 904 (1994).
- [8] D. V. Averin and Yu. V. Nazarov, *Phys. Rev. Lett.* **69**, 1993 (1992).
- [9] M. T. Tuominen, J. M. Hergenrother, T. S. Tighe, and M. Tinkham, *Phys. Rev. Lett.* **69**, 1997 (1992).
- [10] P. Joyez, P. Lafarge, A. Filipe, D. Esteve, and M. H. Devoret, *Phys. Rev. Lett.* **72**, 2458 (1994).
- [11] A. Amar, D. Song, C. J. Lobb, and F. C. Wellstood, *Phys. Rev. Lett.* **72**, 3234 (1994).
- [12] P. Lafarge, P. Joyez, D. Esteve, C. Urbina, and M. H. Devoret, *Phys. Rev. Lett.* **70**, 994 (1993).
- [13] G. Schon, J. Siewert, and A. Zaikin, *Physica B* **203**, 340 (1994).
- [14] C. Bruder and H. Scholler, *Phys. Rev. Lett.* **72**, 1076 (1994).

- [15] D. B. Haviland, Y. Harada, P. Delsing, C. D. Chen, and T. Claeson, *Phys. Rev. Lett.* **73**, 1541 (1994).
- [16] T. A. Fulton, P. L. Gammel, D. J. Bishop, L. N. Dunkleberger, and G. J. Dolan, *Phys. Rev. Lett.* **63**, 1307 (1989).
- [17] A. Maassen van den Brink, A. A. Odintsov, P. A. Bobbert, and G. Schon, *Z. fur Phys. B* **85**, 459 (1991).
- [18] A. Maassen van den Brink, G. Schon, and L. J. Geerligs, *Phys. Rev. Lett.* **67**, 3030 (1991).
- [19] Y. Nakamura, C. D. Chen, and J. S. Tsai, *Phys. Rev. B* **53**, 8234 (1996).
- [20] Y. Nakamura, C. D. Chen, and J. S. Tsai, preprint *parity effects in a superconducting single-electron transistor with a 20-nm island*, 1996.
- [21] B. Geerligs, Ph.D. thesis, Delft University of Technology, 1990.
- [22] P. Joyez, Ph.D. Thesis, University of Paris, p. 134, 1995.
- [23] U. Hanke, M. Gisselalt, and K. A. Chao, *Phys. Rev. B* **54**, 1529 (1996).

---

## Summary

This thesis is focused on the development of the technology of ultra-small tunnel junctions circuits. The area of these junctions is typically smaller than  $0.1 \times 0.1 \mu\text{m}$  and the resistance of the junctions is usually much larger than the resistance quantum  $h/e^2$ . The characteristic energy of these systems is called the charging energy  $e^2/2C$ . Therefore the reduction of the dimensions of these devices increases the charging energy, which can exceed the thermal fluctuations,  $k_B T$ . Consequently the charging energy can block electron transport through the circuit. Since one can control this transport on the scale of a single electron these devices are usually referred to as single-electron tunneling (SET) devices. Using submicron lithography it is possible to fabricate circuits in a controlled manner. Macroscopic pads connect small metallic islands via tunnel junctions. In this thesis the circuits are made of aluminum, which can be either in the normal or the superconducting state, exhibiting different transport properties.

The conventional SET technology was first improved by developing a multilayer SET technology. Better control over the device parameters was obtained, which is necessary in the design of more complex SET circuits which can be used in metrology and logic circuits. The multilayer approach was applied to several known SET circuits, such as the SET transistor with voltage gain, the electron box experiment and the single-electron turnstile. Using the experience of the multilayer technology, the coupling of a cryogenic high-electron mobility transistor (HEMT) on-chip to a metallic SET transistor was realized. Due to the intrinsically large output impedance of the SET transistor, coupled to the capacitive load at the output, the bandwidth of SET devices is basically reduced to dc operation. The HEMT is used in a source follower configuration transforming the output of the SET transistor to a low output impedance. The experiment is the first demonstration of the direct integration and operation of a metallic SET device and a semiconductor HEMT. The results have been used to propose SET experiments where a fast electrometer with sub-electron sensitivity is an essential element.

Using a similar philosophy as in the SET-HEMT circuit, a Josephson junction (JJ) generator was used as an on-chip tunable local microwave generator driving a superconducting SET transistor from a few to approximately 190 GHz. Biasing a shunted Josephson junction above its critical current, the voltage across the junction oscillates at the Josephson frequency  $f = 2eV/h$ . The frequency is in the microwave regime and therefore can be used as a local microwave source. Before the realization of such an integrated circuit, an externally shunted Josephson junction needed to be developed in the existing aluminium technology. Combining the multilayer fabrication with platinum thin film resistors resulted in almost ideal non-hysteretic Josephson junctions. The designed JJ generator was first characterized by measuring its response using an unshunted JJ as a threshold

---

detector. Driving a SET transistor instead of a large JJ with microwave frequencies, resulting in photon-assisted tunneling processes (PAT), in which tunneling electrons can absorb an integer number of photons resulting in an enhancement of the tunnel current. Using the JJ generator, these PAT processes in a superconducting SET transistor were studied. Again the coupled JJ generator - SET transistor circuits forms a hybrid circuit combining to different types of technologies. Furthermore, it is the first successfully proven experiment using a Josephson junction as a microwave generator for the high frequency study of SET circuits. It opens the possibility of numerous different experiments involving microwave spectroscopy. Ultimately all the developments described in this thesis should lead to fully integrated SET experiments and devices. Filtering, oscillators, and output buffering all can be integrated on one chip, leading to a mature SET technology, in which more complicated SET circuits can be implemented.



---

## Samenvatting

Dit proefschrift beschrijft de ontwikkeling van de technologie van ultra-kleine tunneljuncties. De afmetingen van deze tunnelcontacten zijn kleiner dan  $0.1 \times 0.1 \mu\text{m}$  en de tunnelweerstand van deze contacten zijn meestal veel groter dan de weerstands quantum,  $h/e^2$ . De karakteristieke energie van dit systeem wordt de ladingsenergie,  $e^2/2C$ , genoemd. Doordat de ladingsenergie omgekeerd evenredig schaal met de capaciteit van het systeem, zal deze toenemen als de dimensies van het systeem kleiner worden gemaakt. De ladingsenergie kan daardoor groter worden dan de thermische fluctuaties  $k_B T$ , zodat elektron transport door het circuit gebokkeerd wordt. Omdat het elektron transport gecontroleerd kan worden op de schaal van een enkel elektron, worden deze circuits vaak enkele-elektron (SET) circuits genoemd. Met behulp van submicron lithografie is het mogelijk dergelijke circuits op een gecontroleerde manier te maken. Via makroscopisch grote elektroden kan via de tunnelcontacten contact gemaakt worden naar kleine metallische eilanden. In dit proefschrift zijn de enkele elektron circuits vervaardigd uit aluminium. Afhankelijk van de grootte van het aangelegde magnetisch veld kan bij lage temperaturen het aluminium in de normale of in de supergeleidende toestand verkeren en zal hierdoor verschillende transport eigenschappen vertonen.

Door SET circuits te ontwikkelen gebaseerd op een multilaags technologie, is betere controle over de circuit parameters verkregen. Controle over deze parameters is noodzakelijk voor de ontwikkeling van meer complexere circuits, die hun toepassing vinden in de metrologie of SET logica. The multilaags technologie was toegepast op de SET transistor met spannings versterking, het "electron box" experiment, en de enkele elektronen "turnstile". Vervolgens was met behulp de multilaags fabricage de koppeling van een SET transistor aan een hoge elektronen mobiliteit transistor (HEMT) gerealiseerd. De intrinsiek hoge uitgangsimpedantie van de SET transistor, gekoppeld aan de capacitair load reduceert de bandbreedte van de SET transistor slechts tot dc operatie. De HEMT werd in dit geval gebruikt als een buffer, die de uitgang van de SET transistor naar een lage uitgang impedantie transformeerd. Dit experiment was de eerste demonstratie van de directe integratie en operatie van een metallische SET transistor en een halfgeleider HEMT. De resultaten kunnen worden gebruikt in experimenten waarbij een snelle elektrometer met sub-elektron ladingsgevoeligheid een essentieel onderdeel is.

Gebruik makend van dezelfde integratie filosofie als het SET-HEMT circuit, is een Josephson junctie (JJ) gebruikt als een lokale variabele microgolf generator. De generator kan frequenties van een paar tot ongeveer 190 GHz inkoppelen op een supergeleidende SET transistor. Als een geshunte Josephson junctie boven zijn kritische stroom wordt aangestuurd, oscilleert de spanning over de junctie met de Josephson frequentie  $f = 2eV/h$ . De frequentie is in het microgolf gebied

---

en kan daardoor worden gebruikt als een lokale microgolf bron. Voor de realisatie van de microgolf bron moest een extern geshunte Josephson junctie worden ontwikkeld in de bestaande aluminium technologie. Het gebruik van de multi-laags technologie in combinatie met platina dunne film weerstanden resulteerde in bijna ideale niet-hysteretische Josephson juncties. De JJ generator was eerst gekarakteriseerd door zijn respons te meten met behulp van een ongeschunte JJ, die als een detector fungeerde. Als microgolf frequenties worden ingekoppeld op een SET transistor in plaats van een grote Josephson junctie resulteert dit in foton-geassisteerde tunnel (PAT) processen. De tunnelende elektronen kunnen hierbij een geheel aantal fotonen absorberen en zal zo de tunnelstroom door de SET transistor vergroten. Met behulp van de JJ generator zijn de PAT processen in een supergeleidende SET transistor bestudeerd. Ook hier vormt de JJ generator en de SET transistor een circuit waar verschillende technologieën zijn geïntegreerd. Het is bovendien het eerste succesvolle experiment waarbij een Josephson junctie microgolf generator is gebruikt in de hoge frequentie studie van SET circuits. Het opent de weg naar verschillende experimenten waarbij microgolf spectroscopie van belang is. Uiteindelijk moeten alle ontwikkelingen, die in dit proefschrift zijn beschreven leiden tot een volwassen technologie, waarin meer complexe circuits kunnen worden geïmplementeerd.

---

# Curriculum Vitae

Erik Visscher

- Nov. 4, 1967    Born in Utrecht, The Netherlands.
- 1980-1986    V.W.O at the St. Bonifatius College, Utrecht.
- 1986-1992    Applied Physics at the Delft University of Technology,  
graduate research in the Solid State / Quantum transport  
group of prof. dr. ir. J. E. Mooij.  
subject: one-dimensional parallel Josephson junction arrays
- 1992-1996    Ph.D. research at the Delft University of Technology,  
in the Solid State / Quantum transport group of prof. dr.  
ir. J. E. Mooij.  
subject: technology and applications SET devices
- 1996-        Examiner at the European Patent Office, The Hague.

